Health Monitoring and Fault Diagnostics of Wind Turbines

Wang, Chao

DOI (link to publication from Publisher):
10.5278/vbn.phd.engsci.00152

Publication date:
2016

Document Version
Publisher's PDF, also known as Version of record

HEALTH MONITORING AND FAULT DIAGNOSTICS OF WIND TURBINES

BY
CHAO WANG

DISSERTATION SUBMITTED 2016

AALBORG UNIVERSITY
DENMARK

HEALTH MONITORING AND FAULT DIAGNOSTICS OF WIND TURBINES

by

Chao Wang

AALBORG UNIVERSITY
DENMARK

A Dissertation submitted to
the Faculty of Engineering and Science at Aalborg University
in Partial Fulfillment for the Degree of Doctor of Philosophy

Feb. 2016
Aalborg, Denmark

Dissertation submitted: May 2016

PhD supervisor: Prof. Zhe Chen
Aalborg University

Assistant PhD supervisor: Assistant Prof. Xiao Liu
Aalborg University

PhD committee: Professor Stig Munk-Nielsen (chairman)
Aalborg University

Professor David Infield
University of Strathclyde

Professor Keyue M Smedley
University of California

PhD Series: Faculty of Engineering and Science, Aalborg University

ISSN (online): 2246-1248
ISBN (online): 978-87-7112-710-2

Published by:
Aalborg University Press
Skjernvej 4A, 2nd floor
DK – 9220 Aalborg Ø
Phone: +45 99407140
aauf@forlag.aau.dk
forlag.aau.dk

Printed in Denmark by Rosendahls, 2016

Public Defence of PhD Dissertation

Thesis Title:
Health Monitoring and Fault Diagnostics of Wind Turbines

Ph.D. Defendant:
Chao Wang

Supervisor:
Professor Zhe Chen

Co-Supervisor:
Assistant Professor Xiao Liu

Moderator:
Associate Professor Weihao Hu

Assessment Committee:
Professor Stig Munk-Nielsen (Chairman)
Department of Energy Technology
Aalborg University
Pontoppidanstraede 111
9220 Aalborg, Denmark

Professor David Infield
Department of Electronic and Electrical Engineering
University of Strathclyde
Glasgow, Scotland, United Kingdom

Professor Keyue M Smedley
Department of Electrical Engineering and Computer Science
University of California, Irvine, USA

Defence Date and Place:

Monday, 27 June 2016
Pontoppidanstraede 111, Auditorium, Aalborg University

COPYRIGHT STATEMENTS

Thesis Title: Health Monitoring and Fault Diagnostics of Wind Turbines

Name of the PhD student: Chao Wang

Name of the supervisors: Prof. Zhe Chen

Name of Co-supervisors: Assist. Prof. Xiao Liu

List of publication: listed in § 1.5

This thesis has been submitted to the Faculty of Engineering and Science at Aalborg University for assessment in partial fulfilment for the Degree of Doctor of Philosophy (Ph.D.) in Electrical Engineering. The documented thesis is based on the submitted or published academic papers, which are listed in § 1.5. Parts of the papers are used directly or indirectly in this thesis. As part of the assessment, co-author statements have been made available to the assessment committee and are also available at the Faculty of Engineering and Science, Aalborg University.

ACKNOWLEDGEMENTS

First and foremost, I would like to express my sincerest thanks and deepest gratitude to my supervisor Prof. Zhe Chen for his guidance, encouragement and help on my research during my PhD study. I appreciate his vast knowledge and skills in many areas (e.g., renewable energy, power electronics, power system, electrical machine). In particular, I must acknowledge him for his understanding and consent on my temporary absence in 2012 dealing with my personal issues.

I would also like to thank my co-supervisor, Dr. Xiao Liu, for his help on Finite Element modeling and assistance in understanding the operation of electrical machines.

Many thanks go to Prof. Luis Romarol and Dr. Miguel Delgado for their support during my study abroad period at the MCIA Research Center in Polytechnic University of Catalonia, Spain. Moreover, I would like to extend my gratitude to Prof. Frede Blaabjerg and Prof. Francesco Iannuzzo for their assistance on my study abroad.

I must also acknowledge Dr. Shankar Sankararaman form National Aeronautics and Space Administration (NASA), USA, Dr. Eric Bechhoefer from GPMS, USA, Dr. Francois Liard from Alstom, France and Dr. Marcos Orchard from University of Chile for their professional suggestions on my PhD project. I would like to say thank you to Assoc. Prof. Ewen Ritchie for his constructive comments on fault diagnosis of wind turbines. Thanks also go to Prof. Mongens Blanke from Technical University of Denmark for offering me the opportunity attending his prestigious course on “Advanced topics on fault diagnosis and fault tolerant control”. Thanks also go to Mr. Justin Dinale from Department of Defence, Australia for his inspiration on the electromagnetic-field calculation. I would also like to thank Mr. Xiaoxu Zhang for the discussion on thermal analysis of electrical machines.

A special thank you goes to all my colleagues and friends at the Department of Energy Technology Aalborg University for their professional discussions, advice and support. Moreover, my special appreciations are extended to John K. Pedersen, Claus Leth Bak, Tina Larsen, Corina Busk Gregersen, Mette Skov Jensen, Eva Janik, Hanne Munk Madsen and Jan Krogh Christiansen for their assistance in many different ways.

I appreciate the financial support for my research provided by the China Scholarship Council and the Department of Energy Technology, Aalborg University.

Last but not least, I would like to thank my parents, my brothers, my wife and my son for their love, understanding and continuous support.

Chao Wang

Feb. 2016

Aalborg, Denmark

ENGLISH ABSTRACT

Wind power has increased dramatically in the past decades all over the world. The fast expansion of the wind power has also encountered quite a few challenges at the same time, among which major issues are Reliability, Availability and Profitability (RAP). From the life cycle management perspective, efficient Operation & Maintenance (O&M) is one of the most significant means to ensure and improve the RAP of Wind Turbines (WTs) during 20-year lifetime, especially in offshore environments. Health Monitoring and Fault Diagnostics (HMFD) is the enabling technology for RAP oriented maintenance of WTs. The objective of this project is to enhance the RAP of WTs by developing advanced HMFD technologies. HMFD for a Switched Reluctance Generator based Wind Turbine (SRG-WT) has been studied in this project, where gearbox and generator are the main focuses.

The thesis starts with introduction and literature review. Chapter 2 and Chapter 3 are dedicated to the online HMFD of WT gearboxes. Specifically, chapter 2 is on the HM of WT gearboxes where a saddle-coil probe based oil metal debris sensor is proposed to improve the performance of online health monitoring for WT gearboxes, the results demonstrate that the proposed saddle-coil inductive sensor possesses good identification ability of recognizing the ferromagnetic and non-ferromagnetic oil debris particles whose diameters are as small as 100 μm. Chapter 3 is dedicated to the FD of WT gearboxes. Conventional FD approaches including frequency domain analysis and joint time frequency analysis are investigated and evaluated using the signals collected from an experimental gearbox test bench with incipient gear tooth wear fault. Afterwards, an intelligent approach for the incipient gear fault detection based on *t*-Distributed Stochastic Neighbor Embedding (*t*SNE) and K Nearest Neighbor (KNN) is presented. The incipient gear tooth fault has been successfully detected under different operation conditions.

The next two chapters are focused on the HMFD of SRG. A sensor-less approach for online thermal monitoring of stator winding of SRG is addressed in Chapter 4, only voltage and current measurements which already exist in the control system are needed to estimate the temperature of stator winding, neither machine parameters (except initial resistance) nor thermal impedance parameters are required in the scheme. Simulation results under various operating conditions confirm the proposed sensor-less online thermal monitoring approach. Chapter 5 presents a fault diagnostic scheme for a SRG based on the residual between the estimated rotor position and the actual output of the position sensor. Extreme Learning Machine (ELM), which could build a nonlinear mapping among flux linkage, current and rotor position, is utilized to design an assembled estimator for the rotor position detection. The data for building the ELM based assembled position estimator is derived from the magnetization curves which are obtained

from Finite Element Analysis of an SRG. The effectiveness and accuracy of the proposed fault diagnostic method are verified by simulation at various operating conditions. The results provide a feasible theoretical and technical basis for the effective condition monitoring and predictive maintenance of SRG. The thesis ends with conclusions and future works.

The main contribution of this project is on the advanced monitoring and diagnostic methods for WTs. A new probe is designed to improve the performance of the oil metal debris sensor for online health monitoring of WT gearboxes. The proposed probe can also be applied to online health monitoring of general mechanical transmission systems. Furthermore, *t*SNE based nonlinear feature reduction is first applied to intelligent detection of incipient gear fault of WT gearboxes. Moreover, a simple and cost effective method is proposed to estimate the temperature of stator winding of SRG without using thermal sensors. Besides, ELM is applied to the rotor position estimation and position sensor fault diagnostics of SRG for the first time, the results validate the superiority of this method.

DANSK ABSTRAKT

Vindkraft er steget dramatisk i de sidste årtier over hele verden. Den hurtige ekspansion af vindkraften har også stødt på en hel udfordringer på samme tid, blandt hvilke store spørgsmål er Pålidelighed, tilgængelighed og Rentabilitet (RAP). Fra livscyklus management perspektiv, effektiv drift og vedligeholdelse (O & M) er en af de mest betydningsfulde middel til at sikre og forbedre RAP af vindmøller (WTS) i løbet af 20-års levetid, især i offshore miljøer. Sundhedsovervågning og Fejl Diagnostics (HMFD) er nødvendig teknologi for RAP orienterede vedligeholdelse af WTS. Formålet med dette projekt er at forbedre RAP af træsporingssystemet ved at udvikle avancerede HMFD teknologier. HMFD for en Switched Tilbageholdenhed Generator baseret Wind Turbine (SRG-WT) er blevet undersøgt i dette projekt, hvor gearkasse og generator er de vigtigste fokusområder.

Afhandlingen starter med introduktion og gennemgang af litteraturen. Kapitel 2 og kapitel 3 er dedikeret til online HMFD af WT gearkasser. Konkret kapitel 2 er på HM af WT gearkasser, hvor der foreslås en sadel-spole sonde baseret olie metal vragrester sensor til at forbedre effektiviteten af online sundhedsovervågning for WT gearkasser, resultaterne viser, at den foreslåede sadel-coil induktiv sensor besidder god identifikation evne til at genkende de ferromagnetiske og ikke-ferromagnetiske olie debris partikler, hvis diametre er så små som 100 um. Kapitel 3 er dedikeret til FD af WT gearkasser. Konventionel FD tilgange herunder frekvensdomænet analyse og fælles tid frekvens analyse undersøges og vurderes først ved hjælp af de signaler, der er indsamlet fra en eksperimentel gearkasse prøvebænk med begyndende gear tand slid skyld. Bagefter er en intelligent tilgang til den begyndende gear fejlfinding baseret på *t*-Distributed Stochastic Neighbor Embedding (*t*SNE) og K Nærmeste nabo (KNN) præsenteres. Den begyndende gear tand fejlen er blevet opdaget under forskellige driftsbetingelser.

De næste to kapitler er fokuseret på HMFD af SRG. En sensor-mindre tilgang til online termisk overvågning af statorvikling af SRG behandles i kapitel 4, er det kun spænding og strøm målinger, der allerede findes i styresystemet er nødvendig for at vurdere temperaturen i statorvikling, hverken maskine parametre (undtagen indledende modstand) heller termiske impedans parametre er påkrævet i ordningen. Simulation resultater under forskellige driftsbetingelser bekræfter den foreslåede sensor-mindre online termisk overvågning tilgang. Kapitel 5 præsenterer en fejldiagnose ordning for en SRG baseret på det tilbageværende mellem den anslåede rotor position og den faktiske produktion af positionssensoren. Extreme Learning Machine (ELM), som kunne bygge en ulineær kortlægning blandt fluxkobling, strøm og rotor position, er udnyttet til at designe en samlet estimator for rotorens position detektion. Dataene til at bygge ELM baseret samlede stilling estimator er afledt af magnetiseringskurver som er fremstillet af Finite Element Analyse af en SRG. Effektiviteten og nøjagtigheden af den foreslåede diagnostiske

metode skyld er verificerede af simulation ved forskellige driftsforhold. Resultaterne giver et realistisk teoretiske og tekniske grundlag for en effektiv tilstandsovervågning og forebyggende vedligeholdelse af SRG. Afhandlingen slutter med konklusioner og fremtidige værker.

Det vigtigste bidrag med dette projekt er på den avancerede overvågning og diagnostiske metoder til WTS. En ny sonde er designet til at forbedre ydeevnen af olien metal vragrester sensor til online sundhedsovervågning af WT gearkasse. Den foreslåede sonde kan også anvendes på online sundhedsovervågning af generelle mekaniske transmissionssystemer. Desuden er *t*SNE baseret lineær funktion reduktion først anvendes på intelligent detektion af begyndende gear skyld WT gearkasse. Endvidere foreslås en enkel og omkostningseffektiv metode til at estimere temperaturen af statorviklingen af SRG uden brug termiske sensorer. Desuden er ELM påføres rotorens position estimering og positionssensor fejldiagnosticering af SRG for første gang, at resultaterne validere overlegenhed af denne fremgangsmåde.

TABLE OF CONTENTS

LIST OF FIGURES

LIST OF TABLES

ABBREVIATIONS

BEMD	Bivariate Empirical Mode Decomposition
BP	Back Propagation
BTA	Boosting Tree Algorithm
CSA	Current Signature Analysis
DFIG	Doubly Fed Induction Generator
DWT	Discrete Wavelet Transform

ELM	Extreme Learning Machine
EMD	Empirical Mode Decomposition
ETC	Equivalent Thermal Circuits
FDD	Fault Detection and Diagnosis
FEA	Finite Element Analysis
FFT	Fast Fourier Transform
GMF	Gear Mesh Frequency
GWEC	Global Wind Energy Council
HHT	Hilbert-Huang Transformation
HMFD	Health Monitoring and Fault Diagnostics
KNN	K Nearest Neighbor
LM	Leverberg Marquart
LWK	Landwirtschaftskammer Schleswig-Holstein
MAE	Maximum Absolute Error
MSE	Mean Square Error
O & M	Operation and Maintenance
PMSG	Permanent Magnet Synchronous Generator
PSD	Power Spectral Density
RAP	Reliability, Availability and Profitability
RBF	Radial Basis Function
RIV	Relative Inductance Variation
RMSE	Root Mean Squared Error

SCADA	Supervisory Control And Data Acquisition
SLFNs	Single Hidden Layer Feedforward Neural Networks
SOM	Self-Organizing feature Map
SRG	Switched Reluctance Generator
STFT	Short Time Fourier Transform
SVD	Singular Value Decomposition
SVM	Support Vector Machines
***t*SNE**	*t*-Distributed Stochastic Neighbor Embedding
VKF	Vold-Kalman Filter
WBFS	Wrapper with Best Frst Search
WECS	Wind Energy Conversion Systems
WGS	Wrapper with Genetic Search
WMEP	Wissenschaftliches Mess- und Evaluierungsprogramm
WT	Wind Turbine

CHAPTER 1. INTRODUCTION

1.1. BACKGROUND AND MOTIVATION

1.1.1. BACKGROUND

Human society is experiencing an energy revolution – shift from fossil fuels to renewable and sustainable energies among which wind power has been expanding dramatically in the past decades all over the world. According to Global Wind Statistics 2015 published by Global Wind Energy Council (GWEC), the global cumulative installed wind power capacity is more than 430GW by the end of 2015. As shown in Fig. 1.1, the global cumulative installed wind power goes through an exponential growth trend, from less than 17GW in 2000 to over 430GW in 2015 [1]. The top ten countries of cumulative wind power until December 2015 are China, United States, Germany, India, Spain, United Kingdom, Canada, France, Italy and Brazil. The corresponding cumulative wind power capacities of these countries are demonstrated in Fig. 1.2 [1]. Thus wind power has become one of the most significate renewable power sources.

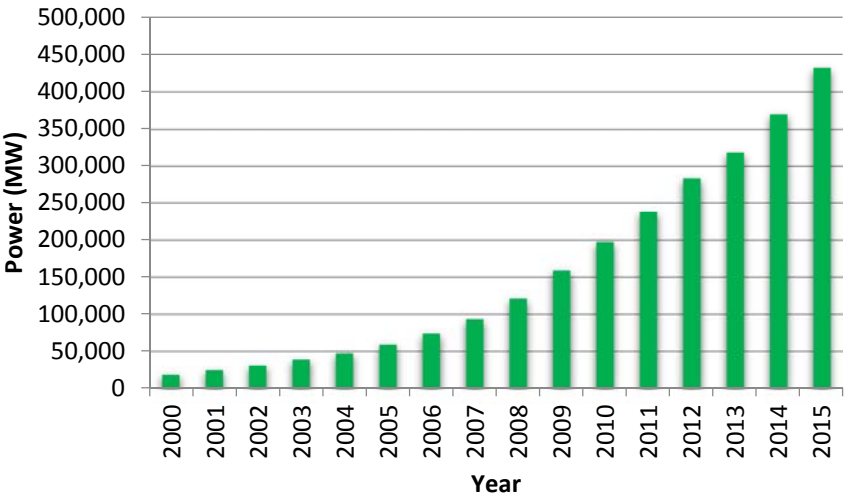

Fig. 1.1. Global cumulative installed wind power capacity from 2000 to 2015. [The figure was made in Microsoft Office Excel using the statistical data from reference [1]].

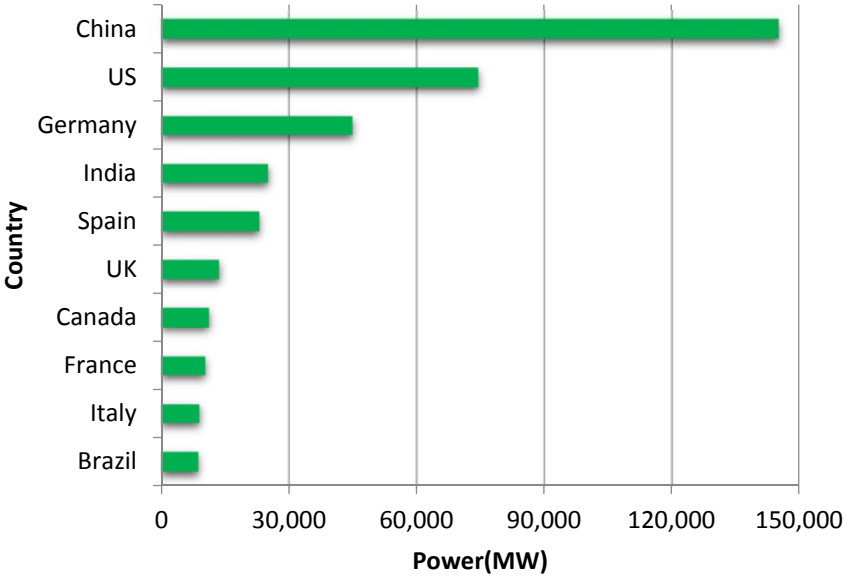

Fig. 1.2. Top ten countries of cumulative wind power until December 2015. [The figure was made in Microsoft Office Excel using the statistical data from reference [1]].

It is estimated that wind power would have a continued growth in the decades to come. Wind power accounts for about 3% of global electricity generation in 2014, the penetration level of wind power will achieve 17-19% of global electricity by 2030 with the capacity of 2,000 GW. The installation capacity of wind power will be 4,042 GW by 2050 [2].

1.1.2. CHALLENGES

There are more than 268,000 Wind Turbines (WTs) installed all over the world by the end of 2014 [3], the quantity of WTs could be 1,000,000 in 2030 and 2,021,000 in 2050 (the numbers are inferred based on the predicted global installation capacity of wind power and the average rated power per WT). The fast expansion of the wind power has been accompanied by many problems at the same time, among which major issues are relatively poor Reliability, Availability and Profitability (RAP). Management and maintenance of this huge number of renewable power generation assets are great challenges.

Reliability

WT, which consists of more than 8000 components [2], has a sophisticated electromechanical system with multi-body structure. Moreover, WTs are usually located in remote or ocean areas where the harsh operating conditions may result in the poor reliability of systems. Thus the reliability of WTs is susceptible to the degradation and failures of its assembly units. Most subsystems in a wind turbine may fail during operation, including blades and rotor, pitch control system, gearbox and bearings, generator, power electronic converters, yaw system, electrical control system and brakes etc. Recently, there are more and more accidents arising in wind farms all over the world with the continuous rapid expansion of wind power. A wind turbine in Netherland was burnt in 2013, two young Dutch technicians died in this fatal accident [4]. Fig. 1.3 demonstrates a disintegrated wind turbine in Ireland owing to a fault of turbine control system [5, 6]. It is observed that the blades are crashed into small pieces of fiberglass. A falling blade with fire in US is shown in Fig. 1.4, the blade is falling down from a firing wind turbine [7]. A wind turbine collapsed and hit the ground in Sweden on Christmas Eve 2015, which is reported in reference [8]. The tower was broken into several segments. The undesirable RAP of wind turbines is a great challenge for the development and utilization of wind power effectively and inexpensively.

Fig. 1.3. Disintegration of a wind turbine in Ireland on 2 January 2015 due to a fault in turbine control system [Reproduced with permission from [Andrew Kusiak, “Renewables: Share data on wind energy,” *Nature*, vol. 529, no. 7584, pp. 19-21, Jan. 2, 2016.] Copyright 2016, Nature Publishing Group], [5, 6].

Fig. 1.4. A falling blade with fire in US, 23July 2015 [Reproduced with permission from Kimberly Watley, Copyright 2016, Kimberly Watley], [7].

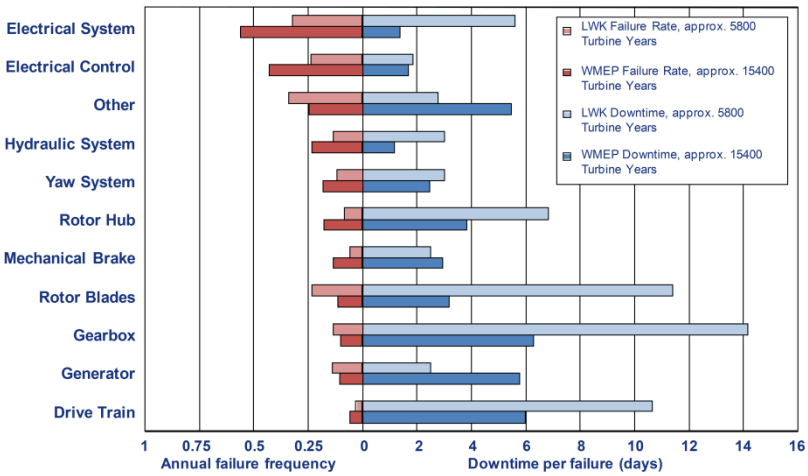

Fig. 1.5. Wind turbine subsystems failure rate and downtime per failure from two surveys including over 20000 turbine years. [The figure was made in Microsoft Office Visio using the statistical data from reference [9]].

Availability

Availability of WT is defined as a ratio of the total operational time (including start, generation, braking time, etc.) during a given interval to the total calendar time of the interval. It could be expressed as a percentage, $A\ (\%) = \frac{T_T - T_D}{T_T} X\ 100$, where A is the availability of WT, T_T is the total calendar time during the given interval, T_D is the total downtime of the WT. T_D can be calculated using frequency of failure multiplied by downtime per failure in WT.

Fig. 1.5 shows the comparison of the failure rate and downtime of different wind turbine subsystems from two German surveys by Wissenschaftliches Mess- und Evaluierungsprogramm (WMEP) and Landwirtschaftskammer Schleswig-Holstein (LWK) [9] which reveal that the gearbox has the longest downtime per failure while the electrical system has the highest failure rate among all the onshore wind turbines. It should be noted that the availability of electrical system is higher compared with mechanical system, even though electrical system has the highest failure rate. The main reason is that the electrical system is easy to be changed and has a shorter repair time. In other words, the electrical system does fail often but recovers quickly, hence it has less influence on the overall availability of the WTs.

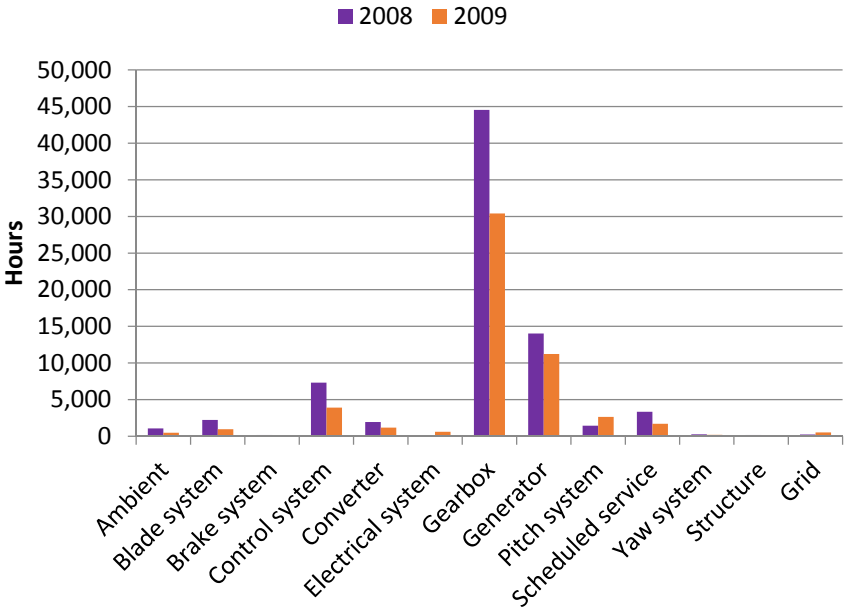

Fig. 1.6. Downtime caused by each subsystem of WTs in Egmond aan Zee wind farm in Netherland during 2008 and 2009. [The figure was made in Microsoft Office Excel using the statistical data from reference [11, 12]].

It is reported that the average availability is 95-98% for onshore WT, and is 80-95% for offshore WT [10]. However, the actual operating statistics of two large offshore wind farms indicate that the availabilities are even lower.

Fig. 1.6 demonstrates the downtime caused by subsystems, which is derived from the operation reports of WTs in Egmond aan Zee wind farm in Netherland during 2008 and 2009 [11-12]. This wind farm consists of 36 Vestas V90 3MW WTs which began operating in 2007. Gearbox and generator are among the top 2 subsystems which cause the longest downtime of WTs. The total downtime T_D in 2008 is 76758 hours,$T_T = 36\ turbines * 8760\ hours = 315360\ turbine\ hours$, thus the availability of the Egmond aan Zee wind farm in 2008 is, $A = (315360 - 76758)/315360 = 75.7\%$. Similarly, the availability in 2009 can be calculated as 82.9%. The operating statistics of Egmond aan Zee wind farm shows that the low availability of wind farms especially offshore wind farms is a significant challenge for the development of wind power.

Profitability

Profitability is another challenge faced by wind power developers, which is mainly due to the high Operation and Maintenance (O&M) cost especially for the offshore wind projects. The lifetime cost distribution of a baseline offshore wind project is shown in Fig. 1.7. It can be observed that the O&M cost takes up 21% of the total cost in this project. In reference [13] and [14], it is revealed that the maintenance cost accounts for 10-15% of the lifetime cost of onshore WTs, and 20-35% that of offshore WTs. The high maintenance cost results from the maintenance strategy of WTs. Periodical maintenance is the dominant maintenance strategy in wind power industry, normally the WTs are inspected twice a year. Although this maintenance strategy is more effective than the posterior maintenance, it still has drawbacks. Firstly, the condition of the WT is assessed and maintenance practices are arranged at fixed intervals based on experience, such strategy is usually high cost and often require shutdown of WT which certainly reduced the availability of wind farm. Another disadvantage is that the condition assessment is only made every certain time and the equipment conditions between maintenance remain unknown, which may result in either excessive maintenance or lack of maintenance of the WTs. Thus the condition based maintenance is preferred for the maintenance cost reduction and profitability improvement of WTs.

Another factor which has a great impact on the profitability of WTs is the unplanned replacement of the critical subsystems especially in offshore wind projects. Costs for unscheduled replacement of WTs are significant. Table I shows the cost for replacement of different subsystems for a 5MW offshore WT [15], which has a value of 50 million DKK. The cost for replacement of gearbox is more than two times of that for generator or blade. Replacement of such subsystems usually requires specialized vessel and crane. In addition, the harsh

marine environment may limit the accessibility of operating personnel to faulty WT, which further increases the cost of human resource.

Therefore, the high O&M and unscheduled replacement costs make the profitability of WTs a big challenge.

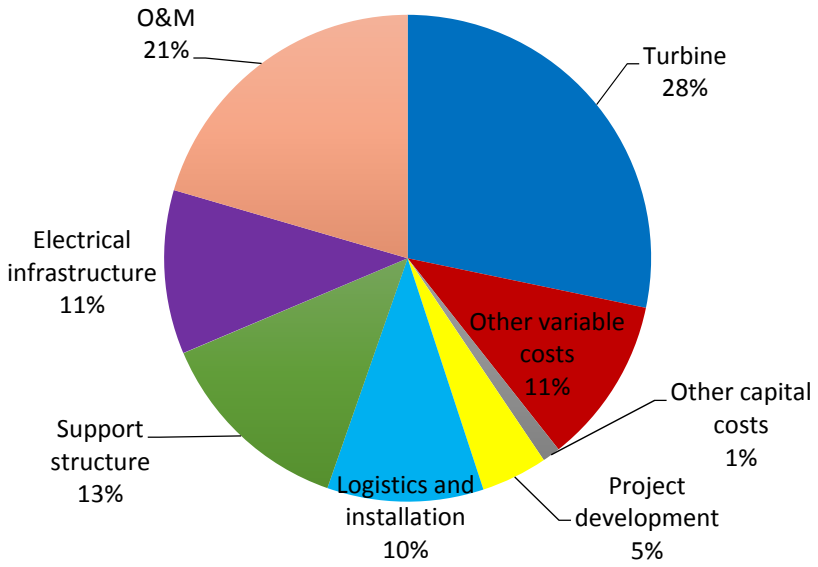

Fig. 1.7. Lifecycle cost distribution of an offshore wind project. [The figure was made in Microsoft Office Excel using the statistical data from reference [10]].

Table 1.1. Subsystem replacement cost of a 5MW offshore wind turbine [15].

Name of Subsystem	**Cost (DKK)**
Gearbox	3,937,000
Generator	1,968,000
Blade	1,625,000

1.1.3. MOTIVATION

Health Monitoring and Fault Diagnostics (HMFD) is the enabling technology for safe and reliable operation as well as efficient maintenance of WTs.

The first motivation is to sense the conditions of WT in real time, identify the potential faults/failures in the early stage, promote condition based and RAP orientated maintenance of WTs by developing advanced and innovative HMFD technologies. The aim is to improve the reliability of WTs and reduce the O&M costs, eventually lower the cost of wind power.

Another driving force of this research is the great market demand of advanced HMFD systems for WTs. It is reported that the global O&M market of WTs was 62.26 Billion DKK in 2014 and is predicted to be 137.92 Billion DKK by 2023[16]. As one of the core technologies for O&M of WTs, the HMFD systems will have a booming market in the decade to come. However, the dominant commercialized HMFD technologies are spectral analysis based on vibration monitoring which is focused on the drive train subsystems of WTs according to survey [17]. O&M market calls for new technologies for HMFD of WTs.

Thus, it is of great significance to conduct research on HMFD of WTs to sense the health status, detect incipient faults, identify severity and locations of faults, predict the remaining useful lifetime and promote RAP orientated maintenance of WTs.

1.2. STATE OF THE ART

Online HM is an effective way to sense the health status of WTs. Based on the data collected from the online HM system, the terminal users need an automatic classification system to provide or predict the assessment results of the health conditions of WTs for them to arrange the maintenance strategies in advance. RAP orientated maintenance require the stable accurate and fast FD techniques to detect, locate the fault as soon as possible and recognize the root causes as accurate as we can, predict the future damage and system failures as early as possible. This will benefit the logistic decisions for wind farm operators.

In the literature, a number of articles have reviewed the state of the art on HMFD of WTs. As the HMFD of WTs is a multidisciplinary research area, the authors of these review papers are from different fields which are mainly in the domains of Electrical Engineering [18-26], Mechanical Engineering [27-31] and Civil Engineering [32-34]. Structural HM in WTs especially corrosion and crack monitoring are often neglected in the review papers from Electrical Engineering and Mechanical Engineering communities, while the review papers from Civil Engineering usually pay little attention on the HM of electrical components in WTs.

In this section, a brief review of the state of the art on HM of WTs will be provided. FD of WTs will be reviewed and classified in a new perspective.

WT is a sophisticated mechanical-electrical-magnetic system. A typical offshore WT configuration is illustrated in Fig. 1.8. The components/subsystems of a WT which have been/should to be monitored include blade, main bearing, main shaft, gearbox, generator, power converter, sensor, nacelle, tower, foundation, hydraulic system, control system, braking system, yaw system, anemometer and key connecting bolts. The common fault modes of main components in a WT have been introduced in [23]. The HM methods applied to WTs have been well investigated and summarized in recent review reference [23, 24, 26] published in the last two years. Thus FD of WTs is the main focus of this overview.

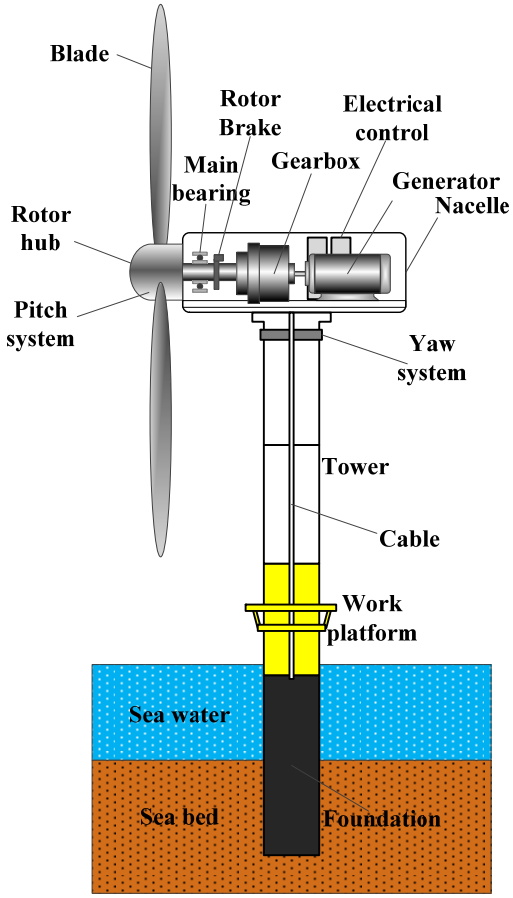

Fig. 1.8. A typical offshore wind turbine.

HM is the foundation for fault detection and diagnostics of WTs. The monitoring solutions applied to WTs include acoustic emission monitoring [35, 36], thermal monitoring [37, 38], ultrasonic monitoring [39, 40], fiber optical monitoring [41, 42], current monitoring [43, 44], voltage monitoring [45, 46], electrical impedance monitoring [47, 48], strain monitoring [49], eddy current monitoring [50], oil monitoring [51, 52, 53], X-radioscopy [29], lightning monitoring and protection [54], fir monitoring [55], and SCADA data analysis [56, 57].

Among the above mentioned HM methods, vibration, thermal and electrical parameters monitoring are often used for WTs' HM. The vibration monitoring is most common and mature and thermal monitoring is usually used in protection of WT generators. Bearing faults in the generators were successfully recognized in [44] by analyzing the current signal in the Permanent Magnet Synchronous Generator (PMSG). Reference [58] also used electrical signal which is output power signal as a medium to detect the shaft misalignment fault in a Doubly Fed Induction Generator (DFIG). As a matter of fact, both mechanical and electrical faults in WTs can be recognized via stator electrical signals as is shown in reference [59]. It is a trend that noninvasive nondestructive methods such as Current Signature Analysis (CSA) and other electrical signal based FD in WTs is more and more popular as they have significant advantages over vibration based methods in terms of cost, implementation and reliability.

The FD methods used in WTs can mainly be divided into the following categories: model based method, signal processing based method, artificial intelligence based method and their combinations.

Model based FD of WTs

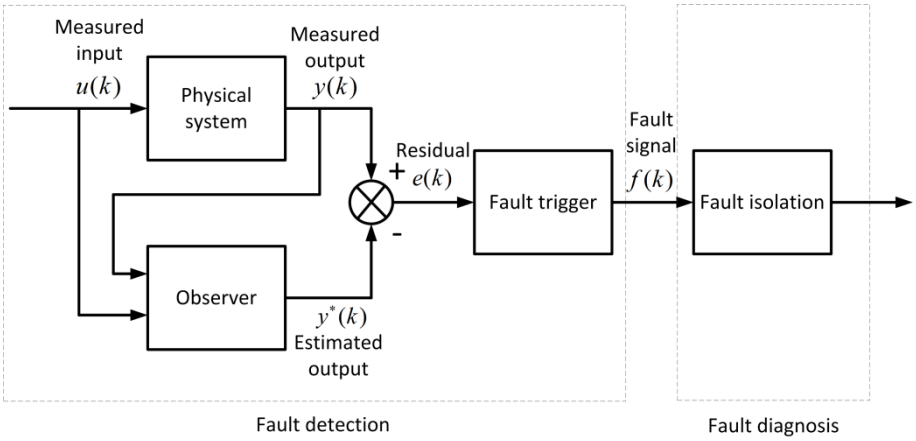

Fig. 1.9. Schematic diagram of model-based fault diagnosis.

Model based FD is popular in control community. The basic idea is using the generated residual between measured behavior and estimated behavior as a fault indictor to trigger the fault detection and fault isolation schemes based on the mathematic models of dynamic systems. Analytical redundancy in the system is fully utilized in the model based FD [60, 61]. The schematic diagram of model-based FD is shown in Fig. 1.9. Fault detection usually means to detect abnormal states. The existence of a fault could be checked by the fault detection block, while fault diagnosis block is trying to identify the location, types as well as severity of the fault. It should be noted that a set of residuals could be required in some cases to isolate the fault.

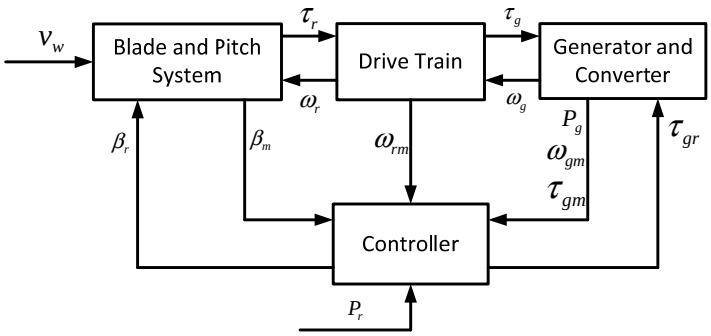

Fig. 1.10. The fault detection bench model in [64].

Recently, model based FD has been gradually applied to WTs. Reference [62] proposed a model based method to detect the current, voltage, and position sensor fault in DFIG based WTs. Kalman filter was used in [63] to detect current sensor faults for a WT. A benchmarking model for three-bladed horizontal variable speed WT with a full converter coupled is proposed in [64] and [65], which is demonstrated in Fig. 1.10. FD schemes for sensors, actuators and system could be tested using this model. Several solutions have been explored based on this model recently. Support Vector Machines (SVM) with Gaussian Kernel has been used to classify the types of faults based on trained vectors which can be found by learning the fault pattern from training dataset. A combined observer and Kalman Filter solution for the fault diagnosis of this bench model has also been developed. These proposed methods have satisfactory results [66-68]. The drawback of model based fault detection method lies in the accurate analytical mathematic model which is usually very hard to be established because modern wind turbines are more and more complicated. However, model based FD is feasible for some subsystems and components.

Signal Processing based FD of WTs

Signal processing based method used in wind turbine fault diagnosis is more common. A literature review in this related papers show that signal processing theory including Power Spectral Density (PSD) analysis, Wavelet, Empirical Mode Decomposition (EMD) and Bivariate Empirical Mode Decomposition (BEMD) etc. have been used in this research field. Also, some noninvasive monitoring methods containing power signal and stator current are favored to be used for the diagnosis of mechanical faults in wind turbines. Most of the researches are focused on the mechanical faults, so there are more to do with respect to the electrical faults in wind turbines. W. Yang et al. proposed to obtain fault related signals from generator output power and rotational speed. They designed an adaptive filter based on continuous wavelet transform to track the energy in the fault related frequency bands from the power signal. Both mechanical and electrical faults were successfully detected by applying this method [69]. Watson, S.J. et al. also used generator output power signal instead of vibration monitoring to gain the features of the faults. But they only study the mechanical faults such as shaft misalignment failure and bearing failure in the wind turbine [70]. BEMD was investigated in paper [71] for detecting incipient mechanical and electrical faults of wind turbines. The results showed that BEMD is more effective than EMD and wavelet-based energy tracking techniques. But this method is too complicated to be implemented in field applications in the near future.

Hilbert-Huang Transformation (HHT) is proposed in [72] to detect the very early stage fault in inter-turn insulation by only analyzing the stator current in the PMSG. Simulation results show that HHT can detect the incipient insulation fault in PMSG successfully. In addition, HHT is more effective than DWT in incipient winding insulation deterioration detection of the PMSG. The decomposition of phase current by Discrete Wavelet Transform (DWT) and EMD are presented in Fig. 1.11(a) and Fig. 1.11(b) respectively. A novel methodology based on tracking the characteristic demagnetization fault orders of stator current by means of Vold-Kalman Filter (VKF) has been proposed in [73] for the partial demagnetization fault detection of PMSMs operating under nonstationary conditions. Only the fault related harmonics are tracked while the rest of components are removed as noise. Amplitude of envelopes of the fault characteristic orders has been used as fault indictors. The results demonstrate the potential of the proposed method for PDFD of PMSMs to be applied in industrial nonstationary applications. Choi-Williams time frequency distribution of the tracked orders of stator current in a healthy and 50% demagnetized PMSM are shown in Fig. 1.12 (a) and Fig. 1.12(b), respectively. By comparing the results in these two scenarios, it can be seen that the envelopes of 1/3, 5/3, 15/3 orders of stator current in 50% demagnetization fault occasion are all higher than those of healthy occasions. Significant difference of Choi-Williams time frequency distributions of the tracked orders of these two cases can be observed easily.

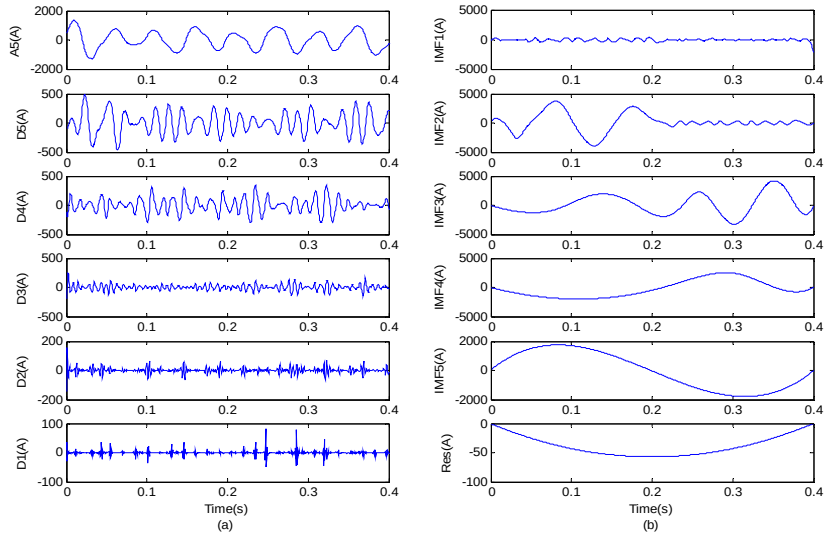

Fig. 1.11. The comparison of DWT and EMD on inter-turn fault detection of PMSWG, (a) DWT of the Phase current, (b) EMD of the Phase current.

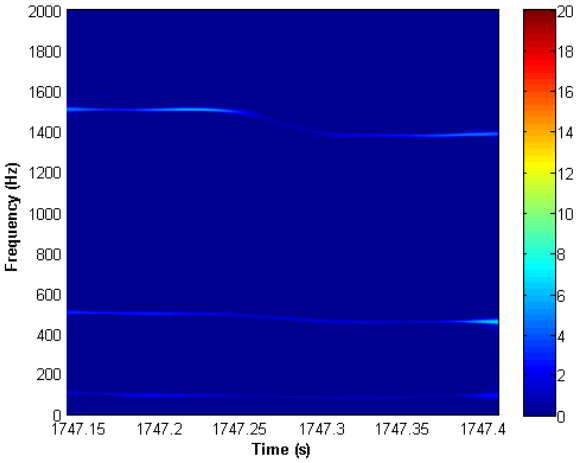

(a)

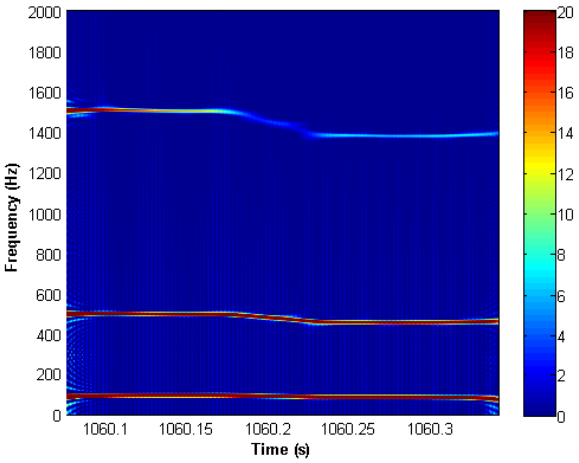

(b)

Fig. 1.12. Choi-Williams time frequency distribution of the tracked orders of stator current in a PMSM with slope speed profile from 6000 to 5550 r/min (a) healthy (b) 50% demagnetized.

Artificial Intelligent based FD of WTs

Recently, some researchers began to apply Artificial Intelligent in the fault diagnosis of wind turbines. Most of these studies are based on artificial neural network which is an efficient tool in dealing with complicated nonlinear fault pattern identification problems in wind turbines. In paper [74], Back Propagation (BP) neural network was applied in the identification four kinds of typical faults of gearbox in wind turbines. Although the research results are satisfying, the author didn't consider the drawbacks of BP neural network such as slow convergence speed and local extremum which will affect the diagnosis accuracy. X. Zhang et al. summarized that the fault diagnosis method based on frequency spectrum analysis and wavelet analysis can be effectively used in the vibration analysis of the gear box, shaft and generator of WTs [75]. Different structure of neural network including feed forward and self-organizing feature map neural network (SOM) and varieties algorithms containing BP, Leverberg Marquart (LM) have been applied in gearbox, yaw system, generator and power electronic equipment in wind turbines [76-77]. Fuzzy algorithm approach, maximum membership grade principle and data mining algorithm are also adopt to diagnose the fault symptom of wind turbine blade and gearbox respectively [78-80].

Other intelligent fault diagnosis technologies used in the wind turbines including Muti-Agent system and Data-Mining Approach. These methods are based on large quantities of data from Supervisory Control and Data Acquisition (SCADA) system in wind power plants. By analysis these data, the health status as well as the condition trend of the turbine and the internal segments will be estimated by different Agents or different data-mining algorithms such as wrapper with genetic search (WGS), wrapper with best first search (WBFS) and boosting tree algorithm (BTA). A. S. Zaher et al. proposed a multi-agent framework which includes abnormal detection and trend prediction for wind turbines. The fault diagnosis system architecture using Multi-Agent techniques is shown in Fig. 1.13. The system includes five agents among which three are fault diagnosis agents [81]. In paper [82], A. Kusiak et al. proposed wind fault prediction models based on data mining algorithms.

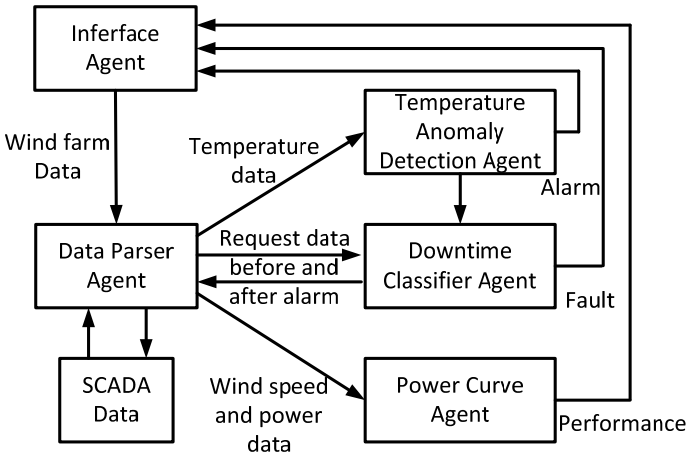

Fig. 1.13. Fault diagnosis system architecture using Multi-Agent techniques [81]

It is a trend that current based bearing fault diagnosis and other electrical signal based fault diagnosis in WTGS is more and more popular because they have significant advantages over vibration based methods in terms of cost, implementation and reliability. X. Gong et al. proposed a wavelet method for incipient bearing fault detection using stator currents of the wind turbine [83]. A method based on stator current PSD analysis was also proposed in paper [84]. Bearing outer race and inner race defects for a direct-drive wind turbine generator were researched in this paper. There are also many works we can do in this area in the future.

Although a great many of the research objects in these studies are generator, it seems that they often concentrate on the mechanical parts such as bearing and shaft in wind generations. In fact, the electrical fault in rotor and stator in wind turbine generator should also be paid more attention on.

Power electronic conversion system, which interfaces the power grid and wind turbines' generator, is one of the most important parts in wind power systems [85-86]. The reliability analysis and faults diagnosis of power electronics conversion system in wind power system become a very important issue. Except for fault diagnosis of universal power electronics devices, converter and power electronics systems, there are also many papers about the fault diagnosis of these devices used in the wind power system. Among these papers, study objects include single fault and multiple faults both in the grid side and generator side converters. The wind power generation systems cover from Permanent Magnet Synchronous Generator (PMSG) to Doubly-Fed Induction Generator (DFIG). The algorithms used in this field include BP neural networks fault diagnosis method and orthogonal power references method [87-91].

In the past few years, some novel generators are gradually applied to WTs. Among them switched reluctance generator (SRG) is attractive for its fault tolerant ability. But fault tolerance doesn't mean fault free. Several articles are about the fault diagnostics of SRGs. Winding fault detectors were designed in [92] to indicate the faulty windings in SRG to make sure the generator can continue operate without the faulty phase. Reference [93] analyzed and simulated the various faulty modes of the SRG. The generator's excitation requirements with and without faults were also investigated in this article. The literature on FD for switched reluctance wind turbine generators is very rare. But the demand for high reliable generators in wind power system is urgent. The fault tolerance capability of SRG should be fully utilized in the wind turbine application to satisfy the high reliability requirement. Hence there are a lot of opportunities in this research field.

To sum up, a brief literature review on fault diagnosis of WTs has been carried out. It can be concluded that although a lot of work has been done in the recent past, the fault diagnosis of WTs is still in the initial stage and there are plenty of work to do. Currently, almost all condition monitoring and fault diagnosis methods used in wind power industry are borrowed from universal equipment fault diagnosis or have been used in other similar applications. Thus, the characteristics of faults pattern and mechanism as well as the uniqueness should be studied before applying those technologies in wind turbine. On the other hand, more attention should be paid on the electrical fault research in generators as well as in the power electronics conversion system of WTs. Also, noninvasive monitoring method such as stator current and other electrical signal based monitoring should be applied in the condition monitoring and fault diagnosis of WTs. Again, because the WTs are very complicated, one fault can be caused by many reasons, just using one method to diagnose the fault is very difficult. So the newest theory in Artificial Intelligence, Machine Learning, Pattern Recognition, Data Mining, Intelligent Computing and other related theory and their combination should be used in the fault diagnosis of WTs. Furthermore, condition prediction, fault warning fault tolerant control, condition based maintenance as well as SCADA data analysis should be further researched based on the intelligent fault

diagnosis of WTs. Therefore, it is thought that there are a lot of opportunities and strong demands in this research field.

1.3. SCOPE OF THIS THESIS

Research object

As mentioned in section 1.1, faults in gearbox and generator result in the longest downtime of WTs and maintenance costs for these subsystems are relative high. Thus, the HMFD of gearbox and generator in WTs is the concentration of this project. In order to fulfill partial objectives for "Research on DC network connection with a novel wind-power-generator system" supported by the Danish Agency for Science, Technology and Innovation through the under Grant DSF-10-094560, a Switched Reluctance Generator (SRG) based WT has been selected to conduct research on HMFD of gearbox and generator.

Specific research objectives

The objective of this project is to enhance the RAP of gearbox and generator in SRG based WTs by applying advanced HMFD technologies. The specific research objectives are,

- ***a.*** To improve the performance of the oil debris sensor for HM of gearboxes, in order to prolong the lifetime of gearboxes and benefit the condition based maintenance of gearboxes.
- ***b.*** To detect the incipient teeth faults of gearboxes based on a novel incipient fault detection scheme using the tri-axis vibration signals aiming at improving the sensitivity of the fault related features and enhancing the accuracy of the incipient fault detection of WT gearboxes.
- ***c.*** To develop a sensor-less scheme for thermal monitoring of stator winding of SRG, neither machine parameters nor thermal impedance parameters are required in the scheme.
- ***d.*** To develop a fault diagnostic scheme for FD of position sensor in a SRG based on the model based FD. The purpose is to provide a feasible theoretical and technical basis for the effective predictive maintenance of SRG.

Methodology

The methodology of this project is shown in Fig. 1.14. Firstly, fault analysis and simulation has been conducted with the focus on gearbox and generator, knowledge of failure mechanism has been obtained. This study requires interdisciplinary knowledge including Electrical Machine, Power Electronics, Artificial Intelligence, Computational Intelligence, Machine Learning and Signal Processing. So some

novel and newest theories in these fields have been investigated. The fault analysis and simulation also provide guidance to the whole procedure including the algorithm development and experimental design. Secondly, parameters for HM of WTs have been selected. For the HMFD of gearbox, the monitored parameters are lubricating oil debris and vibration. For the HMFD of generator diagnosis, the monitored parameters are voltage and current. In addition, the effective and feasible feature extraction methods and fault diagnostic models have been developed for the diagnosis. A new oil debris sensor has been proposed. A novel approach has been proposed to detect the incipient teeth fault in a gearbox based on vibration monitoring. A sensor-less scheme for thermal monitoring of stator winding of a WT generator has been developed. A fault diagnostic scheme for FD of position sensor in a WT generator has been proposed. Some of the proposed HMFD methods have been verified experimentally.

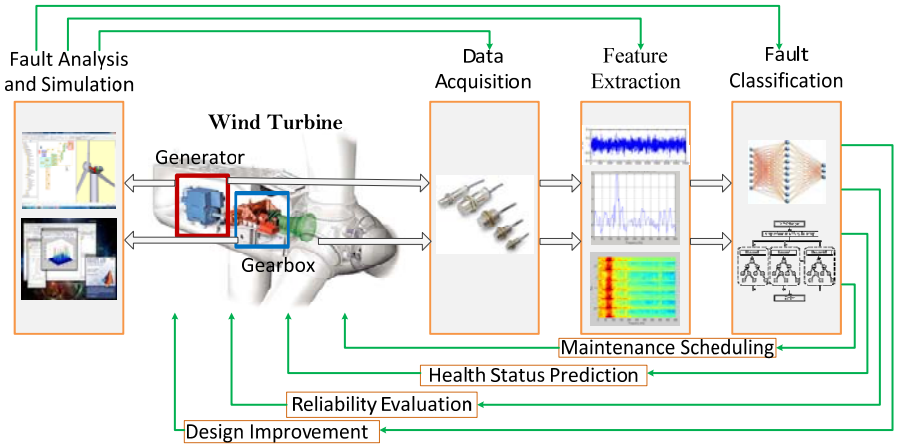

Fig. 1.14. Methodology of this project.

1.4. THESIS LAYOUT

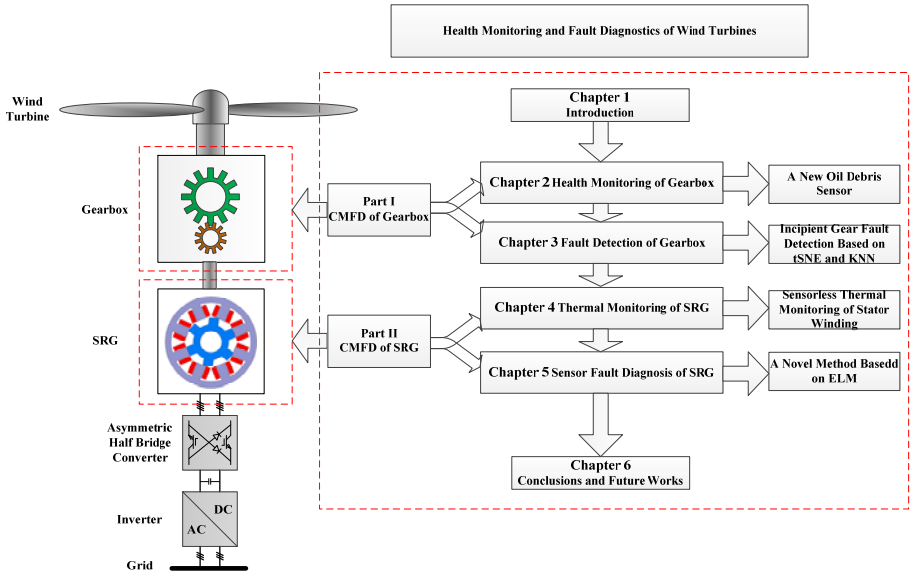

Fig. 1.15. Thesis layout and relationship of the chapters.

The thesis consists of 6 chapters, the thesis layout and relationship of the chapters are demonstrated in Fig. 1.15. The thesis is arranged as below,

Chapter 1 Introduction

The background, challenges and motivations of the research are introduced, the state of the art of HMFD for WTs is reviewed briefly. In addition, the research objects, specific research objectives as well as the methodology of the project are presented. Finally, the thesis layouts and list of publications are given.

Chapter 2 Online health monitoring of wind turbine gearboxes

A new inductive sensor which uses saddle-coil probe to generate a uniform magnetic field for performance improvement on the metal particle detection for HM of WT gearboxes is proposed in this chapter. The detailed geometry and the performance analysis are presented by using finite element analysis. The results demonstrate that the proposed saddle-coil inductive sensor possesses good identification ability of recognizing the ferromagnetic and non-ferromagnetic oil debris particles whose diameters are as small as 100 μm.

Chapter 3 Incipient gear fault detection of wind turbine gearboxes

A new method for detection of early degradation in WT gearboxes is presented in this chapter. Tri-axis vibration signals, which are used as the medium for the fault detection, are collected from an experimental gearbox test bench with incipient gear tooth wear fault. Twenty four statistical features in time domain are extracted from the vibration signals in each sampled instance. The intrinsic low dimensional manifold embedded in the twenty four dimensional fault characteristic space is learned by using the *t*-Distributed Stochastic Neighbor Embedding (*t*SNE) which is an advanced nonlinear dimensionality reduction algorithm. The incipient gear tooth fault has been successfully detected under different operation conditions only via a sample K Nearest Neighbor (KNN) classifier using the reduced features in the manifold.

Chapter 4 Online thermal monitoring of switched reluctance wind turbine generators

A sensor-less approach for online thermal monitoring of stator winding of SRM is proposed in this chapter, only voltage and current measurements which already exist in the control system are needed to estimate the temperature of stator winding, neither machine parameters nor thermal impedance parameters are required in the scheme. Simulation results under various operating conditions confirm the proposed sensor-less online thermal monitoring approach.

Chapter 5 Sensor fault diagnosis of switched reluctance wind turbine generators

This chapter presents a fault diagnostic scheme for a SRG based on the residual between the estimated rotor position and the actual output of the position sensor. Extreme Learning Machine (ELM), which could build a nonlinear mapping among flux linkage, current and rotor position, is utilized to design an assembled estimator for the rotor position detection. The data for building the ELM based assembled position estimator is derived from the magnetization curves which are obtained from Finite Element Analysis (FEA) of an SRG with the structure of 8 stator poles and 6 rotor poles. The effectiveness and accuracy of the proposed fault diagnosis method are verified by simulation at various operating conditions. The results provide a feasible theoretical and technical basis for the effective condition monitoring and predictive maintenance of SRG.

Chapter 6 Conclusion and future works

Contributions and main findings of this thesis are summarized in this chapter. Future works are also discussed in the end.

1.5. LIST OF PUBLICATIONS

Journal papers

[1] **C. Wang**, X. Liu, and Z. Chen, "Incipient Stator Insulation Fault Detection of Permanent Magnet Synchronous Wind Generators Based on Hilbert–Huang Transformation," *IEEE Transactions on Magnetics*, vol. 50, no. 11, Nov. 2014.

[2] **C. Wang**, X. Liu, and Z. Chen, "Probe Improvement of Inductive Sensor for Online Health Monitoring of Mechanical Transmission Systems," *IEEE Transactions on Magnetics,* vol. 51, no. 11, Nov. 2015.

[3] **C. Wang**, M. D. Prieto, L. Romeral, Z. Chen, F. Blaabjerg, and X. Liu, "Detection of Partial Demagnetization Fault in PMSMs Operating under Nonstationary Conditions," *IEEE Transactions on Magnetics.* vol. 52, no. 7, Jul. 2016.

[4] **C. Wang**, X. Liu, H. Liu, and Z. Chen, "A Fault Diagnostic Method for Position Sensor of Switched Reluctance Wind Turbine Generators," *Journal of Electrical Engineering & Technology*. vol. 11, no. 1, Jan. 2016.

[5] X. Liu, **C. Wang,** and Z. Chen, "Characteristics Analysis of an Excitation Assistance Switched Reluctance Wind Power Generator," *IEEE Transactions on Magnetics.* vol. 51, no. 11, Nov. 2015.

[6] **C. Wang**, M. D. Prieto, L. Romeral, Z. Chen, and F. Blaabjerg, "Incipient Fault Detection of Wind Turbine Gearboxes Based on Nonlinear Dimensionality Reduction," *IEEE Transactions on Industrial Electronics.* (submitted)

[7] **C. Wang** and Z. Chen, "Health Monitoring and Fault Diagnostics of Wind Turbines, A Review" *IEEE Transactions on Energy Conversion.* (submitted)

Selected conference papers

[1] **C. Wang**, X. Liu, and Z. Chen, "Rotor Position Estimation for Switched Reluctance Wind Generator Using Extreme Learning Machine," *Proceedings of International Conference on Wind Energy Grid-adaptive Technologies*, Oct. 2014, pp. 1–6.

[2] **C. Wang**, X. Liu, and Z. Chen, "A New Inductive Sensor for Online Health Monitoring of Mechanical Transmission Systems," *Proceedings of the 2015 IEEE Magnetics Conference (INTERMAG), May 2015*, pp: CT–10.

[3] **C. Wang**, H. Liu, X. Liu, X. Zhang, and Z. Chen, "A Sensor-less Method for Online Thermal Monitoring of Switched Reluctance Machine," *Proceedings of 18th International Conference on Electrical Machines and Systems (ICEMS 2015)*, Oct. 2015, pp.1709–1715.

[4] **C. Wang**, H. Liu, X. Liu, and Z. Chen, "A New Oil Debris Sensor for Online Condition Monitoring of Wind Turbine Gearboxes," *Proceedings of European Wind Energy Association Annual Event (EWEA 2015), Nov. 2015*, pp. 1–6.

[5] **C. Wang**, X. Liu, and Z. Chen, "Intelligent fault diagnosis and prognosis for wind turbine generators" presented at *Annual Conference of the Prognostics and Health Management Society - Doctoral Symposium, Oct. 2014*, pp. 1–3.

BIBLIOGRAPHY

[1] GWEC Global Wind Statistics 2015, available: http://www.gwec.net/wp-content/uploads/vip/GWEC-PRstats-2015_LR.pdf. Accessible on 11 Feb. 2016.

[2] Global Wind Energy Outlook 2014, available: http://www.gwec.net/wp-content/uploads/2014/10/GWEO2014_WEB.pdf. Accessible on 1 Dec. 2015.

[3] Wind in Numbers, available: http://www.gwec.net/global-figures/wind-in-numbers/. Accessible on 1 Dec. 2015.

[4] https://www.flickr.com/photos/laurenfortes/11304921953, accessible on 1 Dec. 2015.

[5] BBC news, available: http://www.bbc.com/news/uk-northern-ireland-30671607, accessible on 1 Dec. 2015.

[6] BBC news, available: http://www.bbc.com/news/uk-northern-ireland-31455666, accessible on 1 Dec. 2015.

[7] http://www.downvids.net/sublette-turbine-fire-kimberly-watley-video-644536.html, accessible on 1 Dec. 2015.

[8] http://sverigesradio.se/sida/artikel.aspx?programid=2054&artikel=6333744, accessible on 11 Feb. 2016.

[9] C. J. Crabtree, Y. Feng, and P. J. Tavner, "Detecting Incipient Wind Turbine Gearbox Failure: A Signal Analysis Method for Online Condition Monitoring," in *Proc. Euro. Wind Energy Conf.*, Apr. 2010.

[10] B. Meadows, "Offshore Wind O&M Challenges," presented in 2011 Wind Turbine Condition Monitoring Workshop, Broomfield, CO, USA, September 19−21, 2011.

[11] "Operations Report 2008," Noordzee Wind, Netherland, Tech. Rep. OWEZ_R_000_20090807, Aug. 2009.

[12] "Operations Report 2009," Noordzee Wind, Netherland, Tech. Rep. OWEZ_R_000_20101112, Nov. 2010.

[13] W. Musial and B. Ram, "Large-scale offshore wind power in the United States: Assessment of opportunities and barriers," Technical Report, National Renewable Energy Laboratory, CO, USA, Sept. 2010,

[14] T.W. Verbruggen, "Wind turbine operation & maintenance based on condition monitoring," Final Report, Energy Research Center of the Netherlands (ECN), April 2003.

[15] D. McMillan and G. W. Ault, "Quantification of condition monitoring benefit for offshore wind turbines," *Wind Eng.*, vol. 31, no. 4, pp. 267–285, 2007.

[16] "Wind Turbine Operations and Maintenance Market, by Application - Global Industry Analysis, Size, Share, Growth Trends and Forecast 2015 – 2023," Report by Transparency Market Research, NY, USA, 2015.

[17] C. J. Crabtree, D. Zappala, and P. J. Tavner, "Survey of commercially available condition monitoring systems for wind turbines," Technical Report. Durham University School of Engineering and Computing Sciences

and the SUPERGEN Wind Energy Technologies Consortium, Durham, UK, 2014.

[18] Y. Amirat, BenbouzidMEH, AlAhmarE, BensakerB, TurriS. Abriefstatuson, "A brief status on condition monitoring and fault diagnosis in wind energy conversion systems," *Renew. Sustain. Energy Rev.*, vol. 13, no. 9, pp. 2629–2636, 2009.

[19] B. Lu, Y. Li, X. Wu, and Z. Yang, "A review of recent advances in wind turbine condition monitoring and fault diagnosis," in *Proc. IEEE Symp. Power Electron. Mach. Wind Appl.*, Lincoln, NE, USA, Jun. 2009, pp.1–7.

[20] Z. Daneshi-Far, G. A. Capolino, H. Henao, "Review of Failures and Condition Monitoring in Wind Turbine Generators", in *Proc. XIX International Conference on Electrical Machines - ICEM 2010*, Sep. 2010, pp. 1–6.

[21] C. J. Crabtree, D. Zappalá, P. J. Tavner, "Survey of commercially available condition monitoring systems for wind turbines," Technical report, Durham University School of Engineering and Computing Sciences and the SUPERGEN Wind Energy Technologies Consortium, 2014.

[22] B. Chen, D. Zappalá, C. J. Crabtree, P. J. Tavner, "Survey of commercially available SCADA data analysis tools for wind turbine health monitoring," Technical report, Durham University School of Engineering and Computing Sciences, 2014.

[23] W. Qiao and D. Lu, "A survey on wind turbine condition monitoring and fault diagnosis-part I: Components and subsystems," *IEEE Trans. Ind. Electron.*, vol. 62, no. 10, pp. 6536–6545, Oct. 2015.

[24] W. Qiao and D. Lu, "A survey on wind turbine condition monitoring and fault diagnosis-part II: Signals and signal processing methods," *IEEE Trans. Industrial Electronics*, vol. 62, no. 10, pp. 6546–6557, Oct. 2015.

[25] W. X. Yang, P. J. Tavner, C. J. Crabtree, Y. Feng, and Y. Qiu, "Wind turbine condition monitoring: Technical and commercial challenges," *Wind Energy*, vol. 17, no. 5, pp. 673–693, May 2014.

[26] P. Takoutsing, R. Wamkeue, M. Ouhrouche, et al., "Wind turbine condition monitoring: state-of-the-art review, new trends, and future challenges," *Energies*, vol. 7, no. 4, pp. 2595–2630, Apr. 2014.

[27] Z. Hameed, Y. S. Hong, Y. M. Cho, S. H. Ahn, and C. K. Song, "Condition monitoring and fault detection of wind turbines and related algorithms: A review," *Renew. Sustain. Energy Rev.*, vol. 13, no. 1, pp. 1–39, Jan. 2009.

[28] H. D. M. de Azevedo, A. M. Araújo, and N. Bouchonneau, "A review of wind turbine bearing condition monitoring: State of the art and challenges," *Renew. Sustain. Energy Rev.,* vol. 56, no. 1, pp. 368–379. Apr. 2016.

[29] F. Garcia-Marquez, A. Tobias, J. Pinar-Perez, and M. Papaelias, "Condition monitoring of wind turbines: Techniques and methods," *Renew. Energy*, vol. 46, pp. 169–178, Oct. 2012.

[30] S. T. Kandukuri, A. Klausen, H. Reza Karimi, and K.G. Robbersmyr, "A review of diagnostics and prognostics of low-speed machinery towards wind turbine farm-level health management," *Renew. Sustain. Energy Rev.*, vol. 53, no. 1, pp. 697–708. Jan. 2016.

[31] Z. Zhang, A. Verma, and A. Kusiak, "Fault analysis and condition monitoring of the wind turbine gearbox," *IEEE Trans. Energy Convers.*, vol. 27, no. 2, pp. 526–535, Jun. 2012.
[32] W. Y. Liu, B. P. Tang, J. G. Han, et al., "The structure healthy condition monitoring and fault diagnosis methods in wind turbines: A review," *Renew. Sustain. Energy Rev*., vol. 44, no. 1, pp. 466–472, Apr. 2015.
[33] M. L. Wymore, J. E. V. Dam, H. Ceylan, and D. Qiao, "A survey of health monitoring systems for wind turbines," *Renew. Sustain. Energy Rev*., vol. 52, no. 1, pp. 976–990, Dec. 2015.
[34] C. C. Ciang, J. R. Lee, and H. J. Bang, "Structural health monitoring for a wind turbine system: A review of damage detection methods," *Meas. Sci. Technol.*, vol. 19, no. 12, pp. 1–20, Dec. 2008.
[35] B. F. Sorensen *et al.*, "Fundamentals for remote structural health monitoring of wind turbine blades—A preproject," Riso Nat. Lab., Roskilde, Denmark, Tech. Rep. Risø-R-1336(EN), May 2002.
[36] T. Bouno, T. Yuji, T. Hamada, and T. Hideaki, "Failure forecast diagnosis of small wind turbine using acoustic emission sensor," *KIEE Int. Trans. Elect. Mach. Energy Convers. Syst.*, vol. 5-B, no. 1, pp. 78–83, Jun. 2005.
[37] A. G. Beattie, M. Rumsey, "Non-Destructive Evaluation of Wind Turbine Blades Using an Infrared Camera," SAND98-2824C, Sandia National Laboratory: Albuquerque, NM, USA, 1998.
[38] P. Guo, D. Infield, and X. Yang, "Wind turbine generator condition monitoring using temperature trend analysis," *IEEE Trans. Sustain. Energy*, vol. 3, no. 1, pp. 124–133, Jan. 2012.
[39] G. Aranguren, P. M. Monje, V. Cokonaj, E. Barrera, and M. Ruiz, "Ultrasonic wave-based structural health monitoring embedded instrument," *Rev. Sci. Instrum.*, vol. 84, no. 12, 2013, Art. ID. 125106.
[40] T. E. Michaels and J. E. Michaels, "Application of acoustic wavefield imaging to non-contact ultrasonic inspection of bonded components," *Rev. Quant. Nondestr. Eval.* vol. 820, no. 25, pp. 1484–1491, Aug. 2006.
[41] N. Takeda, "Characterization of microscopic damage in composite laminates and real -time monitoring by embedded optical fiber sensors," *Int. J. Fatigue,* vol. 24, no. 1, pp. 281–291, 2002.
[42] K.-Y. Oh, J.-Y. Park, J.-S. Lee, B. I. Epureanu, and J.-K. Lee, "A novel method and its field tests for monitoring and diagnosing blade health for wind turbines," *IEEE Trans. Instrum. Meas.*, vol. 64, no. 6, pp. 1726–1733, Jan. 2015.
[43] X. Gong and W. Qiao, "Imbalance fault detection of direct-drive wind turbines using generator current signals," *IEEE Trans. Energy Convers.*, vol. 27, no. 2, pp. 468–476, Jun. 2012.
[44] X. Gong and W. Qiao, "Current-based mechanical fault detection for direct drive wind turbines via synchronous sampling and impulse detection," *IEEE Trans. Ind. Electron.*, vol. 62, no. 3, pp. 1693–1702, Mar. 2015.
[45] N. M. A. Freire, J. O. Estima, and A. J. M. Cardoso, "Open-circuit fault diagnosis in PMSG drives for wind turbine application," *IEEE Trans. Ind. Electron.*, vol. 60, no. 9, pp. 3957–3967, Sep. 2013.

[46] J. Hang, J. Zhang, M. Cheng, and J. Huang, "Online interturn fault diagnosis of permanent magnet synchronous machine using zero-sequence components," *IEEE Trans. Power Electron.*, vol. 30, no. 12, pp. 6731–6741, Dec. 2015.

[47] D. C. Seo and J. J. Lee, "Damage detection of CFRP laminates using electrical resistance measurement and neural network," *Compos. Struct.* Vol. 47, no. 1–4, pp. 525–530, Dec. 1999.

[48] A. Todoroki, M. Tanaka, and Y. Shimamura, "Electrical resistance change method for monitoring delaminations of CFRP laminates effect of spacing between electrodes," *Compos. Sci. Technol.,* vol. 65, no. 1, pp. 37–46, 2005.

[49] P. Sendrup, "Fundamentals for remote structural health monitoring of wind turbine blades—A preproject: Annex C—Fiber transducer for damage detection in adhesive layers of wind turbine blades," Riso Nat. Lab., Roskilde, Denmark, Tech. Rep. Risø-R-1342(EN), May 2002.

[50] X. E. Gros, "An eddy current approach to the detection of damage caused by low-energy impacts on carbon fibre reinforced materials," *Mater. Design,* vol. 16, no. 3, pp.167–173, Dec. 1995.

[51] J. Zhu, J. M. Yoon, D. He, and E. Bechhoefer, "Online particle contaminated lubrication oil condition monitoring and remaining useful life prediction for wind turbines," *Wind Energy*, vol. 18, no. 6, pp. 1131–1149, Jun. 2015.

[52] J. Zhu, J. M. Yoon, D. He, Y. Qu, and E. Bechhoefer, "Lubrication oil condition monitoring and remaining useful life prediction with particle filtering," *Int. J. Prognosis Health Manage.*, vol. 4, pp. 2–6, Jul. 2013.

[53] C. Wang, X. Liu, and Z. Chen, "Probe Improvement of Inductive Sensor for Online Health Monitoring of Mechanical Transmission Systems," *IEEE Transactions on Magnetics,* vol. 51, no. 11, pp. 1–4, Nov. 2015.

[54] M.A. Abd-Allah, A. Said, and Mahmoud N. Ali, "A novel lightning protection technique of wind turbine components," *The Journal of Engineering*, vol. 1, no. 1, pp. 1–6. Dec. 2015.

[55] M. Froese, "Making the case for wind-turbine fire detection and suppression systems," available: http://www.windpowerengineering.com/maintenance/safety/making-the-case-for-wind-turbine-fire-detection-and-suppression-systems/, accessible on 31 Dec. 2015.

[56] A. Zaher, S. D. J. McArthur, D. G. Infield, and Y. Patel, "Online wind turbine fault detection through automated SCADA data analysis," *Wind Energy*, vol. 12, no. 6, pp. 574–593, Sep. 2009.

[57] H. Long, L. Wang, Z. Zhang, Z. Song, and J. Xu, "Data-driven wind turbine power generation performance monitoring," *IEEE Trans. Ind. Electron.*, vol. 62, no. 10, pp. 6627–6635, Oct. 2015.

[58] S. J. Watson, B. J. Xiang, W. Yang, P. J. Tavner, and C. J. Crabtree, "Condition Monitoring of the Power Output of Wind Turbine Generators Using Wavelets," *IEEE Trans. Energy Convers.*, vol. 25, no. 3, pp. 715–721, Sept. 2010.

[59] W. Yang, P. J. Tavner, C. J. Crabtree, and M. Wilkinson, "Cost-Effective Condition Monitoring for Wind Turbines," *IEEE Trans. Ind. Electron.*, vol. 57, no. 1, pp. 263–271, Jan. 2010.

[60] R. Isermann, "Model-based fault-detection and diagnosis—Status and applications," *Annu. Rev. Control*, vol. 29, no. 1, pp. 71–85, Jan. 2005.

[61] R. Isermann, "Trends in the application of model-based fault detection and diagnosis of technical processes," *Control Eng. Pract.*, vol. 5, no. 5, pp. 709–719, May 1997.

[62] K. Rothenhagen and F. W. Fuchs, "Doubly Fed Induction Generator Model-Based Sensor Fault Detection and Control Loop Reconfiguration," *IEEE Trans. Ind. Electron.*, vol. 56, no. 10, pp. 4229–4238, Oct. 2009.

[63] H. T. Do and H. Chafouk, "Fault detection and isolation using Kalman filter bank for a wind turbine generator," *Proc. of 19th Mediterranean Conf. on Control & Automation (MED)*, 20-23 Jun. 2011, pp.144–149.

[64] P. Odgaard, J. Stoustrup, and M. Kinnaert, "Fault Tolerant Control of Wind Turbines – a benchmark model," in *Proc. 7th IFAC Symp. on Fault Detection, Supervision and Safety of Technical Processes*, 2009, pp. 155–160.

[65] P. Odgaard, J. Stoustrup, and M. Kinnaert, "Fault-tolerant control of wind turbines: A benchmark model," *IEEE Trans. Control Syst. Technol.*, vol. 21, no. 4, pp. 1168–1182, Jul. 2013.

[66] N. Laouti, N. Othman, and S. Othman, "Support Vector Machines for Fault Detection in Wind Turbines," in *Proc. IFAC World Congress*, 2011, pp. 7067–7072.

[67] W. Chen, S. Ding, A. Sari, A. Naik, A. Khan, and S. Yin, "Observer-based FDI Schemes for Wind Turbine Benchmark," in *Proc. of IFAC World Congress*, 2011, pp. 7073–7078.

[68] H. Sanchez, T. Escobet, V. Puig, and P. Odgaard, "Fault diagnosis of an advanced wind turbine benchmark using interval-based ARRs and observers," *IEEE Trans. Ind. Electron.*, vol. 62, no. 6, pp. 3783–3793, Jun. 2015.

[69] W. Yang, P. J. Tavner, C. J. Crabtree, and M. Wilkinson, "Cost-Effective Condition Monitoring for Wind Turbines," *IEEE Trans. on Indus. Electron.*, vol. 57, no. 1, pp. 263–271, Jan. 2010.

[70] S. J. Watson, B. J. Xiang, W. Yang, P. J. Tavner, and C. J. Crabtree, "Condition Monitoring of the Power Output of Wind Turbine Generators Using Wavelets," *IEEE Trans. on Energy Conversion*, vol. 25, no. 3, pp. 715–721, Sept. 2010.

[71] W. Yang, R. Court, P. J. Tavner, and C. J. Crabtree, "Bivariate empirical mode decomposition and its contribution to wind turbine condition monitoring," *Journal of Sound and Vibration*, vol. 330, no. 15, pp. 3766–3782, Jul. 2011.

[72] C. Wang, X. Liu and Z. Chen, "Incipient Stator Insulation Fault Detection of Permanent Magnet Synchronous Wind Generators Based on Hilbert–Huang Transformation," *IEEE Transactions on Magnetics*, vol. 50, no. 11, pp. 1–4, Nov. 2014.

[73] C. Wang, M. D. Prieto, L. Romeral, Z. Chen, F. Blaabjerg and X. Liu, "Detection of Partial Demagnetization Fault in PMSMs Operating under Nonstationary Conditions," *IEEE Transactions on Magnetics.* vol. 52, no. 7, pp. 1–4, Jul. 2016.

[74] S. Yang, W. Li, and C. Wang, "The intelligent fault diagnosis of wind turbine gearbox based on artificial neural network," in *Proc. of Int. Conf. on CMD*, 2008, pp. 1327–1330.

[75] X. Zhang, S. he, P. Zhou, and W. Wang, "Summerization and study of fault diagnosis technology of the main components of wind turbine generator system," in *Proc. of IEEE ICSET*, 2008, pp. 1223–1226.

[76] X. An, D. Jiang, and S. Li, "Application of back propagation neural network to fault diagnosis of direct-drive wind turbine," in *Proc. of World Non-Grid-Connected Wind Power and Energy Conf.*, 2010, pp. 1–5.

[77] L. Ju, D. Song, B. Shi, and Q. Zhao, "Fault predictive diagnosis of wind turbine based on LM arithmetic of Artificial Neural Network theory," *in Proc. of 7th Int. Conf. on Natural Computation*, 2011, pp. 575–579.

[78] H. Guo and B. Wu, "Fault diagnosis of wind turbine power electronic equipment based on SOM neural network," *in Proc. of 7th Int. Conf. on Natural Computation,* 2010, pp. 1679–1681.

[79] Y. Li, G. Li, and J. Yan, "Fault Diagnosis of Wind Turbine Blades Based on Fuzzy Theory," in *Proc. of Int. Conf. Control, Automation and Systems Engineering*, 2011, pp. 1–3.

[80] Z. Chen, X. Lian, H. Yu, and Z. Bao, "Algorithm of Data Mining and its Application in Fault Diagnosis for Wind Turbine," in *Proc. of 2th Int. Symp. Knowledge Acquisition and Modeling*, 2009, pp. 240–243.

[81] A. S. Zaher and S. D. J. McArthur, "A Multi-Agent Fault Detection System for Wind Turbine Defect Recognition and Diagnosis," *IEEE Power Tech.*, 2007, pp. 22–27.

[82] A. Kusiak and A. Verma, "A Data-Mining Approach to Monitoring Wind Turbines," *IEEE Trans. Sustain. Energy*, vol. 3, no. 1, pp.150–157, Jan. 2012.

[83] X. Gong, W. Qiao, and W. Zhou, "Incipient bearing fault detection via wind generator stator current and wavelet filter," in *Proc. of IEEE IECON, 2010*, pp. 2615–2620.

[84] X. Gong and W. Qiao, "Bearing fault detection for direct-drive wind turbines via stator current spectrum analysis," in *Proc. of IEEE ECCE, 2011*, pp. 313–318.

[85] Z. Chen, J.M Guerrero, and F. Blaabjerg, "A Review of the State of the Art of Power Electronics for Wind Turbines," *IEEE Trans. Power Electron.*, vol. 24, no. 8, pp. 1859–1875, 2009.

[86] F. Blaabjerg, Z. Chen, and S. B. Kjaer, "Power electronics as efficient interface in dispersed power generation systems," *IEEE Trans. Power Electron.,* vol. 19, no. 5, pp. 1184–1194, Sept. 2004.

[87] P. Duan, K. Xie, L. Zhang, and X. Rong, "Open-Switch Fault Diagnosis and System Reconfiguration of Doubly fed Wind Power Converter Used in a Microgrid," *IEEE Trans. on Power Electron.*, vol. 26, no. 3, pp. 816–821,

Mar. 2011.

[88] N. M. Freire, J. O. Estima, and A. J. Cardoso, "Converters fault-diagnosis in PMSG drives for wind turbine applications," in *Proc. of IEEE IECON*, 2010, pp. 403–408.

[89] Z. Wang and Q. Guo, "The Diagnosis Method for Converter Fault of the Variable Speed Wind Turbine Based on the Neural Networks," in *Proc. of 2th Int. Conf. Innovative Computing, Information and Control*, 2007, pp. 615–618.

[90] Q. Duan, L. Zhang, and L. Zhang, "A fault detection and tolerant scheme for back-to-back converters in DFIG-based wind power generation systems," in *Proc. of 3th Int. Conf. Advanced Computer Theory and Engineering*, 2010, pp. 95– 99.

[91] P. F. Odgaard, P. B. Thøgersen, and J. Stoustrup, "Fault isolation in parallel coupled wind turbine converters," in *Proc. of 3th Int. Conf. Control Applications*, 2010, pp. 1069–1072.

[92] C. M. Stephens, "Fault detection and management system for fault-tolerant switched reluctance motor drives," *IEEE Trans. Ind. Appl.*, vol. 27, no. 6, pp. 1098–1102, Nov./Dec. 1991.

[93] I. Husain, A. Radun, and J. Nairus, "Fault analysis and excitation requirements for switched reluctance-generators," *IEEE Trans. Energy Convers.*, vol. 17, no. 1, pp. 67–72, Mar. 2002.

CHAPTER 2. ONLINE HEALTH MONITORING OF WIND TURBINE GEARBOXES[1]

Metal debris in lubricating oil contains abundant information regarding the ageing and wear/damage of WT gearboxes. The health condition of the lubricated WT gearboxes can be indicated by the concentration and size of the metal abrasive particles, which may provide very early warnings of faults/failures and benefit the condition based maintenance of WTs. A new inductive sensor which uses saddle-coil probe to generate a uniform magnetic field for performance improvement on the metal particle detection is proposed in this chapter. The detailed geometry and the performance analysis are presented by using finite element analysis. The results demonstrate that the proposed saddle-coil inductive sensor possesses good identification ability of recognizing the ferromagnetic and non-ferromagnetic oil debris particles whose diameters are as small as 100 μm.

2.1. INTRODUCTION

Gearbox, which is a crucial subsystem in many WTs, causes the longest downtime per failure as mentioned in section 1.1. Meanwhile, the unscheduled replacement cost of the faulty WT gearbox is extremely high. Online HM is an effective means to ensure the availability and reduce the maintenance cost of WTs.

As modern WTs frequently change the operating mode according to the wind and grid conditions, WT gearboxes suffer severe transient loadings during start, shutdown and abnormal grid connections (low or high voltage ride through) [1]. The extreme loads may accelerate the degradation and damage of bearing and gear which are the crucial components of a WT gearbox. Most of WT gearbox failures result from the faults of bearing and gear. There are many different wear and damage patterns of these two critical components. Common bearing damages in WT gearboxes are demonstrated in Fig. 2.1, Fig. 2.1 (a) presents the crack fault of the intermediate bearing, Fig. 2.1 (b) shows the macro pitting on rotor bearing. Similarly, the Fig. 2.2 displays the common gear faults in WT gearboxes. Scuffing

[1] This chapter is based on the paper which was originally published with following details. [C. Wang, X. Liu, and Z. Chen, "Probe Improvement of Inductive Sensor for Online Health Monitoring of Mechanical Transmission Systems," IEEE Transactions on Magnetics, vol. 51, no. 11, Nov. 2015], materials are reused with permission from IEEE. Copyright 2015, IEEE.

of the high-speed gear is shown in Fig. 2.2(a). Corrosion of the sun pinion is presented in Fig. 2.2 (b),

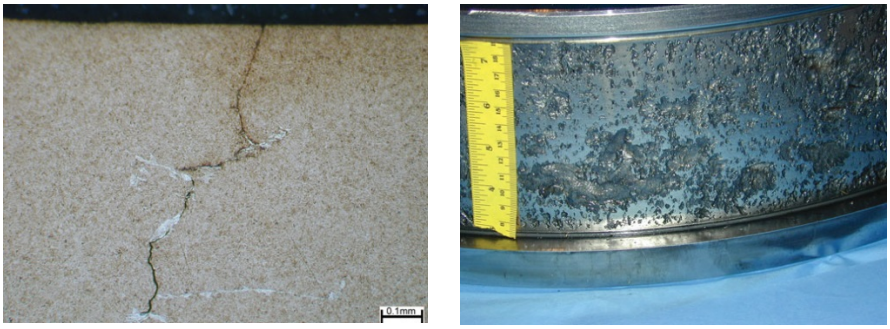

(a) (b)

Fig. 2.1. Common bearing damages in WT gearboxes, (a) Axial crack on the intermediate bearing, (b) Macro pitting on rotor bearing [2]. Reproduced with permission from [R. Errichello, R. Budny, and R. Eckert, "Investigations of Bearing Failures Associated with White Etching Areas (WEAs) in Wind Turbine Gearboxes," Tribology Transactions, vol. 56, no. 6, pp.1069–1076, Jul. 2013.]. Copyright 2013, Taylor & Francis.

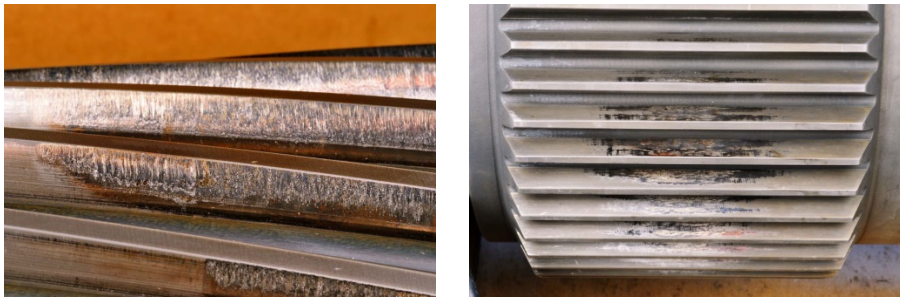

(a) (b)

Fig. 2.2. Common gear damages in WT gearboxes, (a) Scuffing of the high-speed gear, (b) Corrosion of the sun pinion [2]. Reproduced with permission from [R. Errichello, R. Budny, and R. Eckert, "Investigations of Bearing Failures Associated with White Etching Areas (WEAs) in Wind Turbine Gearboxes," Tribology Transactions, vol. 56, no. 6, pp.1069–1076, Jul. 2013.]. Copyright 2013, Taylor & Francis.

There are many different HM methods for the WT gearboxes including vibration monitoring, acoustic monitoring, oil monitoring and current monitoring as concluded in section 1.2. The vibration based HM is the most popular approach in the wind industry applications, however, the very early faults could not be detected

using vibration based HM. Fault symptoms evolution with time is illustrated in Fig. 2.3. As we can see in this figure, after a fault occurs, there are many different symptoms over time such as oil debris, acoustic emission, vibration, noise, heat, smoke and eventually breakdown. The oil debris may come out very soon after the fault occurs, thus if this fault indicator could be detected and recognized, the fault can be detected in a very early stage.

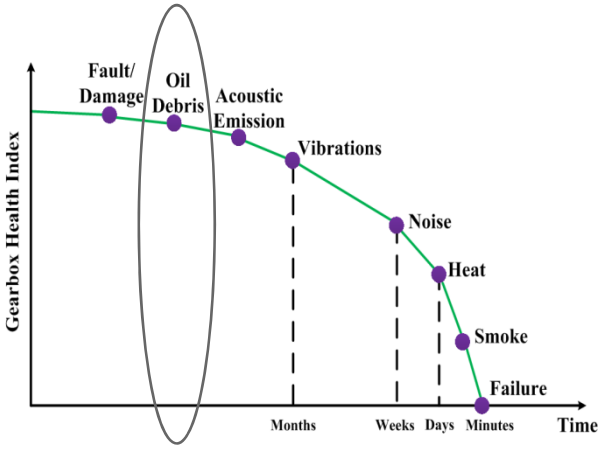

Fig. 2.3. Fault symptoms evolution with time.

Lubricating oil is the life blood of the WT gearboxes. “Blood test” is one of the most effective approaches to monitor the health and detect the incipient fault of WT gearbox. Metal debris in lubricating oil contains abundant information regarding the ageing and wear/damage of WT gearbox. The health condition of the WT gearbox can be indicated by the quantity and size of the metal abrasive particles, which may provide very early warnings of faults/failures and benefit the condition based maintenance of the system [3]. Fig. 2.4 illustrates the lubrication-oil circulating system of a WT gearbox. The step-up gearbox consists of one stage planetary gear and two stage parallel shaft gears. The inductive sensor can be implemented in the primary oil channel (as shown in Fig. 2.4) or bypass oil channel which is in parallel with the primary channel for the online HM.

Generally speaking, the quantity per volume of the oil metal debris indicates the ageing rate of the system, while the size presents the severity of the wear status. Particle diameter under 20μm implies normal wear condition of the system, diameter from 50 μm to 100 μm indicates the infancy failure of the system [4]. Conventional oil metal debris detection methods such as spectroscopic analysis and ferrographic analysis are costly and time consuming, which cannot be used for online monitoring. Optical oil debris sensor is susceptible by the color and transparency of the oil, while the acoustic sensor is susceptible by the vibration,

capacitive sensor can't recognize the ferromagnetic and non-ferromagnetic particles [4-5].

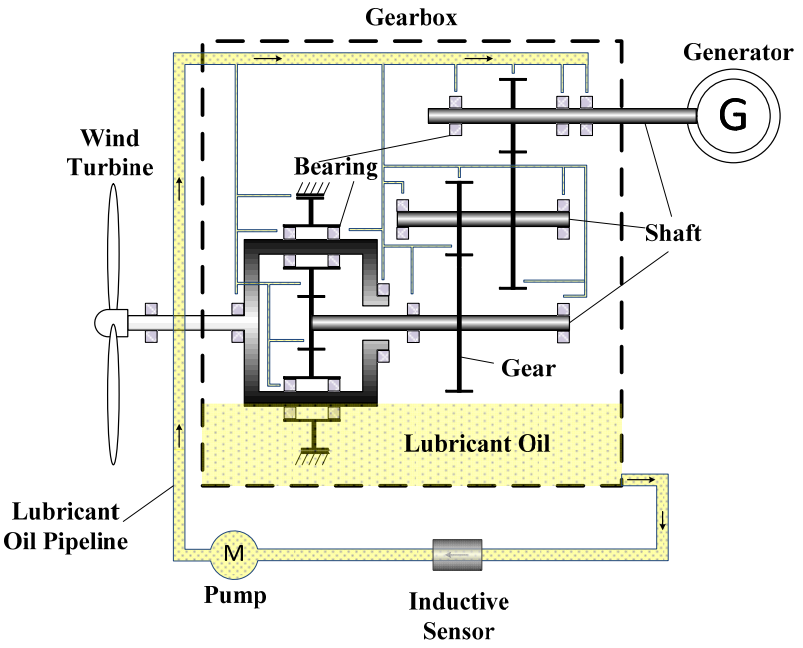

Fig. 2.4. The lubricating system of a WT gearbox.

Inductive sensor, which transforms the quantity per volume and size of the metal particles into the number and magnitude variation of pulses of coil inductance, is a good choice for the online health monitoring of mechanical transmission systems. It is low-cost, high-accuracy, robust and easy to install. Moreover, it can also distinguish between the ferromagnetic and non-ferromagnetic metal debris particles.

An inductive sensor with solenoid coil probe with excitation frequency of 10.06MHz is described in [5] for estimating the composition and size of the metal particles in a glass tube whose outer diameter is 6mm. The smallest detectable particles are diameter of 200μm for nonferrous and diameter of 100μm for ferrous particles. A high throughput inductive pulse sensor for online lubricating oil debris monitoring is presented in [6], the inner diameter of the oil tube is 1mm, two-layer planar coil is used in this study, the excitation frequency is 2MHz, the diameters of the tested particles in this paper is 75-105μm for ferromagnetic particles and 105-150μm for non-ferromagnetic particles. The oil debris sensor was first applied for the condition assessment of the Pratt & Whitney F119 engine for F22 fighter in 1990s [7]. Previous works on the inductive oil debris sensor using solenoid or

planar coils didn't take the diameter effect of such coils into consideration. The works have been done under the assumption that the magnetic field in the oil tube through which the particles pass is uniform. However, solenoid or planar coils which are used in references [4-9] around or inside the lubricating oil tubes could not provide uniform magnetic field, which may result in confused inductance variation output of the sensor. A debris particle passing the oil tube at different positions in the cross section may cause different inductance changes, which may results in detection errors.

Hence, a new inductive sensor which applies saddle coils to generate a uniform magnetic field for metal particle detection is proposed in this chapter, aiming at eliminating the diameter effect and improving the performance of the oil debris detection sensor. The remaining parts of this chapter are arranged as follows, section 2.2 describes the principle of inductive sensor, the uniformity of magnetic field produced by the proposed saddle coil probe is presented in the section 2.3, in section 2.4, the performance of the proposed inductive sensor is simulated and verified by Finite Element Analysis, section 2.5 concludes this chapter.

2.2. PRINCIPLE OF INDUCTIVE OIL DEBRIS SENSOR

2.2.1. PRINCIPLE

The schematic diagram of the inductive oil debris sensor is depicted in Fig. 2.5, when the non-ferromagnetic particle passes the alternated magnetic field together with the oil flow inside the lubricating oil tube, the magnetic field generated by the coil will be weakened (the red lines in Fig. 2.5) owing to the eddy current damping effects. Thus the inductance of the coil in the probe will decrease. During the non-ferromagnetic particle passing through the alternated magnetic field, a negative polarity pulse will be produced on the inductance of the coil. While if a ferromagnetic particle moves across the magnetic field in the oil tube, the magnetic permeability effect of ferromagnetic material and eddy current effect of metallic material are superimposed. Due to the higher permeability of ferromagnetic particle, the magnetic field can be strengthened (purple lines in Fig. 2.5(b)) which results in an increase of the coil inductance. Meanwhile, the eddy current will also be generated inside or on the surface of the ferromagnetic particles dependent on the excitation frequency, which decreases the coil inductance.

If the excitation frequency is set appropriately, the ferromagnetic particle would generate a positive polarity pulse on the inductance when it passes through the magnetic field, thus the ferromagnetic particles and non-ferromagnetic particles can be distinguished by the polarity of the inductance pulses. The quantity and size of the particles can also be identified by the number and amplitude of the pulses.

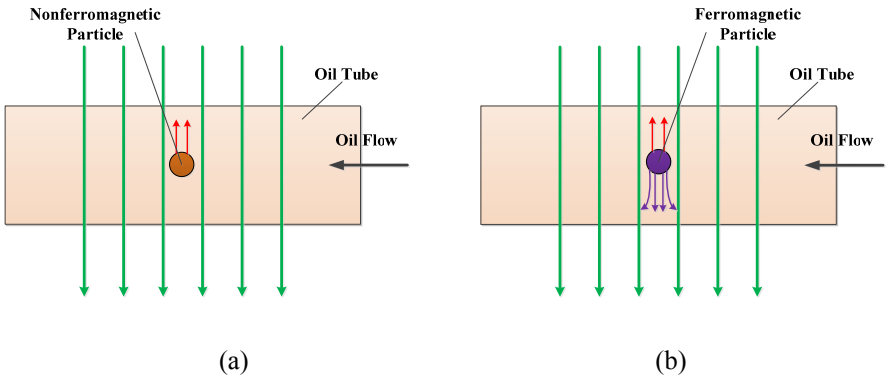

Fig. 2.5.The schematic diagram of the inductive sensor, (a) non-ferromagnetic particle, (b) ferromagnetic particle.

2.2.2. EQUIVALENT CIRCUIT MODEL

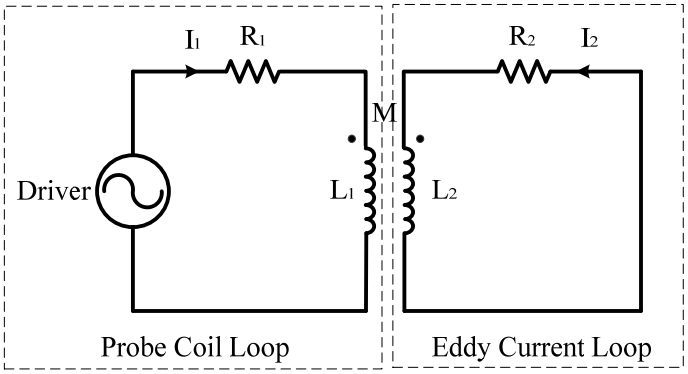

Fig. 2.6. The equivalent circuit model of the oil debris inductive sensor.

The presented inductive sensor can be modeled as a transformer with coupled primary and short circuited secondary windings. The equivalent lumped parameter circuit model of the oil debris inductive sensor is illustrated in Fig. 2.6. The primary winding is the probe coil loop, while the secondary winding is the eddy current loop. Instead of a high permeable ferromagnetic core in a typical transformer, the core material in this inductive oil debris sensor equivalent transformer is air. Thus the coupling factor between the primary and the secondary winding is much smaller than the typical transformer. The equivalent transformer has a leaky and incompact coupling of its two windings. When there is no particle passing through the oil debris sensor, the L_2 in the secondary winding can be viewed as zero which means the secondary coil has nothing to do with the primary winding in this case. If a

ferromagnetic particle passes through the oil debris inductive sensor, the model can be regarded as an air core transformer with an additional small ferromagnetic core.

The voltage equations of the primary and secondary windings are,

$$\dot{U}_1 = R_1\dot{I}_1 + j\omega L_1\dot{I}_1 - j\omega M\dot{I}_2 \tag{2.1}$$

$$0 = R_2\dot{I}_2 + j\omega L_2\dot{I}_2 - j\omega M\dot{I}_1 \tag{2.2}$$

where $\dot{U}_1$, R_1, $\dot{I}_1$ and L_1 are the voltage, resistance, current and inductance in the primary winding, respectively. Driver is the AC power source of the probe, $\dot{I}_2$, R_2 and L_2 are the current, equivalent resistance and inductance of the secondary winding. M is the mutual inductance.

The equivalent impedance of the sensor probe Z can be obtained by solving the above two equations,

$$Z = \frac{\dot{U}_1}{\dot{I}_1} = R_1 + \frac{\omega^2 M^2}{R_2^2 + (\omega L_2)^2)}R_2 + j\left[\omega L_1 - \frac{\omega^2 M^2}{R_2^2 + (\omega L_2)^2)}\omega L_2\right] \tag{2.3}$$

Thus the equivalent inductance is

$$L = L_1 - \frac{\omega^2 M^2}{R_2^2 + (\omega L_2)^2)}L_2 \tag{2.4}$$

here formula (2.4) can be employed to explain the principle of the inductive sensor. The metallic particles exposed in the alternating magnetic field induce the last parts in (2.4) which leads to a decrease of L. On the other hand, the ferromagnetic particle would increase the self-inductance of L_1 which could enlarge the L.

2.3. SADDLE COIL PROBE

2.3.1. THE PROPOSED SADDLE COIL PROBE

Fig. 2.7 displays the geometry of the proposed saddle coil pair whose length diameter ratio and circular arcs are 2 and 120° respectively. This specific saddle coil pair can generate uniform stationary or alternating magnetic field and it has found applications in biomedical fields [10-11].

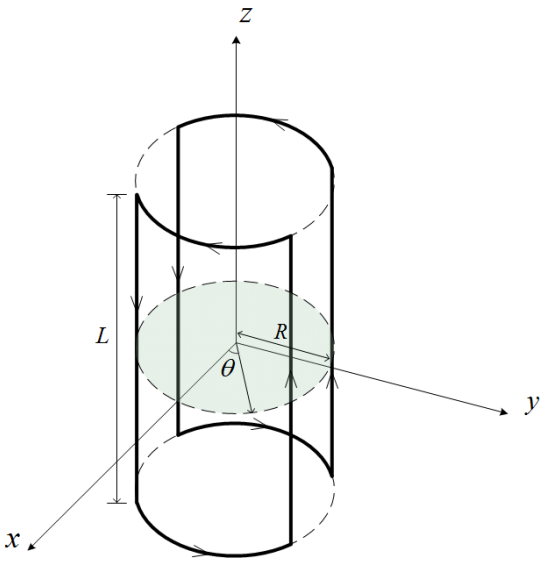

Fig. 2.7.The probe in Cartesian coordinate system.

2.3.2. MAGNETIC FIELD CALCULATION OF THE PROPOSED SADDLE COIL PROBE

According to Biot-Savart law, the magnetic flux density of any point $P(x_0, y_0, z_0)$ in the coordinate space can be calculated by,

$$\overrightarrow{dB} = \frac{\mu_0 I \overrightarrow{dL} \times \vec{r}}{4\pi r^3} \tag{2.5}$$

The magnetic field source consists of two broad parts, namely the coils in the upper and lower arcs and the four straight lines on the cylindrical shell. Thus the integral calculation of magnetic field can be divided into two parts for convenience.

For the upper and lower arcs,

$$\overrightarrow{dl_1} = (Rcos\theta, Rsin\theta, L/2)$$

$$\overrightarrow{r_1} = (x_0 - Rcos\theta, y_0 - Rsin\theta, z_0 - L/2)$$

$$\overrightarrow{dl_2} = (Rcos\theta, Rsin\theta, -L/2)$$

$$\overrightarrow{r_2} = (x_0 - Rcos\theta, y_0 - Rsin\theta, z_0 + L/2)$$

$$\overrightarrow{B_k} = \int_{-\frac{\pi}{3}}^{\frac{\pi}{3}} \frac{\mu_0 I}{4\pi} \frac{\overrightarrow{dl_k} \times \overrightarrow{r_k}}{{r_k}^3}\, d\theta + \int_{-\frac{5\pi}{6}}^{\frac{3\pi}{2}} \frac{\mu_0 I}{4\pi} \frac{\overrightarrow{dl_k} \times \overrightarrow{r_k}}{{r_k}^3}\, d\theta, k = 1, 2 \qquad (2.6)$$

For the four straight lines,

$$\overrightarrow{dl_3} = (\frac{R}{2}, -\sqrt{3}R/2, z)$$

$$\overrightarrow{r_3} = (x_0 - \frac{R}{2}, y_0 + \sqrt{3}R/2, z_0 - z)$$

$$\overrightarrow{dl_4} = (\frac{R}{2}, \sqrt{3}R/2, z)$$

$$\overrightarrow{r_4} = (x_0 - \frac{R}{2}, y_0 - \sqrt{3}R/2, z_0 - z)$$

$$\overrightarrow{dl_5} = (-\frac{R}{2}, -\sqrt{3}R/2, z)$$

$$\overrightarrow{r_5} = (x_0 + \frac{R}{2}, y_0 + \sqrt{3}R/2, z_0 - z)$$

$$\overrightarrow{dl_6} = (-\frac{R}{2}, \sqrt{3}R/2, z)$$

$$\overrightarrow{r_6} = (x_0 + \frac{R}{2}, y_0 - \sqrt{3}R/2, z_0 - z)$$

$$\overrightarrow{B_j} = \int_{-\frac{L}{2}}^{\frac{L}{2}} \frac{\mu_0 I}{4\pi} \frac{\overrightarrow{dl_j} \times \overrightarrow{r_j}}{{r_j}^3}\, d\theta, j = 3, 4, 5, 6 \qquad (2.7)$$

where,

$$r_{k(j)} = |\overrightarrow{r_{k(j)}}| \qquad (2.8)$$

2.4. PERFORMANCE OF THE PROPOSED OIL DEBRIS SENSOR

2.4.1. SIMULATION

The saddle coil oil debris sensor model is developed in Comsol Mutiphysics

environment.

Table 2.1
PARAMETERS OF THE STUDIED OIL DEBRIS SENSOR.

Parameter	Value
Excitation frequency	10MHz
Saddle coils diameter	1mm
Saddle coils length	2mm
Copper particle diameter	100 μm
Ferro particle diameter	100 μm
Excitation current density	$6.83 \times 10^6 \mathrm{A}/m^2$
Nominal inductance	7.1795nH

The materials of the ferromagnetic and non-ferromagnetic particles used in this study are iron and copper, respectively. The particles pass through the sensor along the positive direction of Z axis from different locations in XY plane. Three locations are studied in this paper, namely $\mathrm{r}/\mathrm{R} = 0$, $\mathrm{r}/\mathrm{R} = 0.5$, $\mathrm{r}/\mathrm{R} = -0.5$, where r is the perpendicular distance from the point to Z axis, R is the radius of the saddle coils.

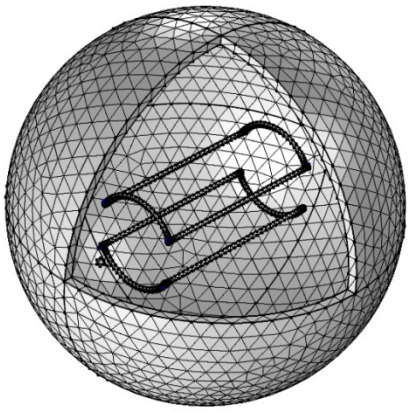

Fig. 2.8. Mesh of the saddle coil.

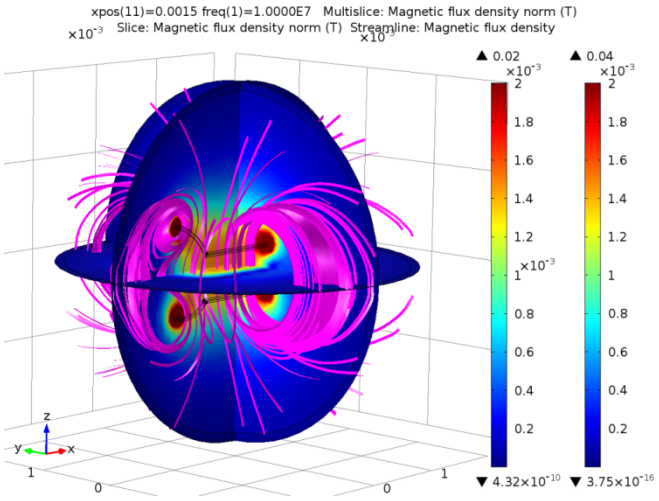

Fig. 2.9. Slice and streamline of the magnetic flux density.

Mesh of the saddle coil is shown in Fig. 2.8. Slice and streamline of the magnetic flux density is illustrated in Fig. 2.9. The magnetic flux density of the cross section and longitudinal surface of this saddle coil probe are shown in Fig. 2.10 and Fig. 2.11, respectively. As can be seen, the magnetic flux density in cross section along radius direction is nearly uniform in most regions except near the wires.

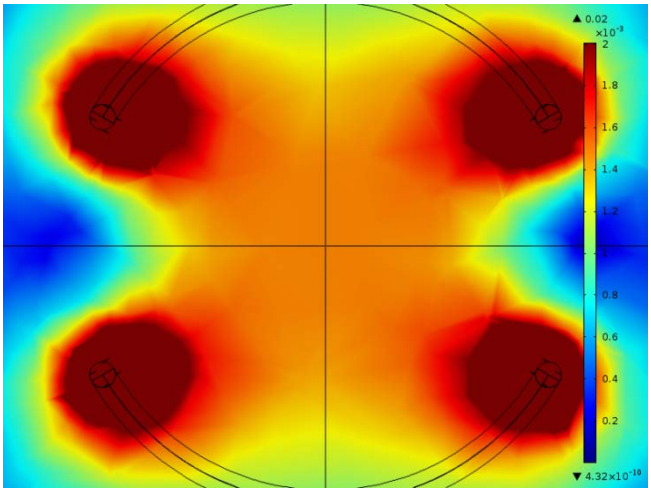

Fig. 2.10.The magnetic flux density of the cross section of saddle coil probe.

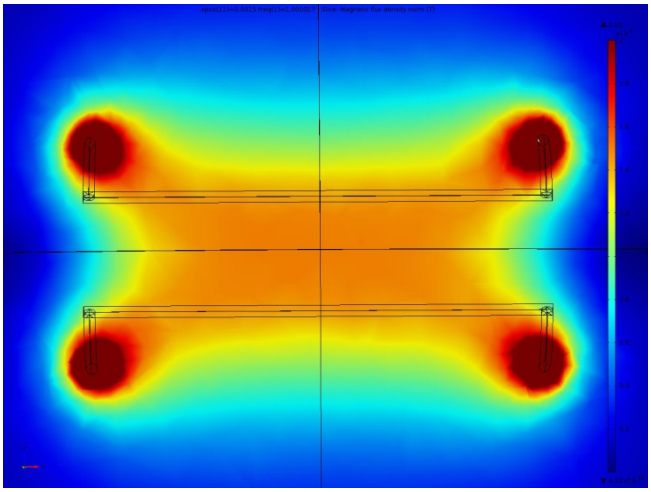

Fig. 2.11. The Magnetic flux density of longitudinal surface of the saddle coil probe.

2.4.2. RESULTS ANALYSIS

The Relative Inductance Variation (RIV) ΔL/Lversus excitation frequency when the 100μm-diameter Cu and Fe particles pass through the probe is demonstrated in Fig. 2.12.

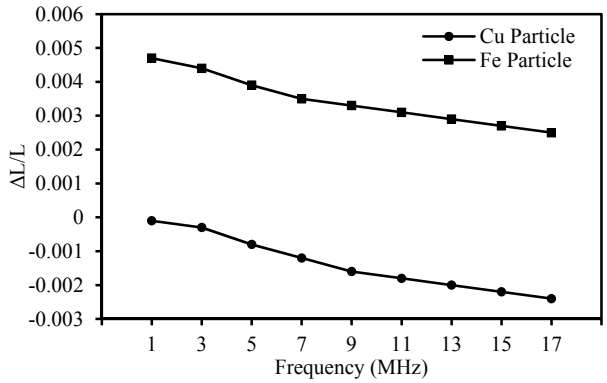

Fig. 2.12. The relative inductance variation versus excitation frequency.

It is observed that the RIVs induced by Cu and Fe particles are in different polarity. The absolute value of RIV (ARIV) caused by the Cu particle decrease with the increase of frequency, it is opposite for the Fe particle. The Cu particle is easy to be

detected with high excitation frequency, while low excitation frequency is favored for detection of the Fe particle. Thus 10MHz can be a compromised frequency in this study.

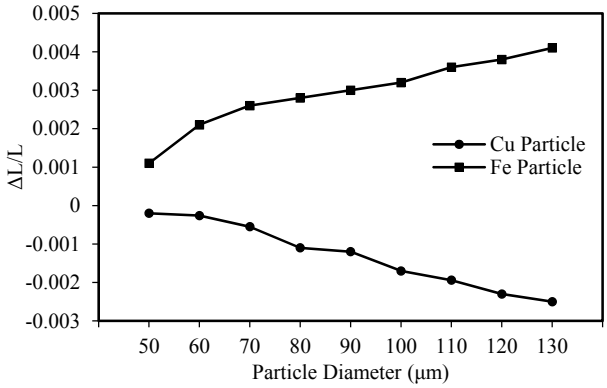

Fig. 2.13. The relative inductance variation versus particle diameter.

Fig. 2.13 depicts the RIV versus particle diameter with excitation frequency of 10MHz. The ARIVs for Cu and Fe particles are both increased with the enlargement of diameter. The RIV curves are nearly linear when the diameters are larger than 90 μm. The parameters of the studied oil debris sensor are shown in Tab. I.

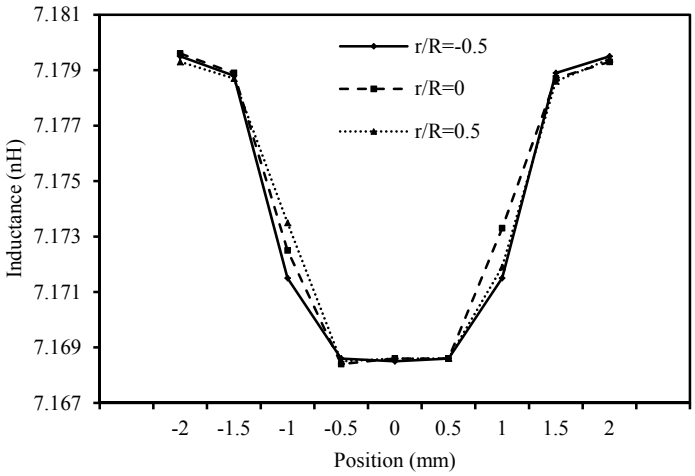

Fig. 2.14.The inductance of the saddle probe versus Z axis positions when non-ferromagnetic particle passes through the sensor from different locations in XY plane.

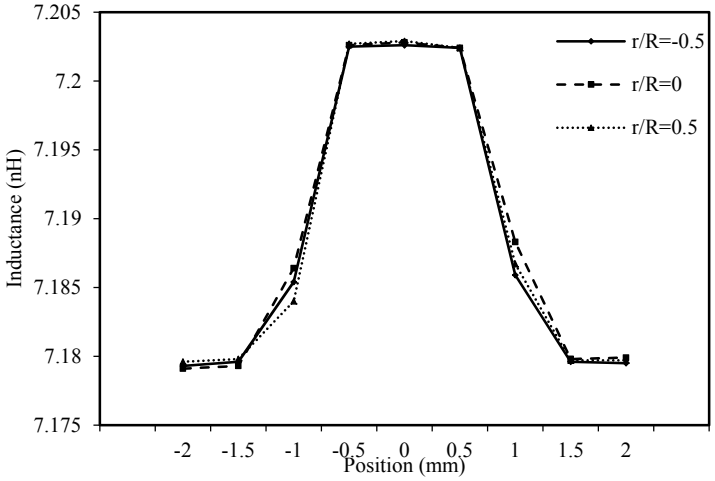

Fig. 2.15.The inductance of the saddle probe versus Z axis positions when ferromagnetic particle passes through the sensor from different locations in XY plane.

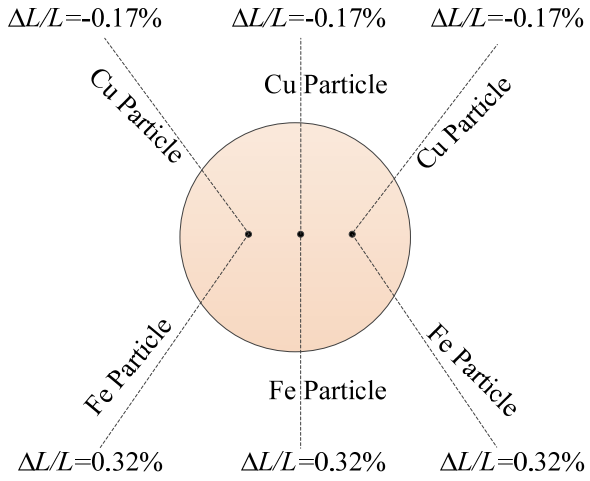

Fig. 2.16.The relative inductance variation of saddle coils at different locations in the cross section of the oil tube.

The inductance profiles of the saddle probe versus Z axis positions when non-ferromagnetic particle and ferromagnetic particles pass through the sensor from

different locations in XY plane are demonstrated in Fig. 2.14 and Fig. 2.15, respectively. As is presented in Fig. 2.16, the relative inductance variations of saddle coils $\Delta L/L$ at different locations in the cross section of the oil tube for Cu particle are all -0.17%, while for Fe particle, the relative inductance variation are all 0.32%, which verifies the theoretical analysis of the proposed inductive sensor.

2.5. SUMMARY

A new inductive sensor probe is proposed in this chapter for the online health monitoring of WT Gearboxes. The magnetic field homogeneity as well as the performance of the proposed saddle coil are analyzed and verified by finite element analysis. Future work will be the experimental verification of the proposed saddle coil probe. Although the proposed inductive sensor is used in 100 μm-diameter metallic particle detection, it can also find applications in the smaller size particle counting in biomedical engineering or larger particle identification in industry.

BIBLIOGRAPHY

[1] R. Errichello and J. Muller, "Gearbox Reliability Collaborative Gearbox 1 Failure Analysis Report," Nat. Renew. Energy Lab., Golden, CO, USA, Tech. Rep. NREL/TP-5000-54530, Feb. 2012.

[2] R. Errichello, R. Budny, and R. Eckert, "Investigations of Bearing Failures Associated with White Etching Areas (WEAs) in Wind Turbine Gearboxes," *Tribology Transactions*, vol. 56, no. 6, pp.1069–1076, Jul. 2013.

[3] J. Edmonds, M. S. Resner, and K. Shkarlet, "Detection of precursor wear debris in lubrication systems," in *Proc. IEEE Aerospace Conference*. Mar. 2000, pp. 73–77.

[4] L. Du, X. L. Zhu, Y. Han, L. Zhao, and J. Zhe, "Improving sensitivity of an inductive pulse sensor for detection of metallic wear debris in lubricants using parallel LC resonance method," *Measurement Science and Technology*, vol. 24, no. 7, pp. 1–10, Jul. 2013.

[5] K. W. Chambers, M. C. Arneson, and C. A. Waggoner, "On-line ferromagnetic wear debris sensor for machinery condition monitoring and failure detection," *Wear*, vol. 128, no. 3, pp. 325–337, Dec. 1988.

[6] L. Du and J. Zhe, "A high throughput inductive pulse sensor for online oil debris monitoring," *Tribology International*, vol. 44, no. 2, pp. 175–179, Feb. 2011.

[7] J. L. Miller and D. Kitaljevich, "In-line oil debris monitor for aircraft engine condition assessment," in *Proc. IEEE Aerospace Conference*. Mar. 2000, pp. 49–56.

[8] I. M. Flanagan, J. R. Jordan, and H. W. Whittington, "An inductive method for estimating the composition and size of metal particles," *Measurement Science and Technology*, vol.1, no. 5, pp. 381–384, 1990.

[9] F. Quintaes, A. O. Salazar, A. L. Maitelli, F. Fontes, M. A. A. Vieira, and T. Eslley, "Magnetic sensor used to detect contamination of insulating oil in motors applied to electrical submersible pump," *IEEE Transactions on Magnetics*, vol. 47, no. 10, pp. 3756–3759, Oct. 2011.

[10] D. M. Ginsberg and M. J. Melchner, "Optimum Geometry of Saddle Shaped Coils for Generating a Uniform Magnetic Field," *Review of Scientific Instruments*, vol. 41, no. 1, pp. 122–123, 1970.

[11] S. Jeon, G. Jang, H. Choi, and S. Park, "Magnetic navigation system with gradient and uniform saddle coils for the wireless manipulation of micro-robots in human blood vessels," *IEEE Transactions on Magnetics*, vol. 46, no. 6, pp. 1943–1946, 2010.

.

CHAPTER 3. INCIPIENT FAULT DETECTION OF WIND TURBINE GEARBOXES

A new method for detection of early degradation in WT gearboxes is presented in this chapter. Tri-axis vibration signals, which are used as the medium for the fault detection, are collected from an experimental gearbox test bench with incipient gear tooth wear fault. Twenty four statistical features in time domain are extracted from the vibration signals in each sampled instance. The intrinsic low dimensional manifold embedded in the twenty four dimensional fault characteristic space is learned by using the *t*-Distributed Stochastic Neighbor Embedding (*t*SNE) which is an advanced nonlinear dimensionality reduction algorithm. The incipient gear tooth fault has been successfully detected under different operation conditions only via a simple K Nearest Neighbor (KNN) classifier using the reduced features in the manifold.

3.1. INTRODUCTION

FD of WT gearbox is highly desired by the wind farm operators to benefit the predictive maintenance and to reduce the cost of wind power [1-5]. In the literature, the fault detection and diagnosis of gear and bearing in WT gearboxes have been achieved by generator current signature analysis [6-10], piezoelectric strain based monitoring [11], acoustic emission analysis [12], frequency based analysis of rotation speeds [13], signature analysis of output power signal [14], Supervisory Control And Data Acquisition (SCADA) data based approach [15], and vibration based analysis [16-17].

However, the early fault detection of WT gearbox is still a challenging task because the incipient fault signatures are very weak and are often buried in the noise. There are few papers on the incipient fault detection of WT gearbox. The trends of vibration and oil debris count versus cumulative wind energy production are analyzed in reference [16] for detection of early damage of WT gearbox. A side band fault detection algorithm which could be incorporated into a commercial condition monitoring system for automatic gear fault detection and diagnosis is presented in [17]. The incipient gear faults including 3mm × 2mm chip, 5mm × 5mm chip, 7mm × 5mm chip, missing tooth on an and pinion damage are detected and identified by using the proposed algorithm. In [18], an artificial neural network-based condition monitoring approach is applied to detect the damages in the gearbox bearings of a WT gearbox successfully. The intelligent and automatic fault detection, which is the trend of the next generation HMFD of wind turbines, could reduce the

quantity of the information and inspection that the operators and maintainers of wind turbines must handle. In the automatic fault detection framework, the feature extraction and reduction is one of the most important steps which play a determinative role to the performance of incipient fault detection.

Hence a *t*SNE based incipient fault detection scheme using the tri-axis vibration signals is proposed in this chapter aiming at improving the sensitivity of the fault related features and enhancing the accuracy of the incipient fault detection of WT gearboxes. The remaining parts of this chapter are arranged as follows. Section 3.2 illustrates the fault setting and experimental setup. Evaluation of commonly used methods for the incipient gear FD is presented in section 3.3, frequency domain and joint time-frequency domain analysis are investigated in this section. A novel FD method based on *t*SNE and KNN is proposed in section 3.4, the detection results are analyzed. Section 3.5 summarizes this chapter.

3.2. FAULT SETTING AND EXPRIMENTAL SETUP

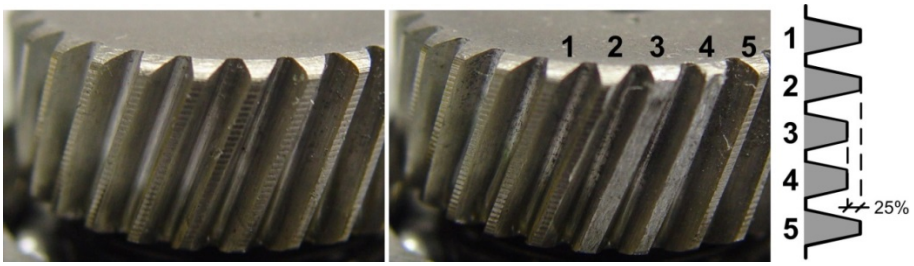

Fig. 3.1. The seeded incipient tooth fault.

The seeded incipient tooth fault and experimental setup are presented in Fig. 3.1 and Fig. 3.2, respectively. 25% abrasion of two adjacent teeth in gear d of a two stage gearbox is set to emulate the incipient gear fault of WT gearboxes. The numbers of teeth in the gears are, a. 54, b. 29, c. 40, d. 29, which makes the gear ratio to be 2.568. Tri-axis vibration signals, which are used as the medium for the fault detection, are collected from the experimental gearbox test bench with incipient gear tooth wear fault. The sampling frequency is 20kHz. Three datasets are generated to be used in section 3.3 and section 3.4.

Dataset 1. Tri-axis vibration signals with a length of 2 seconds when the rotational speed is 1500 rpm of the healthy gearbox. Tri-axis vibration signals with a length of 2 seconds when the rotational speed is 1500 rpm of the faulty gearbox. Tri-axis vibration signals with a length of 0.5 second when the rotational speed is 3000 rpm of the healthy gearbox. Tri-axis vibration signals with a length of 0.5 second when the rotational speed is 3000 rpm of the faulty gearbox.

Dataset 2. Segments of 0.6 second tri-axis vibration signals during a nonstationary operation condition with the speed profile of 1500-0-1500 rpm are collected using the health and faulty gearbox, respectively.

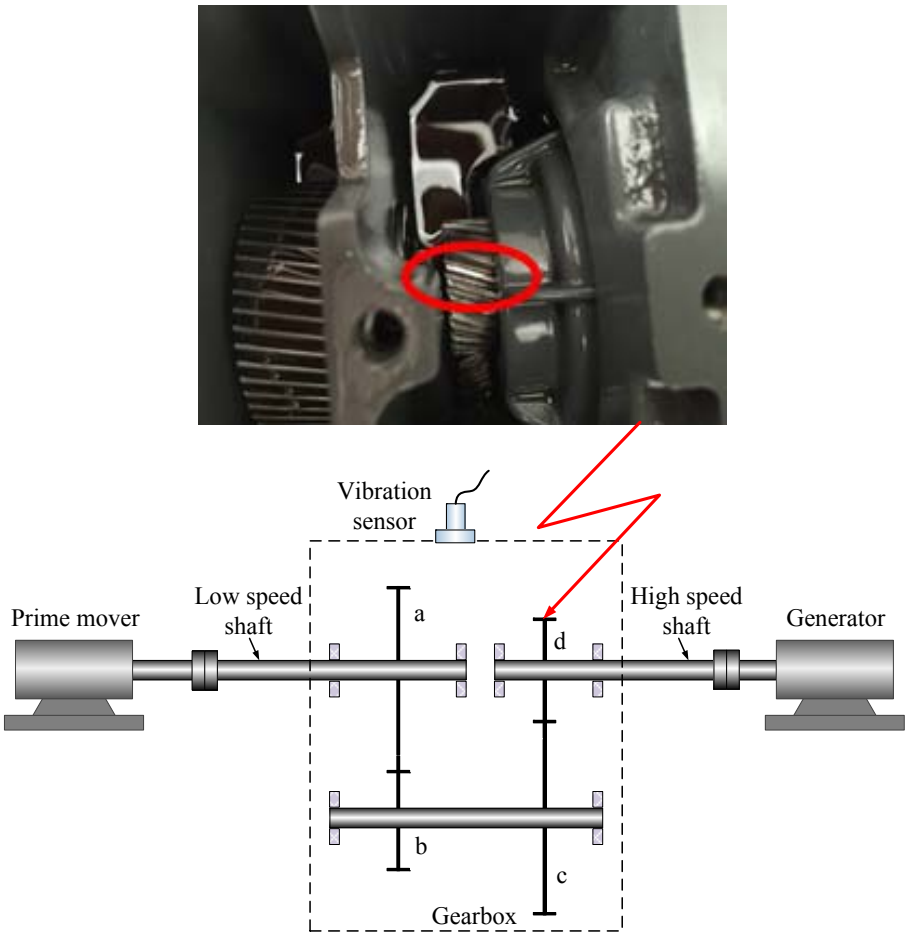

Fig. 3.2. Experimental setup.

Dataset 3. Four operation conditions, case I: tooth healthy @1200-1600rpm, case II: tooth faulty @1200-1600rpm, case III: tooth healthy @2700-3100rpm, case IV: tooth faulty @2700-3100rpm are conducted for the data acquisition. 50 specimens of the tri-axis vibration signals, each of which contains more than 5 rotating cycles of the HSS, are collected from each operation condition. Among these collected instances, 25 instances are randomly selected as testing instances in each case. Hence there are totally 200 specimens collected from the experiment, among which 100 specimens are testing specimens.

It should be noted that the above mentioned rotating speed is the speed of High Speed Shaft (HSS) in the gearbox.

3.3. INVESTIGATION OF REGULAR FD APPROACHES

3.3.1. FREQUENCY DOMAIN ANALYSIS

When two gears mesh each other, the number of teeth involved in the process varies from one pair to two pair then back to one pair, which forms a periodic impulse to the teeth. The shock between the contacting teeth results in the gear meshing vibration. Gear Mesh Frequency (GMF) is,

$$f_m = n\frac{N}{60}Z \tag{3.1}$$

where f_m is GMF, n is integer, N is the rotational speed of the shaft (rpm), Z is the teeth number of the gear. When the rotational speed is 1500 rpm, GMF of different gears in the gearbox shown in Fig. 3.2 is presented in Table 3.1. Table 3.2 shows the rotating frequency of different Shafts, where fs1, fs2 and fs3 represent the rotating frequency of low speed shaft, intermediate shaft and high speed shaft, respectively.

Table 3.1. GMF of different gears with rotational speed of 1500 rpm.

Gear Pair	Gear Ratio	Gear Mesh Frequency (Hz)
a/b	1.862	525.42
c/d	1.379	725

Table 3.2. Shaft rotating frequency with rotational speed of 1500 rpm.

Shaft	Shaft rotating frequency (Hz)
fs1	9.73
fs2	18.13
fs3	25

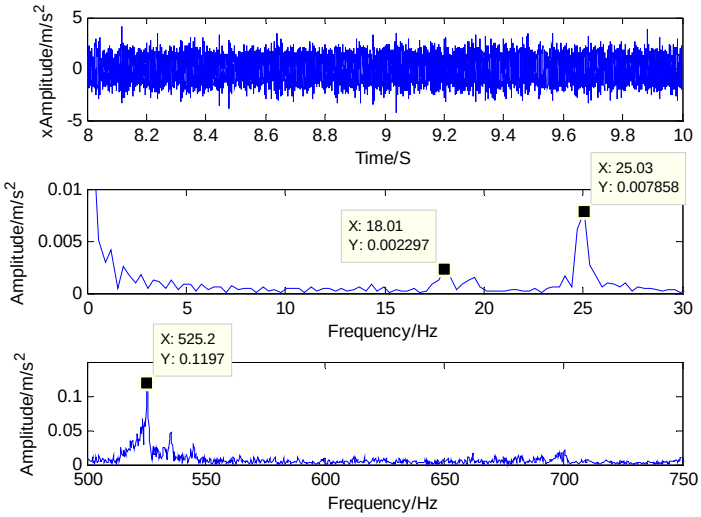

(a)

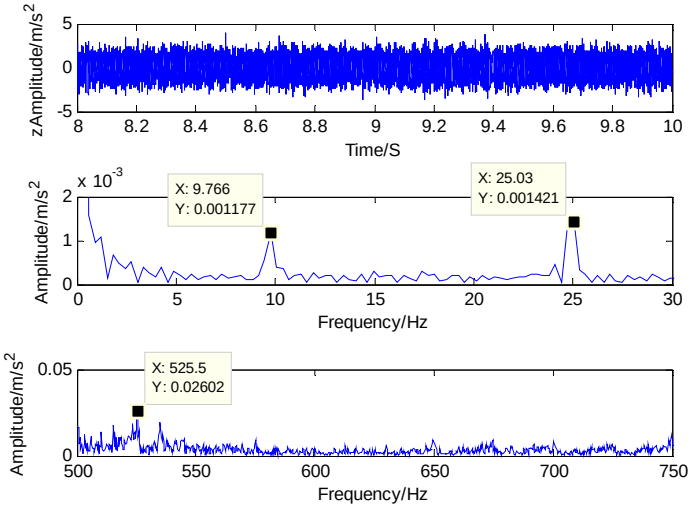

(b)

Fig. 3.3. Frequency spectrum of the of vibration signals from healthy gearbox, (a) x axis vibration signal of the sensor, and (b) z axis vibration signal of the sensor .

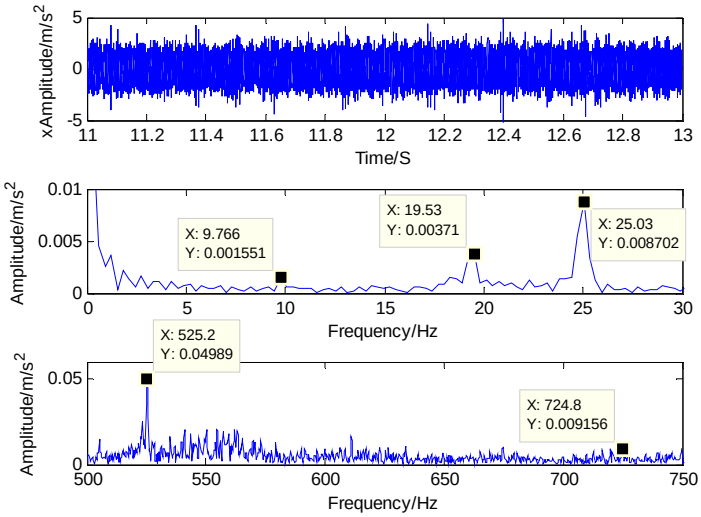

(a)

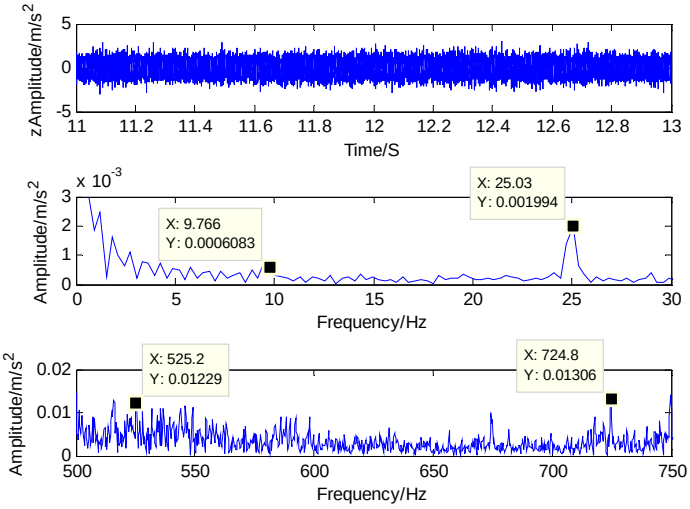

(b)

Fig. 3.4. Frequency spectrum of the of vibration signals from faulty gearbox, (a) x axis vibration signal of the sensor, and (b) z axis vibration signal of the sensor.

Shafts, gears and bearings in a gearbox could produce vibration during normal operation. The energy distribution of the vibration subjects to change once there is a fault in the gear teeth. Thus the vibration signal is the carrier of fault signatures and could be used as the medium for FD of gearboxes. Fault characteristics could be extracted from the vibration signals. Frequency spectrum analysis is the most commonly used approach for the FD of gear fault. Fast Fourier Transform (FFT) is used to obtain the spectrum in frequency domain. If there is damage in the gear teeth, the amplitude of the fault characteristic frequencies should increase. Dataset 1 is used in this subsection.

Fig. 3.3 presents the frequency spectrum of vibration signals from healthy gearbox, it should be noted that only the signals in x and z directions are shown in this figure. This is because the gear fault can only affect the vibration signals in radial direction. Hence y axis signal of the tri-axis accelerometer, which is in the axial direction, is not analyzed here. As shown in Fig. 3.3(a), the upper graph is the time domain waveform of vibration in x axis between 8 and 10 second, spectrum in two frequency bands, 0-30Hz and 500-750Hz, is also presented in this figure. Vibration signal in z direction is transformed into frequency and shown in Fig. 3.3(b). The corresponding frequency spectrum analysis for the faulty gearbox is presented in Fig. 3.4.

Table 3.3. Comparison of fault characteristic frequencies from healthy and faulty gearboxes with rotational speed of 1500 rpm.

	Fs1 (9.73Hz)	Fs2 (18.13Hz)	Fs3 (25Hz)	Fgm1 (525.4Hz)	Fgm2 (725Hz)
xMag(healthy)	0.0002	0.0023	0.0078	0.12	0.008
xMag(faulty)	0.0016	0.0037	0.0087	0.05	0.009
zMag(healthy)	0.0012	0.001	0.0014	0.025	0.012
zMag(faulty)	0.0006	0.001	0.002	0.012	0.013

Table 3.3 shows the comparison of fault characteristic frequencies from healthy and faulty gearboxes with rotational speed of 1500 rpm, the magnitude of Fs2, Fs3 and Fgm2 have slight increases both in x and z axis when the incipient gear fault occurs. However, there are opposite changes on the magnitude of Fs1 and Fgm1. Therefore frequency spectrum is not effective for the FD of incipient gear fault.

In order to evaluate the spectrum analysis method comprehensively, vibration data collected from healthy and faulty gearboxes with rotational speed of 3000 rpm are also analyzed. GMF of different gears is shown in Table 3.4. The rotating frequency of different Shafts is presented in Table 3.5.

Table 3.4. GMF of different gears with rotational speed of 3000 rpm.

Gear Pair	Gear Ratio	Gear Mesh Frequency (Hz)
a/b	1.862	1050.84
c/d	1.379	1450

Table 3.5. Shaft rotating frequency with rotational speed of 3000 rpm.

Shaft	Shaft rotating frequency (Hz)
fs1	19.46
fs2	36.26
fs3	50

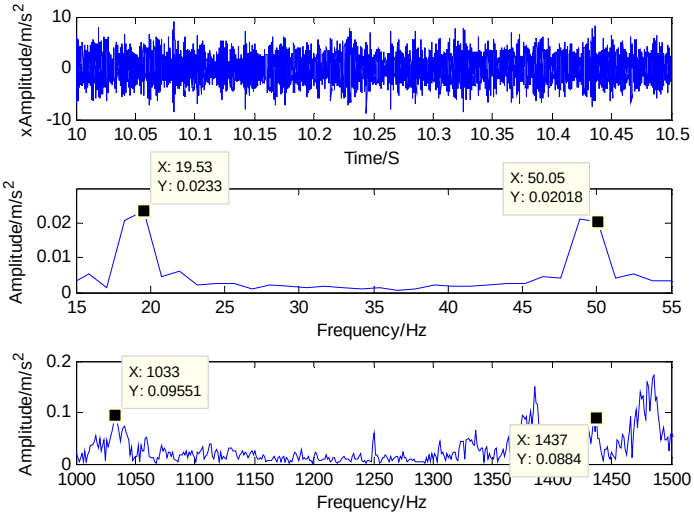

(a)

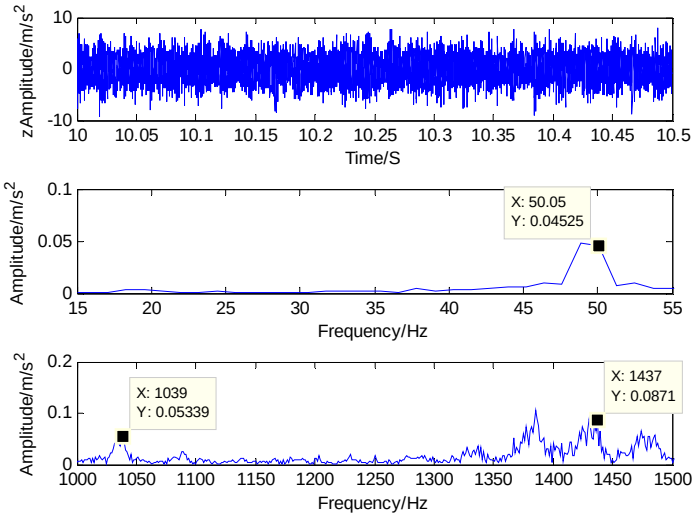

(b)

Fig. 3.5. Frequency spectrum of the of vibration signals from healthy gearbox (3000rpm), (a) x axis vibration signal of the sensor, and (b) z axis vibration signal of the sensor.

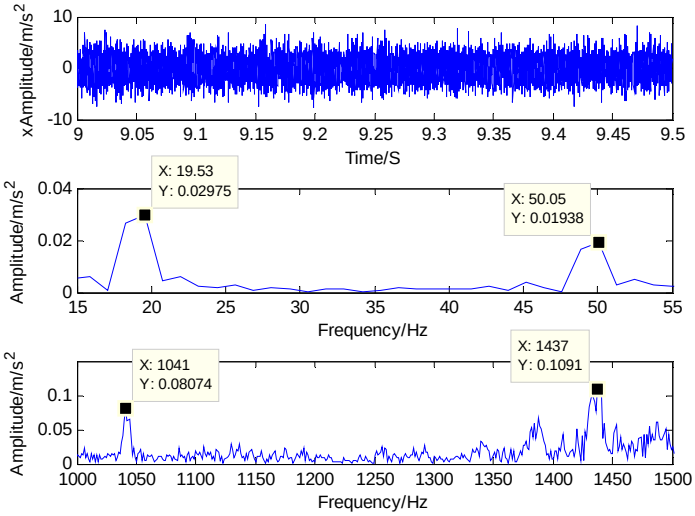

(a)

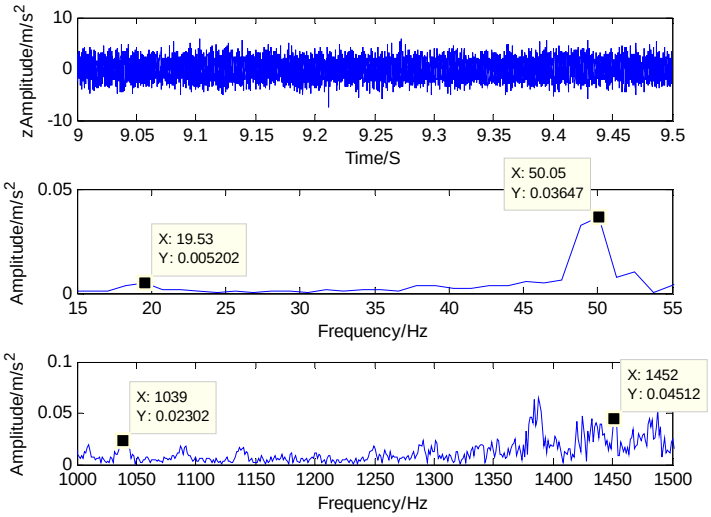

(b)

Fig. 3.6. Frequency spectrum of the of vibration signals from faulty gearbox (3000rpm), (a) x axis vibration signal of the sensor, and (b) z axis vibration signal of the sensor.

Table 3.6. Comparison of fault characteristic frequencies from healthy and faulty gearboxes with rotational speed of 3000 rpm.

	Fs1 (19.46Hz)	Fs2 (36.26Hz)	Fs3 (50Hz)	Fgm1 (1050.8Hz)	Fgm2 (1450Hz)
xMag(healthy)	0.023	0.003	0.02	0.09	0.08
xMag(faulty)	0.029	0.003	0.02	0.08	0.1
zMag(healthy)	0.006	0.008	0.04	0.05	0.09
zMag(faulty)	0.005	0.009	0.03	0.02	0.05

Fig. 3.5 presents the frequency spectrum of vibration signals from healthy gearbox, As shown in Fig. 3.5(a), the upper graph is the time domain waveform of vibration

in x axis between 8 and 10 second. Spectrum in two frequency bands, 15-55Hz and 1000-1500Hz, is also presented in this figure. Vibration signal in z direction is transformed into frequency and shown in Fig. 3.5(b). The corresponding frequency spectrum analysis for the faulty gearbox is presented in Fig. 3.6.

The comparison of fault characteristic frequencies from healthy and faulty gearboxes with rotational speed of 3000 rpm is presented in Table 3.6, the magnitude of Fs1, Fs2 and Fgm1 have tiny increases in x or z axis when the incipient gear fault occurs. Other indicators hold the level or descend. The results from both operation conditions indicate that the frequency spectrum is not reliable for the FD of incipient gear fault.

3.3.2. JOINT TIME-FREQUENCY DOMAIN ANALYSIS

Fourier Transform (FT) is widely used for the FD of gearboxes operating under stationary conditions. However, most modern WTs rotate at variable speed to extract the maximum power from wind [19]. In such cases, FT is not effective for analyzing the time varying signals. Short Time Fourier Transform (STFT) is the most widely used method for analysis of nonstationary signals. Thus STFT is utilized in this subsection to analyze the nonstationary vibration signals in dataset 2.

The idea of STFT is using a sliding window $w(t)$ to segment the signal $s(t)$ into small sections, which is narrow enough to be considered as stationary. FT is applied to each segment of the $s(t)$, which gives a bank of spectral information for the narrow time intervals. Thus STFT is a joint time frequency representation method which provides both time and frequency information of $s(t)$.

The definition of Continuous-time STFT is,

$$S(\tau,\omega) = \int_{-\infty}^{\infty} s(t)w(t-\tau)e^{-j\omega t}dt \tag{3.2}$$

Discrete-time DTFT $D(\tau,\omega)$ of $s(n)$ is

$$D(n,\omega) = \sum_{m=-\infty}^{\infty} s(m)w(n-m)e^{-j\omega m} \tag{3.3}$$

Discrete DTFT $X(\tau,\omega)$ of $s(n)$ is

$$X(n,k) = \sum_{m=-\infty}^{\infty} s(m)w(n-m)e^{-j\frac{2\pi}{N}km} \tag{3.4}$$

where N is the width of the window, $0 \le k \le N-1$.

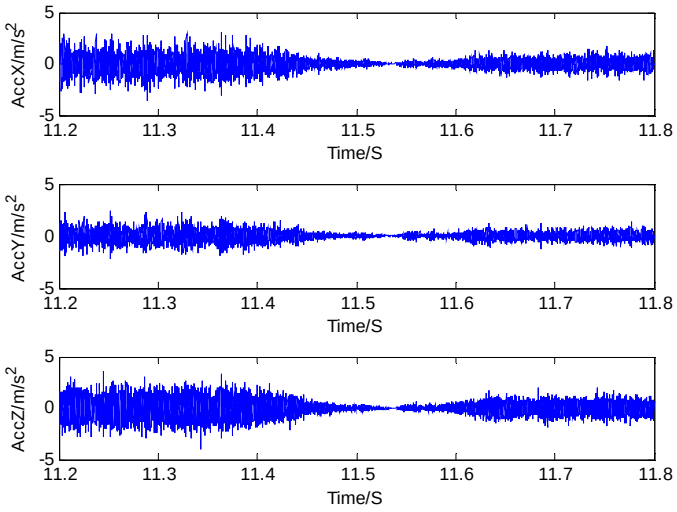

(a)

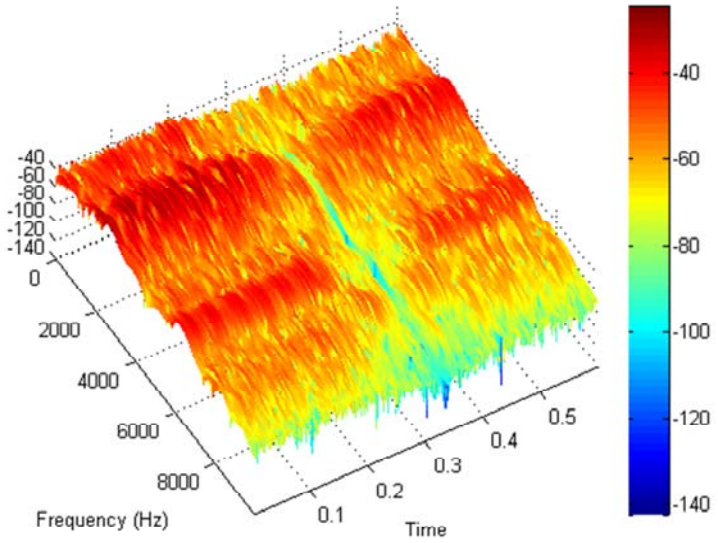

(b)

Fig. 3.7. STFT of vibration signals (healthy gear), (a) time domain waveform, and (b) STFT representation.

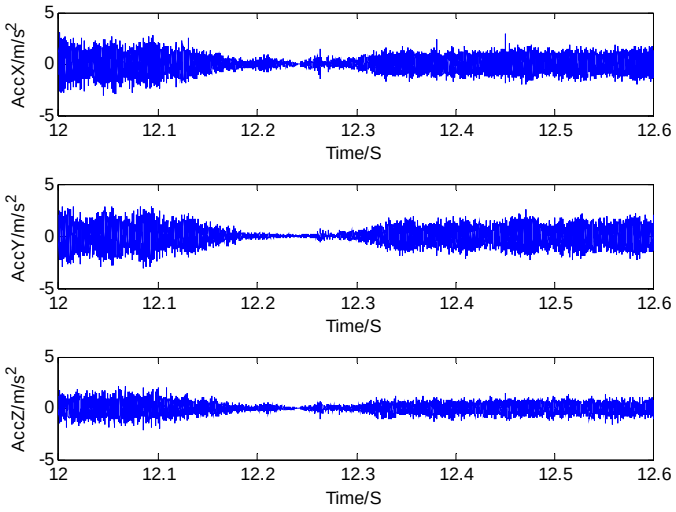

(a)

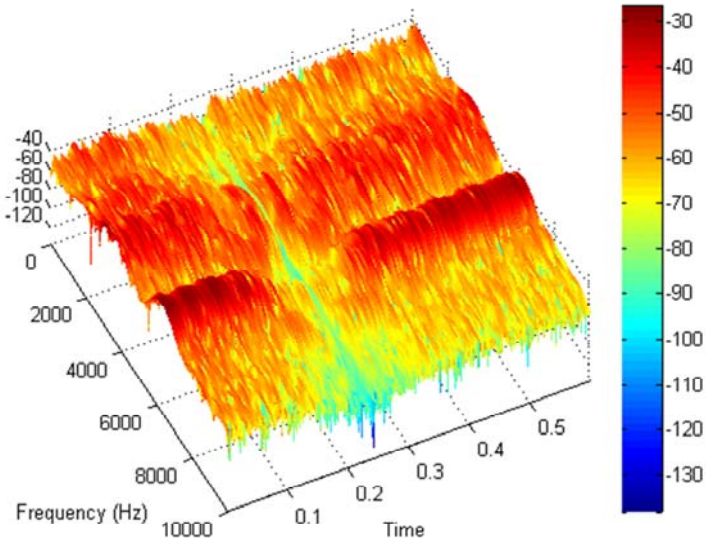

(b)

Fig. 3.8. STFT of vibration signals (faulty gear), (a) time domain waveform, and (b) STFT representation.

Two pieces of data in dataset 2 is analyzed in this subsection. STFT of vibration signals from healthy gearbox and faulty gearbox are shown in Fig. 3.7 and Fig. 3.8, respectively. Hanning window is used in this study, the overlap is 100. The length of the vibration signal is 0.6 second. By comparing the joint time frequency representation of the signals from healthy and faulty gears, only the trend of the spectrum change following the variable rotational speed profile 1500-0-1500 could be observed. The change of fault characteristic frequencies related to the incipient gear fault is not found in the time frequency representation.

3.4. INCIPIENT GEAR FAULT DETECTION BASED ON TSNE AND KNN

3.4.1. EXTRACTION OF FAULT CHARACTERISTICS

The incipient gear fault related features extracted in this section is the statistical characteristics in time domain. Suppose the time series x: $\{x_1, \dots, x_k, \dots, x_n\}$ is the sampled vibration instance, the fault related features are shown as follows.

Mean value:

$$\bar{x} = \frac{1}{n} \cdot \sum_{k=1}^{n} x_k \tag{3.5}$$

Max value:

$$\hat{\mathrm{x}} = \max(\mathrm{x}) \tag{3.6}$$

Root mean square:

$$\mathrm{RMS} = \sqrt{\frac{1}{\mathrm{n}} \cdot \sum\nolimits_{\mathrm{k}=1}^{\mathrm{n}} (\mathrm{x_k})^2} \tag{3.7}$$

Variance:

$$\sigma^2 = \frac{1}{n} \cdot \sum_{k=1}^{n} (x_k - \bar{x})^2 \tag{3.8}$$

Crest factor:

$$CF = \frac{\hat{x}}{RMS} \tag{3.9}$$

Shape factor:

$$SF = \frac{RMS}{\frac{1}{n} \cdot \sum_{k=1}^{n} |x_k|} \tag{3.10}$$

Kurtosis:

$$k = \frac{E[(x_k - \bar{x})^4]}{\sigma^4} \tag{3.11}$$

Skewness:

$$s = \frac{E[(x_k - \bar{x})^3]}{\sigma^3} \tag{3.12}$$

3.4.2. NONLINEAR DIMENSIONALITY REDUCTION USING TSNE

The intrinsic low dimensional manifold embedded in the twenty four dimensional fault characteristic space is obtained by using *t*SNE [20-21], which is a promising approach of manifold learning [22-23], to improve the sensitivity of the fault related features and facilitate the incipient FD of WT gearbox. The principle of *t*SNE is briefly introduced here.

*t*SNE consists of two steps. Firstly, a probability distribution is constructed for the high dimensional objects, which makes the objects with high similarity could be selected easily and the objects with low similarity have a low probability to be selected. Given a set of *N* high dimensional objects $x_1, x_2 \ldots x_N$, it should be noted that *N* is the number of object not the dimensionality. The similarity between objects $x_i$and x_j is,

$$p_{j|i} = \frac{\exp(-\left\|x_i - x_j\right\|^2 / 2\sigma^2)}{\sum_{k \neq i} \exp(-\|x_i - x_k\|^2 / 2\sigma^2)} \tag{3.13}$$

$$p_{ij} = \frac{p_{j|i} + p_{i|j}}{2N} \tag{3.14}$$

Here Gaussian kernel σ is used to establish the probability distribution.

The second step is to build a probability distribution in the target low-dimensional space. The constructed two probability distributions in two different dimensional

spaces should be as similar as possible. Suppose $y_1, y_2 \dots y_N$ is mapped low dimensional objects, the similarity of $y_i$and y_j is defined as,

$$q_{i|j} = \frac{(1 + \|y_i - y_j\|^2)^{-1}}{\sum_{k \neq l}(1 + \|y_k - y_l\|^2)^{-1}} \tag{3.15}$$

where *t* distribution is used to evaluate the similarity of the objects in low-dimensional space.

The positions of the mapped low dimensional points y_i in the manifold are obtained by Kullback–Leibler divergence optimization of the two distributions P and Q via gradient descent method. The objective function *C* is,

$$C = KL(P||Q) = \sum_{i \neq j} p_{ij} log \frac{p_{ij}}{q_{ij}} \tag{3.16}$$

Gradient is,

$$\frac{dC}{dy_i} = 4 \sum_j (p_{ij} - q_{ij})(y_i - y_j)(1 + \|y_i - y_j\|^2)^{-1} \tag{3.17}$$

3.4.3. FAULT CLASSIFICATION BASED ON KNN

Now that the intrinsic low dimensional manifold embedded in the high dimensional fault characteristic space is learned by using *t*SNE, the next step of the incipient gear FD of WT gearbox is fault classification. KNN is applied to fulfill this step. The basic theory of KNN is presented shortly in this subsection.

Suppose $X = (x_1, \dots, x_N)$ is the training sample set, $X_i = (x_{i1}, \dots, x_{ik})$ is the k nearest neighbors of x_i, $X_t = (x_{t1}, \dots, x_{tM})$ testing sample set, x_0 is an arbitrary testing sample. $X_0 = (x_{01}, \dots, x_{0k})$ is the k nearest neighbors of x_0, whose labels are $L_0 = (l_1, \dots, l_k)$. It should be noted that these k nearest neighbors are from the training sample set. Assume $\theta = (\theta_1, \dots, x_C)$ is the class set. There are totally C categories [24].

The voting rules of KNN is,

$$j^* = arg \max_{j=1,\dots C} \sum_{i=1}^{k} \delta(l_i, j) \tag{3.18}$$

where δ is the Kronecker delta.

The training data set is used by the testing instance to search the k Nearest Neighbors. The class label is determined by major class of k Nearest Neighbors. Equation (3.18) is used in this decision-making procedure.

3.4.4. RESULTS ANALYSIS

The time domain waveforms of tri-axis vibration signals of a specimen in operation case II are shown in Fig. 3.9 (a). It can be observed that the actual rotation speed varies from 1200 rpm to 1400 rpm in this 0.2s specimen. A multi-band FIR filter is designed to remove the noise and fault unrelated frequencies. Fig. 3.10 demonstrates the Amplitude-frequency characteristics of the FIR multi-band filter. Spectrum comparison before and after filtering is illustrated in Fig. 3.11.

The filtered signals in time domain are highlighted in Fig. 3.9(a). Twenty four statistical time domain features are extracted from the filtered tri-axis vibration signals in each specimen using the formula (3.5) to (3.12), from which the intrinsic features in 3 dimensional manifold are obtained via *t*SNE. The intrinsic features of the 100 specimens in case I and II are demonstrated in Fig. 3.9(b). It is observed that the healthy and faulty instances are projected to two compact clusters with great margins which can be totally separated using a linear classifier.

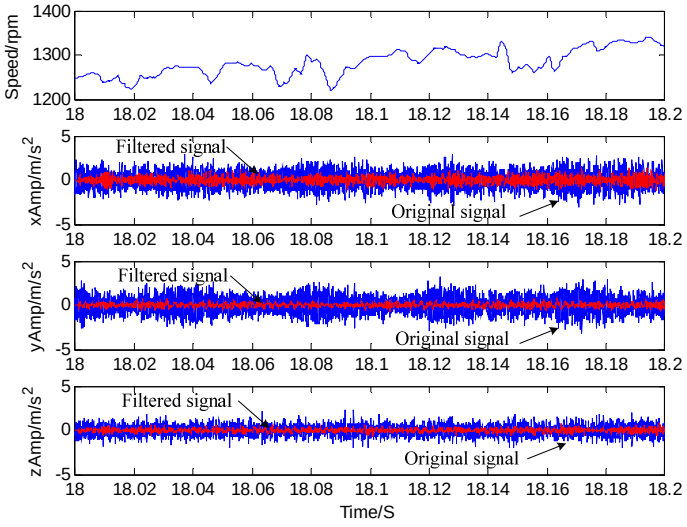

(a)

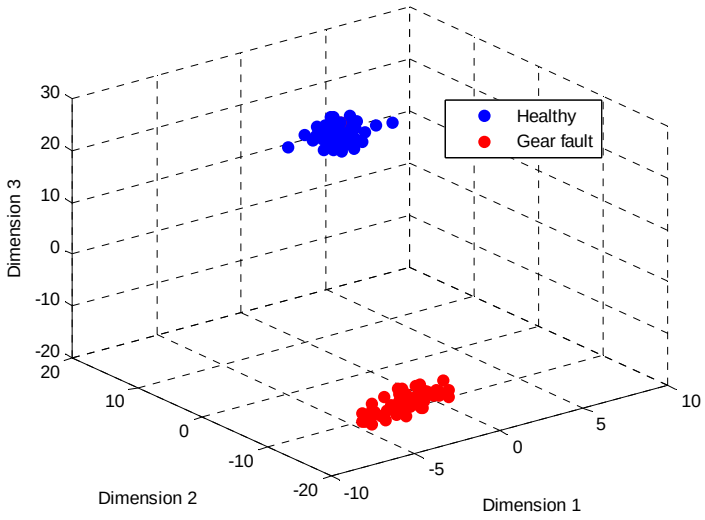

(b)

Fig. 3.9. Dimensionality reduction for case I and II, (a) tri-axis vibration signals (b) intrinsic features.

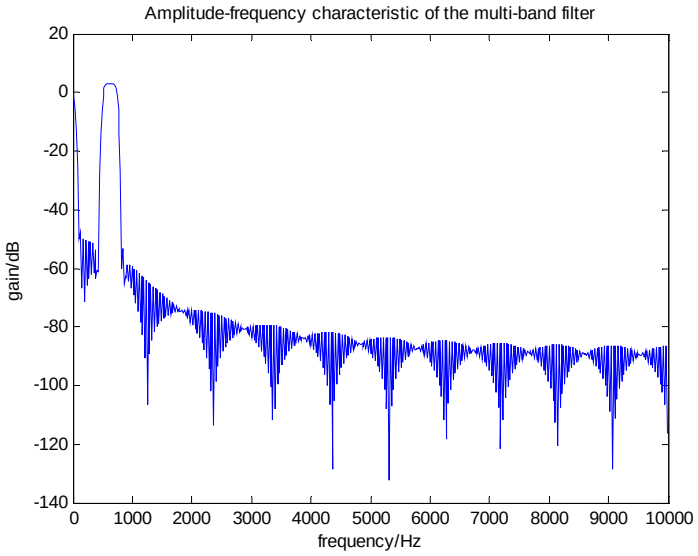

Fig. 3.10. Amplitude-frequency characteristics of the FIR multi-band filter.

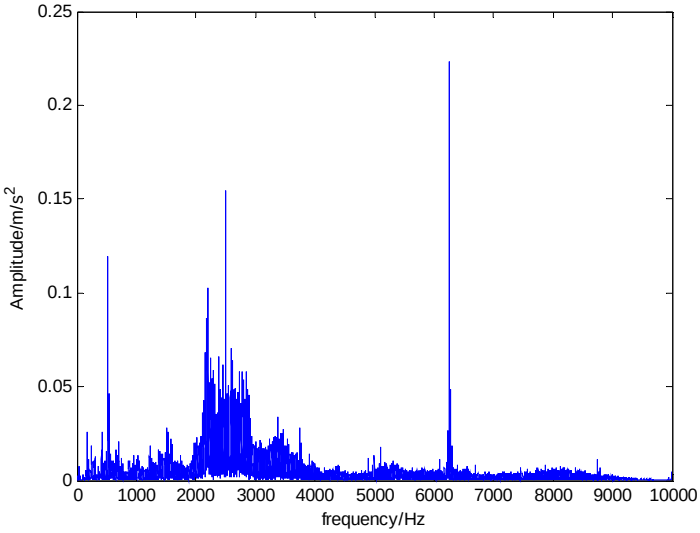

(a)

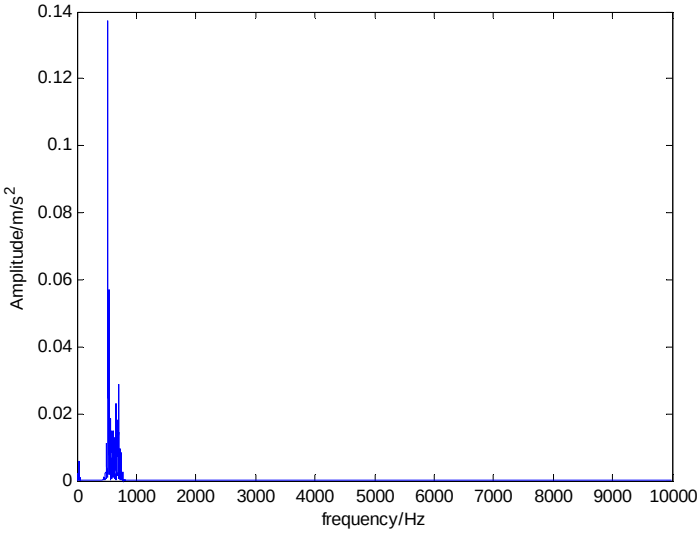

(b)

Fig. 3.11. Spectrum comparison, (a) before filtering, (b) after filtering.

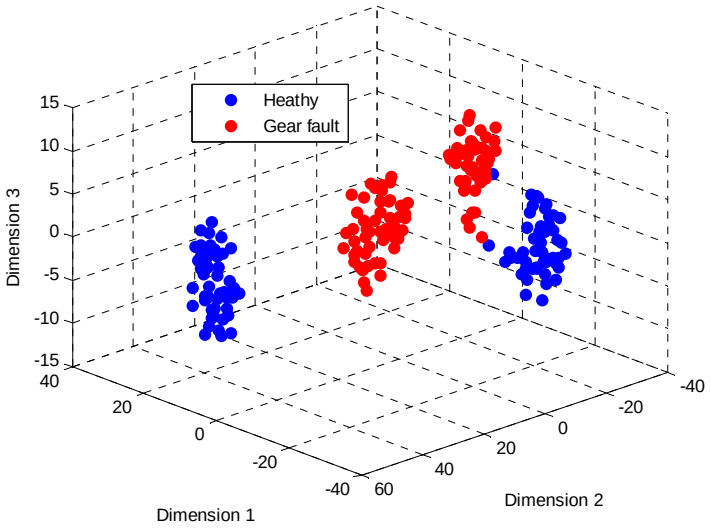

(a)

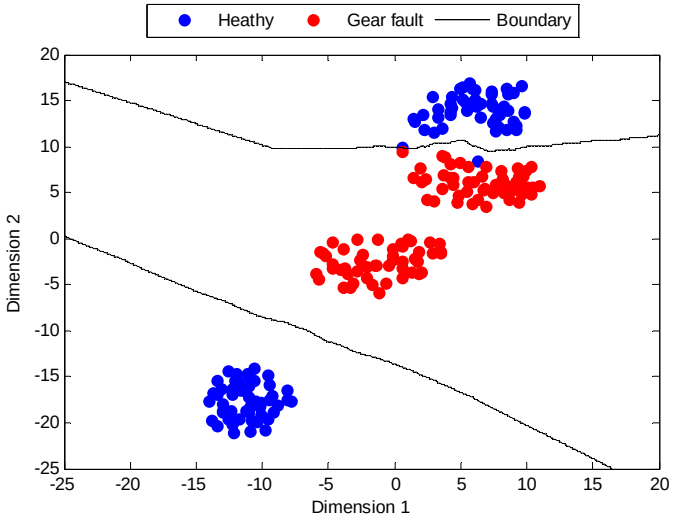

(b)

Fig. 3.12. Results of (a) *t*SNE based nonlinear dimensionality reduction and (b) KNN based fault detection (k=3)

Fig. 3.12 shows the results of the nonlinear dimensionality reduction using *t*SNE and incipient gear fault detection based on KNN (k=3) classification. The reduced dimensional intrinsic features of the specimens in four operation cases aggregate to four separated clusters after *t*SNE, which is demonstrated in Fig. 3.12(a). As is presented in Fig. 3.12(b), the boundaries for the incipient gear fault detection are depicted in the two dimensional intrinsic feature plane. The classification accuracy for training dataset is 100%, while it is 97% for the test dataset because there are two instances on the boundary and one wrongly classified instance of the healthy category.

3.5. SUMMARY

A new approach for the incipient gear fault detection based on *t*SNE and KNN is proposed in this chapter, incipient gear fault is analyzed and set on the high speed gear in the experimental gearbox, commonly used FD approaches including frequency domain analysis and joint time frequency analysis are investigated and evaluated, followed by the detailed procedure of the proposed FD method. Statistical characteristics in time domain are chosen as fault features. The principles of *t*SNE and KNN are briefly introduced. Finally, the results are analyzed.

BIBLIOGRAPHY

[1] J. Ribrant and L. Bertling, "Survey of failures in wind power systems with focus on Swedish wind power plants during 1997–2005," *IEEE Trans. Energy Convers.*, vol. 22, no. 1, pp. 167–173, Mar. 2007.

[2] W. Qiao and D. Lu, "A survey on wind turbine condition monitoring and fault diagnosis-part I: Components and subsystems," *IEEE Trans. Ind. Electron.*, vol. 62, no. 10, pp. 6536–6545, Oct. 2015.

[3] W. Qiao and D. Lu, "A survey on wind turbine condition monitoring and fault diagnosis-part II: Signals and signal processing methods," *IEEE Trans. Industrial Electronics*, vol. 62, no. 10, pp. 6546–6557, Oct. 2015.

[4] S. Faulstich, B. Hahn, P. J. Tavner, "Wind turbine downtime and its importance for offshore deployment," *Wind Energy*, vol. 14, no. 3, pp. 327–337, 2011.

[5] S. Sheng and P. Veers, "Wind turbine drivetrain condition monitoring – an overview," NREL, Golden, CO, Tech. Rep. NREL/CP-5000-50698, May 2011.

[6] X. Gong and W. Qiao, "Bearing fault diagnosis for direct-drive wind turbines via current-demodulated signals," *IEEE Trans. Ind. Electron.*, vol. 60, no. 8, pp. 3419–3428, Aug. 2013.

[7] J. Zhang, J. Dhupia, and C. J. Gajanayake, "Stator current analysis from electrical machines using resonance residual technique to detect faults in planetary gearboxes," *IEEE Trans. Ind. Electron.*, early access article, 2015.

[8] P. Zhang and P. Neti, "Detection of gearbox bearing defects using electrical signature analysis for doubly fed wind generators," *IEEE Trans. Ind. Appl.*, vol. 51, no. 3, pp. 2195–2200, Dec. 2014.

[9] D. Lu and W. Qiao, "Adaptive feature extraction and SVM classification for real-time fault diagnosis of drivetrain gearboxes," *Proceedings of IEEE Transportation Electrification Conference and Expo (ITEC),* 2013, pp. 1 – 6.

[10] D. Lu and W. Qiao, "Current-based diagnosis for gear tooth breaks in wind turbine gearboxes*," Proceedings of IEEE Energy Conversion Congress and Exposition (ECCE),* 2012, pp. 3780 – 3786.

[11] J. Yoon, D. He, and B. Hecke, "On the use a single piezoelectric strain sensor for wind turbine planetary gearbox fault diagnosis," *IEEE Trans. Ind. Electron.*, early access article, 2015.

[12] Y. Qu, D. He, J. Yoon, B. Hecke, E. Bechhoefer and J. Zhu, "Gearbox Tooth Cut Fault Diagnostics Using Acoustic Emission and Vibration Sensors — A Comparative Study," *Sensor*, vol. 14, no. 1, pp. 1372–1393, Jan. 2014.

[13] P. F. Odgaard and A. R. Nejad, "Frequency based Wind Turbine Gearbox Fault Detection applied to a 750 kW Wind Turbine," *Proceedings of IEEE Conference on Control Applications*, Oct. 2014, pp. 1383–1388.

[14] S. J. Watson, B. J. Xiang, W. Yang, P. J. Tavner and C. J. Crabtree "Condition monitoring of the power output of wind turbine generators using wavelets", *IEEE Trans. Energy Convers.*, vol. 25, no. 3, pp.715–721, 2010.

[15] Y. Wang and D. Infield, "Supervisory control and data acquisition data-based non-linear state estimation technique for wind turbine gearbox condition monitoring," *IET Renewable Power Generation,* vol. 7, no. 4, pp. 350–358, Jul. 2013.

[16] C. J. Crabtree, Y. Feng, and P. J. Tavner, "Detecting Incipient Wind Turbine Gearbox Failure: A Signal Analysis Method for Online Condition Monitoring," in *Proc. Euro. Wind Energy Conf.*, 2010, pp. 1–6.

[17] D. Zappalá, P. J. Tavner, C. J. Crabtree, S. Sheng, "Side-band algorithm for automatic wind turbine gearbox fault detection and diagnosis," *IET Renewable Power Generation,* vol. 8, no. 4, pp. 380–389, 2014.

[18] P. Bangalore, and L. B. Tjernberg, "An Artificial Neural Network Approach for Early Fault Detection of Gearbox Bearings," *IEEE Trans. Smart Grid*, vol. 6, no. 2, pp. 980–987, Jan. 2015.

[19] Z. Chen and E. Spooner, "Grid power quality with variable speed wind turbines," *IEEE Trans. on Energy Conversion*, vol. 16, no. 2, pp. 148–154, 2001.

[20] L. J. P. Maaten and G. E. Hinton, "Visualizing High-Dimensional Data Using t-SNE," *Journal of Machine Learning Research,* vol. 9, no. 11, pp. 2579–2605, Nov. 2008.

[21] L. J. P. Maaten, "Accelerating t-SNE using Tree-Based Algorithms," *Journal of Machine Learning Research,* vol.15, no. 10, pp. 3221–3245, Oct. 2014.

[22] J. Tenenbaum, D. Silva, J. Langford, "A global geometric framework for nonlinear dimensionality reduction," *Science*, vol. 290, no. 5500, pp. 2319–2323, Dec. 2000.

[23] S. T. Roweis, L. K. Saul, "Nonlinear dimensionality reduction by locally linear embedding," *Science*, vol. 290, no. 5500, pp. 2323–2326, Dec. 2000.

[24] L. Ma, M. M. Crawford, and J. Tian, “Local manifold learning-based *k*-nearest-neighbor for hyperspectral image classification,” *IEEE Trans. Geosci. Remote Sens.*, vol. 48, no. 11, pp. 4099–4109, Nov. 2010.

CHAPTER 4. ONLINE SENSORLESS THERMAL MONITORING OF SWITCHED RELUCTANCE MACHINE[2]

Stator winding is one of the most vulnerable parts in Switched Reluctance Machine (SRM), especially under thermal stresses during frequently changing operation circumstances and susceptible heat dissipation conditions. Thus real-time online thermal monitoring of the stator winding is of great significance to the system protection and lifetime extension of SRM. A sensor-less approach for online thermal monitoring of stator winding of SRM is proposed in this chapter, only voltage and current measurements which already exist in the control system are needed to estimate the temperature of stator winding, neither machine parameters nor thermal impedance parameters are required in the scheme. Simulation results under various operating conditions confirm the proposed sensor-less online thermal monitoring approach.

4.1. INTRODUCTION

Although the SRM is robust, the stator winding is one of the most vulnerable points under thermal stresses during operation. The maximum temperature limits for the different classes of insulation materials used in the windings are presented in Tab. 4.1 by referring to the IEC standards [1-2]. The winding's insulation is ranked by the ability to bear the thermal load. The limit temperature of class A is 105 °C, while it is 180 °C for H class. According to [3], the lifespan of the winding could decrease one half given that the temperature rises by every 10 °C higher than the designed limits. Thus real-time online thermal monitoring of the stator winding is of great significance to the system protection and lifetime extension of SRM.

The temperature rise and distribution of the SRM has been studied using lumped parameter thermal model and numerical methods recently [4-7]. However, few literatures can be found on the real-time thermal monitoring for SRM. The thermal monitoring methods for electrical machines can be generally divided into two categories, namely with and without additional devices.

[2] This chapter is based on the paper which was originally published with following details.
[C. Wang, H. Liu, X. Liu, X. Zhang, and Z. Chen, "Online Sensorless Thermal Monitoring for Switched Reluctance Machine," Proceedings of 18th International Conference on Electrical Machines and Systems (ICEMS 2015), 2015, pp.1709–1715.], materials are reused with permission from IEEE. Copyright 2015, IEEE.

For the former, embedded sensors such as thermistors or thermocouples in the machine are the most common and straightforward configurations. Another method in this category is the signal injection by auxiliary circuits which run independently with the system. The resistance can be identified via the signal injection from which the temperature of the stator could be estimated indirectly by the variation of the stator winding resistance [8-10]. Although the results of these approaches are accurate, they are intrusive. Furthermore, the additional sensors and circuits may also increase the cost and reduce the reliability of the system.

Table 4.1
Winding insulation classes and the limited temperatures [1-2].

Insulation Class	Temperature Limit (°C)
A	105
B	130
F	155
H	180

The latter category is model based methods which consist of thermal models and electrical models for the thermal monitoring of machines [11-18]. The thermal model based methods employ equivalent thermal circuits (ETC) for the temperature estimation. The parameters of the ETCs can be obtained based on the specifications of the machine and heat transfer path, complicated temperature test as well as calibration [11-13]. The main disadvantage of this approach is that the accuracy is susceptible to different heat dissipation conditions. The electrical model based approach estimates the average stator winding temperature using the stator resistance which varies with the temperature. In this case, the stator winding itself can be regarded as a temperature sensor. By changing the control references and pulse width modulation, the active flux or torque [14], DC current [15], DC voltage [16] is injected into the machine, the generated DC offset in the stator winding can be used to calculate the stator resistance. Another stator resistance evaluation method is to design a resistance estimator based on the analytical model of the machine [17]. The electrical models based temperature estimation method overcome the drawbacks of thermal models, it is not affected by the change of cooling conditions.

In this chapter, a novel temperature estimation scheme for the SRM is proposed without using thermal sensors. The arrangement of the remaining parts of this chapter is as follows, section 4.2 presents the nonlinear analytical model of the

studied SRM, section 4.3 demonstrates the online sensor-less stator winding thermal monitoring scheme for SRM, simulation and results analysis are shown in section 4.4, conclusions are drawn in section 4.5.

4.2. MODELLING OF SRM

SRM has a doubly salient structure, and there is no magnet or winding on the rotor. The transversal section view of an 8/6 SRM is shown in Fig. 4.1. The stator has 8 poles while the rotor has 6 poles. The nonlinear relationship of flux linkage as a function of phase current and rotor position represents the magnetization characteristics of a SRM. The SRM model used in this chapter is a nonlinear analytical model proposed in [19] and [20]. The magnetic curve clusters of one phase in a SRM are displayed in Fig. 4.2. As can be seen in Fig. 4.2, the flux linkage rises monotonically with the increase of phase current at each position. When the phase current reaches to certain value, the variation of the flux linkage is becoming unapparent due to the flux saturation. The unaligned stator inductance, initial aligned stator inductance, and saturated aligned stator inductance used in the analytical SRM model can be obtained by derivative operation of flux linkage on stator current.

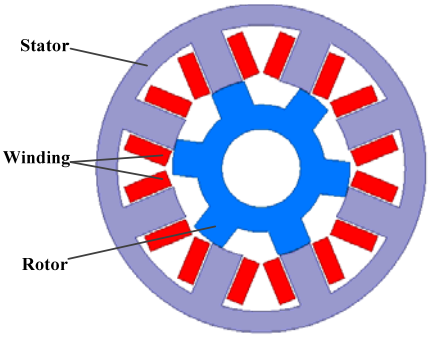

Fig. 4.1. The transversal section of an 8/6 SRM.

The flux linkage Ψ_{ua} at the totally unaligned rotor position is approximated as a linear function of stator current i,

$$\Psi_{ua}(i) = L_1 \cdot i \tag{4.1}$$

where L_1 is the unaligned stator inductance.

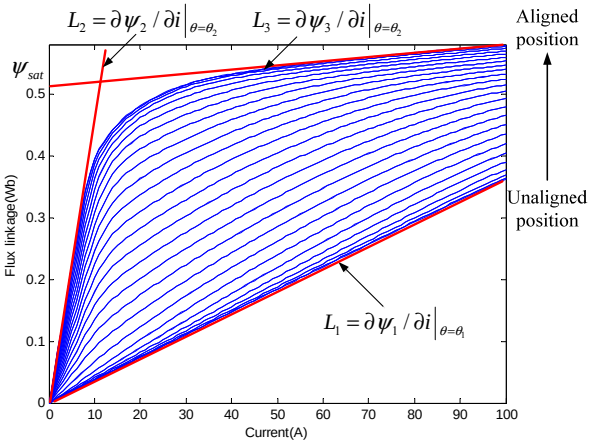

Fig. 4.2. The magnetic curve clusters of one phase in a SRM.

At the totally aligned rotor position, the flux linkage $\Psi_a(i)$ is a non-linear function of the stator current,

$$\Psi_a(i) = \Psi_{sat} \cdot (1 - e^{-K \cdot i}) + L_3 \cdot i \tag{4.2}$$

where

$$K = \frac{L_2 - L_3}{\Psi_{sat}}$$

Ψ_{sat}, L_2 and L_3 can be obtained by using the equations in Fig. 4.2.

The flux linkage $\Psi(i, \theta)$ for the middle rotor positions is calculated using the above two flux linkages,

$$\Psi(i, \theta) = \Psi_{ua}(i) + \eta(\theta) \cdot (\Psi_a(i) - \Psi_{ua}(i)) \tag{4.3}$$

where $\eta(\theta)$ is a weighting function,

$$\eta(\theta) = \frac{1}{2} + \frac{1}{2}\cos(N_r\left(\theta + 2\pi \cdot \frac{x}{N_s}\right)) \tag{4.4}$$

N_r is the number of rotor poles, N_s is the number of stator poles, and $x = 0, \ldots, \frac{N_s}{2} - 1$ denotes the phase.

The voltage equations are,

$$U_k = R_k \cdot i_k + \frac{d\Psi_k}{dt} = R_k \cdot i_k + \frac{\partial \Psi_k}{\partial i_k} \cdot \frac{di_k}{dt} + \frac{\partial \Psi_k}{\partial \theta} \cdot \frac{d\theta}{dt} \tag{4.5}$$

whre U_k, R_k, i_k and Ψ_k are the voltage, resistance, current and flux linkage of phase k, θ is the rotor angle.

Electromagnetic torque produced by phase k is,

$$T_k(i, \theta) = \frac{\partial}{\partial \theta} \int_0^i \Psi_k(i^*, \theta)\, di^* \tag{4.6}$$

Mechanical movement equation is,

$$J\frac{d^2\theta}{dt^2} = T_e - F\frac{d\theta}{dt} - T_l \tag{4.7}$$

where J is rotational inertia, F is frictional coefficient, T_e is total electromagnetic torque, T_l is load torque.

4.3. THE PROPOSED ONLINE SENSORLESS THERMAL MONITORING OF SRM

According to the electromagnetic characteristics of SRM, the phase current and phase flux linkage are all zero at the beginning of winding magnetizing as well as the end of winding discharging, which is illustrated in Fig. 4.3.

If the two time spots mentioned above are denoted as t_{on} and t_2, then we can get

$$\varphi_2 = \int_{t_{on}}^{t_2} [u(t) - i(t) \cdot R] dt$$

$$= \int_{t_{on}}^{t_2} u(t) dt - R \cdot \int_{t_{on}}^{t_2} i(t) dt = 0 \tag{4.8}$$

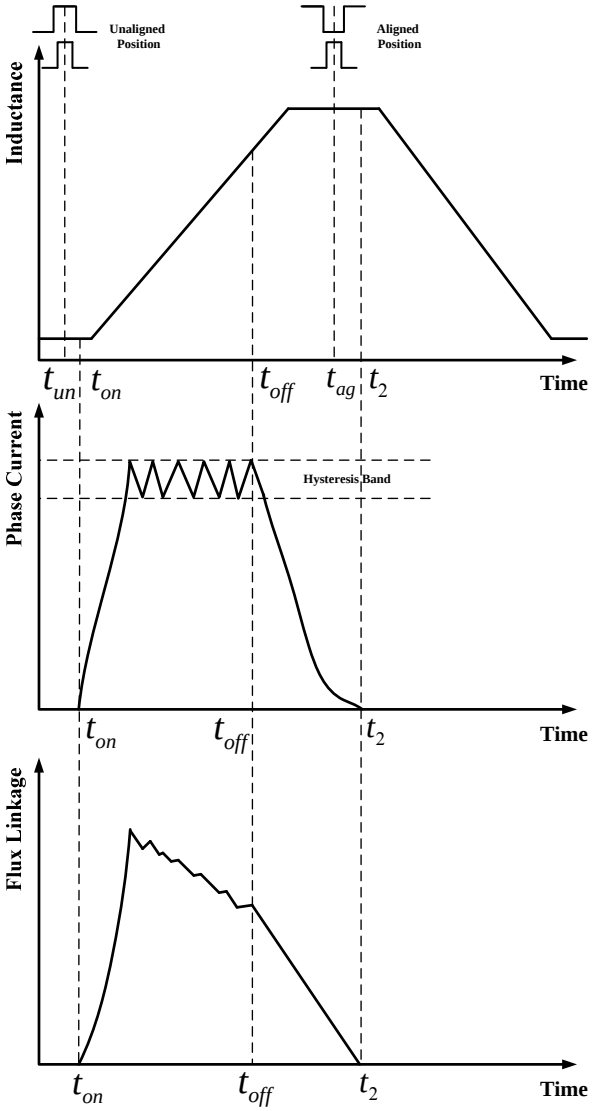

Fig. 4.3. Illustration of the two characteristic flux linkage points.

where φ_2 is the flux linkage of one phase in SRM at t_2, $u(t)$ and $i(t)$ are phase voltage and phase current between t_1 and t_2, thus the phase resistance R can be estimated by

$$\hat{R} = \frac{\int_{t_{on}}^{t_2} u(t)dt}{\int_{t_{on}}^{t_2} i(t)dt} \tag{4.9}$$

It should be noted that R in (4.8) is a function of time in reality. However, the temperature variation of the stator windings in one duty period during normal operation conditions is so little that it is reasonable to assume that the stator winding resistance is constant in one duty cycle.

The resistivity of the copper, which is the typical material of stator winding in a SRG, changes with the temperature of the coil, the relationship is

$$\rho_t = \rho_0 + \alpha_c \rho_0 (t - t_0) \tag{4.10}$$

where ρ_t is the resistivity of copper at temperature t ℃, ρ_0 is the resistivity of copper at temperature t_0℃, α_c is the temperature coefficient of copper (3.93×10^{-3}/℃).

If we assume the length and cross sectional area of the copper is invariant, the resistance of the winding is proportional to its resistivity

$$R \propto \rho \tag{4.11}$$

The temperature of the copper conductor t can be derived as

$$t = t_0 + \frac{R_t/R_0 - 1}{\alpha_c} \tag{4.12}$$

4.4. SIMULATION AND RESULTS ANALYSIS

4.4.1. SIMULATION OF THE SRM SYSTEM

A 7.5kw 8/6 poles four-phase SRM is modelled in Matlab/Simulink, the specifications of the studied SRM system is shown in Tab. 4.2. The unaligned stator inductance, initial aligned stator inductance, and saturated aligned stator inductance are calculated by magnetization characteristics obtained from Finite Element modelling.

A PI controller is designed to regulate the rotational speed. The stator currents of the four phases in two cycles when rotational speed is 1000 rpm and load torque is 20 Nm are shown in Fig. 4.4. It takes 0.01 second for the rotor to turn 60° of mechanical angle. Fig. 4.5 displays the voltage profile of phase A during two

periods. The totally aligned position of phase A is defined as 0°. The turn-on angle and turn-off angle of phase A are set to be 30° and 55°. The voltage of phase A is 240V when the rotor position is 30° at 0.045 second, where the current of phase A is rising quickly due to low inductance at the unaligned position. The phase A gets into current chopping mode from about 0.0455 second until 0.048 second. After which it goes into discharging mode up to 0.00496 second. The currents of Phase B, C and D have 15° phase delays successively.

Table 4.2
Main parameters of the studied SRM system.

Parameters	**Value**
Rated power	7.5 kw
Phase number	4
DC supply voltage	240 V
Structure	8/6 poles
Stator outer diameter	210 mm
Inner diameter	113.8 mm
Air gap	1 mm
Rotor diameter	50 mm
Stator resistance R	0.224 ohm @25°C
Unaligned stator inductance	3.1386 mH
Initial aligned stator inductance	46.4714 mH
Saturated aligned stator inductance	0.94 mH
Aligned saturation flux linkage	0.4716 Wb
Inertia	0.02 $kg \cdot m^2$
Friction coefficient	0.02
Rated load	20 Nm
Initial rotor speed	1000 rpm

Three cases are studied in this chapter, the results and analysis are given in the next section. It should be noted that the thermal time constant of electrical machines are relatively large, hence it may take tens of minutes for the temperature rising curve getting to steady state. However, the time scale of the proposed thermal estimation method is 10 milliseconds (1000rpm), it is unnecessary to simulate the temperature rising or change in tens of minutes. The time scale used in this study is 0.15 second. It is assumed that the temperature of stator winding is constant in the steady state, while it is slope response in the transient state. It is reasonable because thermal analysis is not necessary and not the focus of this chapter. Specifically, the temperature profiles in different operating conditions are assumed as follows, the stator resistances are set according to the temperature.

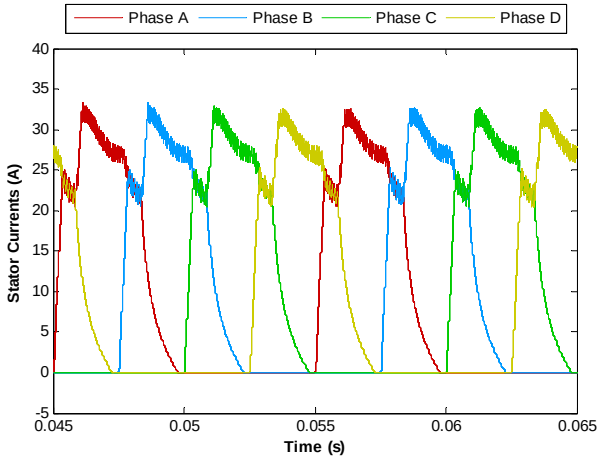

Fig. 4.4. The four-phase stator currents during two cycles.

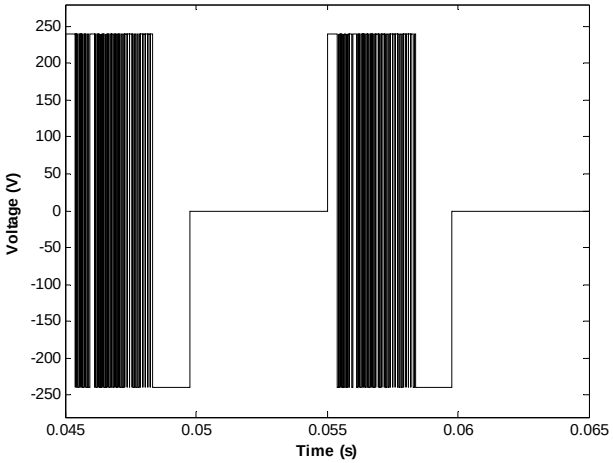

Fig. 4.5. Voltage of phase A during two cycles.

In Case 1: constant speed (1000rpm), constant load (20Nm), It is assumed that the temperature is constant (70.4°C) in this steady state. The phase resistance is 0.264 ohm. In Case 2: step change of speed (1000rpm to 1500rpm), constant load (20Nm), It is assumed that the temperature is constant during 0.05 and 0.1 second, phase temperature is 70.4°C. The phase resistance is 0.264 ohm. From 0.1s to 0.15s, the temperature increases linearly from 70.4°C to 87.5°C. The phase resistance increases linearly from 0.264 ohm to 0.278 ohm correspondingly. In Case 3:

constant speed (1000rpm), step change of load (40Nm to 20Nm), during 0.05 and 0.1 second, the temperature in the steady state is assumed to be 93.16°C. From 0.1s to 0.15s, the temperature decreases linearly from 93.16°C to 81.8°C. The phase resistance increases linearly from 0.284 ohm to 0.2748 ohm correspondingly. In industrial applications, the stator winding temperature could be calculated every few minutes to reduce calculation amount.

4.4.2. RESULTS ANALYSIS

Case 1: constant speed (1000rpm), constant load (20Nm)

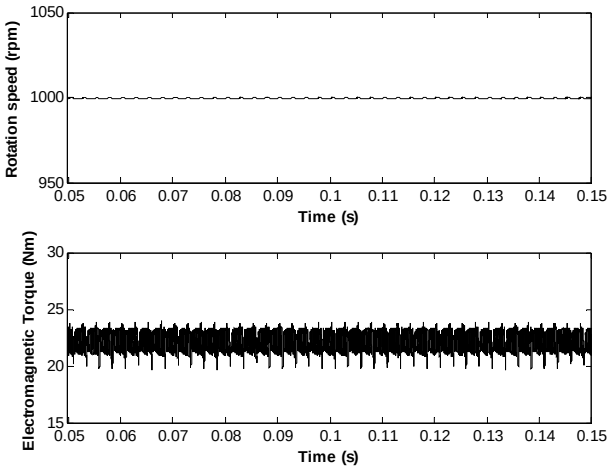

Fig. 4.6. The rotational speed and electromagnetic torque profiles of the SRM system in case 1.

The rotational speed and electromagnetic torque profiles of the SRM system are shown in Fig. 4.6. The speed controller is well designed and the rotational speed can be maintained at 1000 rpm with little error. The torque ripple is less than 20%, which is accepted for this kind of machine. The torque ripple could be reduced by optimizing the turn-on and turn-off angles which is not in the scope of this chapter.

The current, current integration, voltage and voltage integration profiles of phase A in the SRM system in case 1 are shown in Fig. 4.7. The voltage and current profiles are the same as the steady state discussion in section A. The integrations of current and voltage are reset at the turn-on occasion. The temperature of stator winding is estimated using equations (4.9) – (4.12), which is demonstrated in Fig. 4.8. Due to constant resistance of phase A in this case during the 0.15 second, the estimated phase resistance by (4.9) is exactly an accurate estimation.

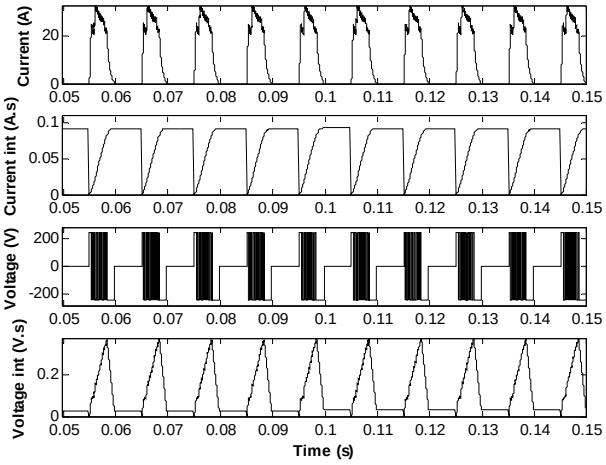

Fig. 4.7. The current, current integration, voltage and voltage integration profiles of phase A of the SRM system in case 1.

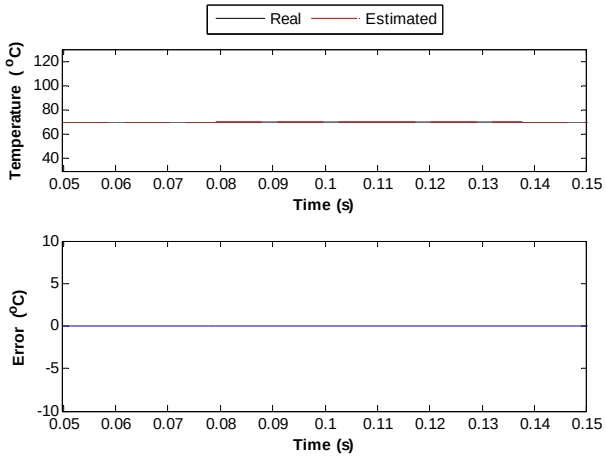

Fig. 4.8. The estimated temperature and error of stator winding in case 1.

Case 2: step change of speed (1000rpm to 1500rpm), constant load (20Nm)

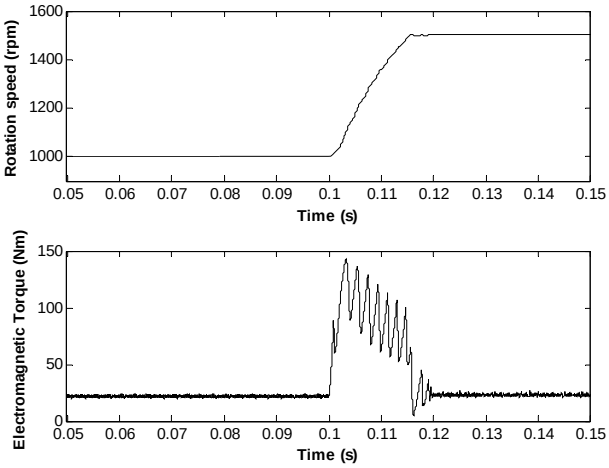

Fig. 4.9. The rotational speed and electromagnetic torque profiles of the SRM system in case 2.

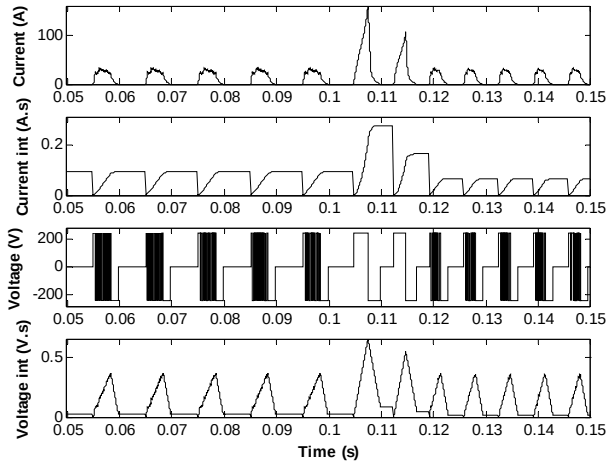

Fig. 4.10. The current, current integration, voltage and voltage integration profiles of phase A of the SRM system in case 2.

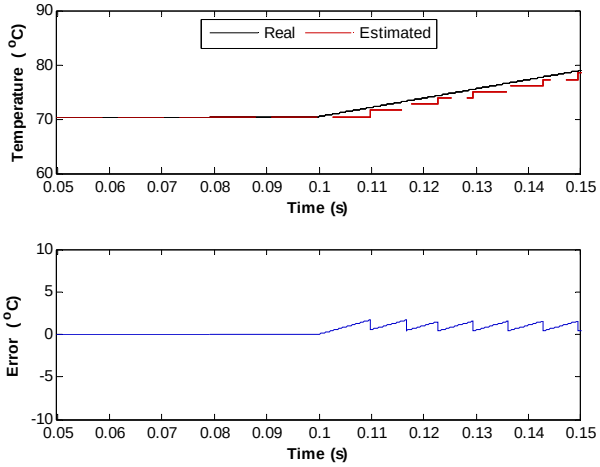

Fig. 4.11. The estimated temperature and error of stator winding in case 2.

A step change of rotational speed is imposed at 0.1 second in this case study. The response curve is shown in Fig. 4.9. The adjustment time of the speed controller is less than 0.02 second. The overshoot is very little and the response speed is very fast. The torque ripple is extremely large during the transient stage, which returns to normal after the rotational speed reaches a stable level around 1500 rpm.

In Fig. 4.10, the current, current integration, voltage and voltage integration profiles of phase A in the SRM system in case 2 is demonstrated. In the transient period, there are two cycles during which the phase A is charging consistently until the turn-off position. Phase A operates in single pulse mode during these two cycles.

The estimated temperature and error curve are shown in Fig. 4.11. Before the speed change, the proposed temperature estimation method can track the resistance and temperature without error, while the temperature has a ramp-up from 70.8°C after the step change of rotational speed. Because the estimated temperature can only be updated once in a cycle, a zero order holder is utilized for the interpolation between two updated points. Thus the error is relatively large, but it is still acceptable as the maximum error is only 2°C. It is observed that the estimated values are always lower than the real ones, which can be explained by (9), where we suppose that the resistance R is constant in a short period, in reality R is slowly rising up after 0.1 second, therefore the estimated value using (9) is lower than the real value.

Case 3: constant speed (1000rpm), step change of load (40Nm to 20Nm)

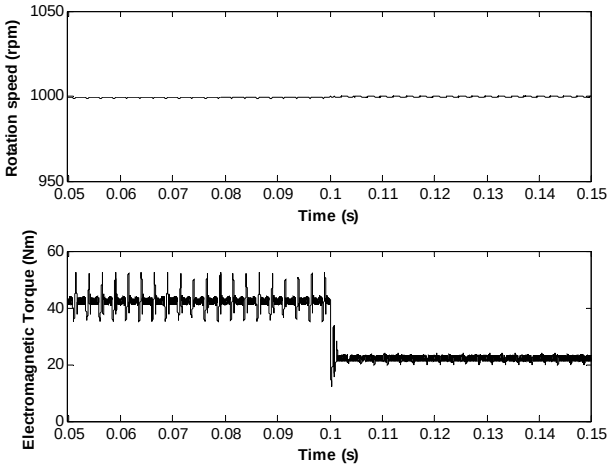

Fig. 4.12. The rotational speed and electromagnetic torque profiles of the SRM system in case 3.

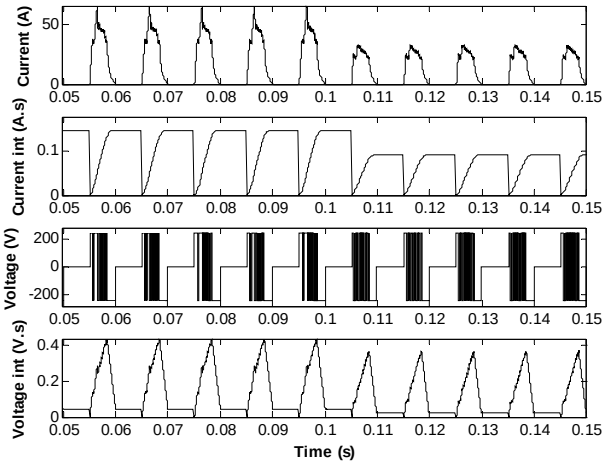

Fig. 4.13. The current, current integration, voltage and voltage integration profiles of phase A of the SRM system in case 3.

A step change of load torque from 40Nm to 20Nm at 0.1 second is presented in Fig. 4.12. The rotational speed is kept to be 1000 rpm in this case. The torque ripple before 0.1 second is over 40%, while it reduces to the same level of case 1 after 0.1 second. The current, current integration, voltage and voltage integration of phase A in the SRM system change dramatically at 0.1 second, which is shown in Fig. 4.13.

The estimated temperature and error in this circumstance are shown in Fig. 4.14. The proposed temperature estimation method can accurately estimate the resistance and temperature before the load change. Nonetheless, the temperature falls off from 93.2°C after 0.1 second due to load change. The estimation error becomes large owing to interpolation and zero order holding. It can be seen that the estimated values are always larger than the real ones. The reason is that the resistance of winding in phase A at t_{on} is larger than the resistance at t_2. The assumption of constant winding resistance introduces an incremental error to the resistance and temperature estimation.

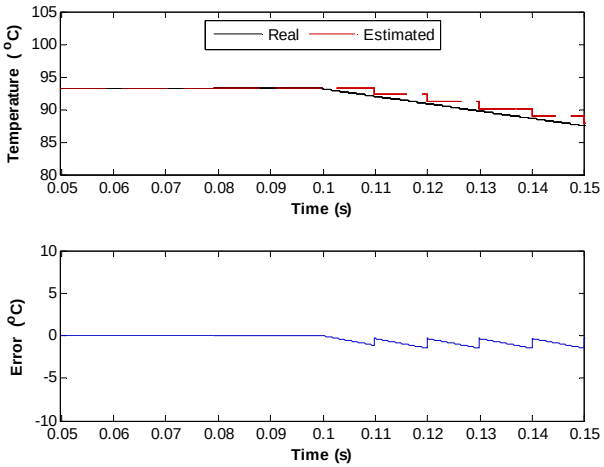

Fig. 4.14. The estimated temperature and error of stator winding in case 3.

4.5. SUMMARY

A novel approach for online thermal monitoring of stator winding of SRM without thermal sensors is presented in this chapter. The proposed approach has been verified with high accuracy under variable rotational speed and torque conditions. The stator winding itself has an additional function as a thermal sensor in this scheme. The accuracy of the winding temperature estimation may be affected by the resistance-temperature characteristic and the resolution and precision of the voltage and current measurements. It doesn't need parameters of the machine, it is nondestructive, and can be easily implemented in the machine control and monitoring system only by adding the temperature estimation algorithms in the software. It is cost-effective and has a vast application potential on the online condition monitoring and health management of SRMs.

BIBLIOGRAPHY

[1] IEC Standard 60034-1: Rotating electrical machines - Part 1: Rating and performance, Edition 12.0, 2010.

[2] IEC Standard 60085: Electrical insulation - Thermal evaluation and designation, Edition 4.0, 2007.

[3] P. Zhang, B. Lu, and T. G. Habetler, "A remote and sensorless stator winding resistance estimation method for thermal protection of soft-starterconnected induction machines," *IEEE Trans. Ind. Electron.*, vol. 55, no. 10, pp. 3611–3618, Oct. 2008.

[4] S. Inamura, T. Sakai, and K. Sawa,"A temperature rise analysis of switched reluctance motor due to the core and copper loss by FEM," *IEEE Trans. Magn.*, Vol. 39, no.3, pp. 1554–1557, May 2003.

[5] J. Faiz, B. Ganji, C. E. Carstensen, K. A. Kasper, and R. W. De Doncker, "Temperature rise analysis of switched reluctance motors due to electromagnetic losses," *IEEE Trans. Magn.*, vol. 45, no. 7, pp. 2927–2934, Jul. 2009.

[6] H. Chen, Y. Xu, and H. H. Iu, "Analysis of temperature distribution in power converter for switched reluctance motor drive," *IEEE Trans. Magn.*, vol. 48, no. 2, pp. 991–994, Feb. 2012.

[7] G. J. Li, J. Ojeda, E. Hoang, M. Lecrivain and M. Gabsi, "Comparative studies between classical and mutually coupled switched reluctance motors using thermal-electromagnetic analysis for driving cycles," *IEEE Trans. on Magn.*, pp. 839–846, Vol.47, No.4, Apr. 2011.

[8] S. B. Lee and T. G. Habetler, "A remote and sensorless thermal protection scheme for small line-connected ac machines," *IEEE Trans. Ind. Appl.*, vol. 39, no. 5, pp. 1323–1332, Sep./Oct. 2003.

[9] P. Zhang, Y. Du, B. Lu, and T. G. Habetler, "A DC signal injection-based thermal protection scheme for soft-starter-connected induction motors," *IEEE Trans. Ind. Appl.*, vol. 45, no. 4, pp. 1351–1358, Jul./Aug. 2009.

[10] D. Reigosa, F. Briz, P. Garcia, J. M. Guerrero, and W. Degner, "Magnet temperature estimation in surface PM machines using high-frequency signal injection," *IEEE Trans. Ind. Appl.*, vol. 46, no. 4, pp. 1468–1475, Jul./Aug. 2010.

[11] Boglietti, A. Cavagnino, M. Lazzari, and M. Pastorelli, "A simplified thermal model for variable-speed self-cooled industrial induction motor," *IEEE Trans. Ind. Appl.*, vol. 39, no. 4, pp. 945–952, Jul./Aug. 2003.

[12] P. Milanfar and J. H. Lang, "Monitoring the thermal condition of permanent-magnet synchronous motors," *IEEE Trans. Aerosp. Electron. Syst.*, vol. 32, no. 4, pp. 1421–1429, Oct. 1996.

[13] G. D Demetriades, H. Z. de la Parra, E. Andersson, and H. Olsson, "A real time thermal model of a permanent-magnet synchronous motor," *IEEE Trans. Power Electron.*, vol. 25, no. 2, pp. 463–474, Feb. 2010.

[14] L. He, S. Cheng, Y. Du, R. G. Harley, T. G. Habetler, "Stator temperature estimation of direct-torque-controlled induction machines via active flux or torque injection," *IEEE Trans. Power Electron*., vol. 30, no. 2, pp. 888–899, 2015.

[15] S. Cheng,Y. Du, J. A. Restrepo, P. Zhang, and T. G. Habetler, "A nonintrusive thermal monitoring method for induction motors fed by closed-loop inverter drives," *IEEE Trans. Power Electron*., vol. 27, no. 9, pp. 4122–4131, Sep. 2012.

[16] P. Zhang, B. Lu, and T. G. Habetler, "An active stator temperature estimation technique for thermal protection of inverter-fed induction motors with considerations of impaired cooling detection," *IEEE Trans. Ind. Appl*., vol. 46, no. 5, pp. 1873–1881, Sep./Oct. 2010.

[17] B. Nahid-Mobarakeh, F. Meibody-Tabar, and F. M. Sargos, "Mechanical sensorless control of PMSM with online estimation of stator resistance," *IEEE Trans. Ind. Appl*., vol. 40, no. 2, pp. 457–471, Mar./Apr. 2004.

[18] S. D. Wilson, P. Stewart, and B. P. Taylor, "Methods of resistance estimation in permanent magnet synchronous motors for real-time thermal management," *IEEE Trans. Energy Conver*., vol. 25, no. 3, pp. 698–707, Sep. 2010.

[19] D. A. Torrey, J.A. Lang, "Modelling a nonlinear variable-reluctance motor drive", *IEE Proceedings B-Electric Power Applications*, vol. 137, no. 5, pp. 314–326, Sept. 1990.

[20] D. A. Torrey, X. M. Niu, and E. J. Unkauf, "Analytic modeling of variable-reluctance machine magnetization characteristics,'' *IEE Proceedings B-Electric Power Applications,* vol. 142, no. 1, pp. 14–22, Jan. 1995.

.

CHAPTER 5. A FAULT DIAGNOSTIC METHOD FOR POSITION SENSOR OF SWITCHED RELUCTANCE WIND POWER GENERATORS[3]

Fast and accurate fault diagnosis of the position sensor is of great significance to ensure the reliability as well as sensor fault tolerant operation of the Switched Reluctance Generators (SRGs). This chapter presents a fault diagnostic scheme for a SRG based on the residual between the estimated rotor position and the actual output of the position sensor. Extreme Learning Machine (ELM), which could build a nonlinear mapping among flux linkage, current and rotor position, is utilized to design an assembled estimator for the rotor position detection. The data for building the ELM based assembled position estimator is derived from the magnetization curves which are obtained from Finite Element Analysis (FEA) of a SRG with the structure of 8 stator poles and 6 rotor poles. The effectiveness and accuracy of the proposed fault diagnosis method are verified by simulation at various operating conditions. The results provide a feasible theoretical and technical basis for the effective condition monitoring and predictive maintenance of SRGs.

5.1. INTRODUCTION

With the increasing concern on the reliability and cost, Switched Reluctance Generator (SRG) has been attracting more and more attentions from the wind power academia and industry. Unlike the most commonly used Doubly Fed Induction Generator (DFIG) and Permanent Magnet Synchronous Generator (PMSG) in wind energy conversion systems, there is no winding or magnet on the rotor of SRG, in addition, each phase is independent of each other in terms of structure and electromagnetism. These significant features help SRG possess high reliability and good fault tolerant ability, making SRG a candidate for the next generation variable speed wind generator [1-7].

Although Switched Reluctance Machine (SRM) has a robust structure and high fault tolerant ability, it does not mean that it is fault free. The relatively vulnerable parts in a SRM are stator windings, power transistors, bearings and sensors. There are

[3] This chapter is based on the paper which was originally published with following details.
[C. Wang, X. Liu, H. Liu, and Z. Chen, "A Fault Diagnostic Method for Position Sensor of Switched Reluctance Wind Turbine Generators," Journal of Electrical Engineering & Technology. vol. 11, no. 1, Jan. 2016.], materials are reused with permission from KIEE.

some researches on Fault Detection and Diagnosis (FDD) of winding, power converter and bearing of SRM [8-12] but very few publications about the position sensor FDD [13]. Although it is a trend that the position sensor will be eliminated with the mature of sensorless control technology [15-19], most SRMs still have position sensors in a considerable period of time. When the position sensor fails, the system should be able to detect it and then switch to the backup sensor or execute proper system reconfiguration and fault tolerant control. Thus the fast and accurate fault diagnosis of the position sensor is essential to ensure the reliability as well as sensor fault tolerant operation of the SRG.

Reference [13] proposed a square wave position edge prediction method for the position signal fault diagnosis and position faults recovery of SRM. However, the position sensor system investigated in this chapter is three optical encoders based measurement system, which may limit the application scope of this approach. Despite few investigations of position sensor FDD, the rotor position estimation of SRM from which the sensor health status can be inferred has been studied a lot [15-27]. One possible solution for position sensor FDD in SRM which widely used in control theory community is to extract and analyze the residual between the actual output and the estimated output if this estimated value is accurate enough [28]. Flux-current characteristics method, which is first proposed by [17], is the most popular method for rotor position estimation in medium and high speed operating of SRM. Flux linkage-current-angle relationship data is stored in a 2D lookup table which is used to estimate the rotor angle. The drawback of this method lies in occupation of mass software and hardware resources as well as long computing time due to table searching and interpolation processing. In order to overcome these shortcomings, plenty of nonlinear approximation solutions have been developed in the last decades based on the basic idea of flux linkage-current-angle characteristics of SRM. These solutions include fuzzy logic [17-21], Back-Propagation (BP) neural networks, Radial Basis Function (RBF) neural networks, adaptive neuro-fuzzy inference system [22-25]. The above methods substitute fuzzy or neural network models for the 2D lookup tables, which release large amount of memory. However, the fuzzy logic rules in the fuzzy logic model are massive and require experience to create, meanwhile, most artificial neural networks models are based on iterative learning algorithm which is time consuming and hard to achieve global optimum.

This chapter presents a fault diagnostic approach for position sensor in SRG based on the residual between the actual output of the position sensor and the estimated rotor position which is obtained from an assembled estimator. Section 5.2 gives the position sensor fault pattern analysis of the SRG. Section 5.3 presents the procedure of magnetization characteristics acquisition via FEA. The rotor position estimation of SRG based on Extreme Learning Machine (ELM) is proposed in section 5.4. Section 5.5 illustrates the fault diagnostic approach for position sensor in SRG based on analysis of the residual. The performance of the proposed approach is verified

under various operating conditions and sensor fault scenarios. Section 5.6 presents the conclusion of this chapter.

5.2. POSITION SENSOR FAULT PATTERN ANALYSIS OF SRG

5.2.1. POSITION SENSOR OF SRG

Accurate rotor position information is indispensable for the SRG to determine the conducting phase/phases and turn-on/turn-off angles to achieve desired control performance. A typical wind power generation system configuration with SRG is depicted in Fig. 5.1, the position sensor measures the position angle of high speed shaft of the gearbox and feedbacks this signal to the controller of the asymmetric half bridge converter. The common used position sensors are optical encoders, hall-effect sensors and magnetic resolvers [13-14].

5.2.2. POSITION SENSOR FAULT ANALYSIS

Owning to the harsh environments most Wind Energy Conversion Systems (WECS) usually work in, especially for offshore occasions, the position sensors are fragile under long-time extreme temperature, high humidity and salt mist conditions. In dusty environment, the optical encoders tend to be affected and may lost signals, while the hall-effect sensors are more susceptible to temperature.

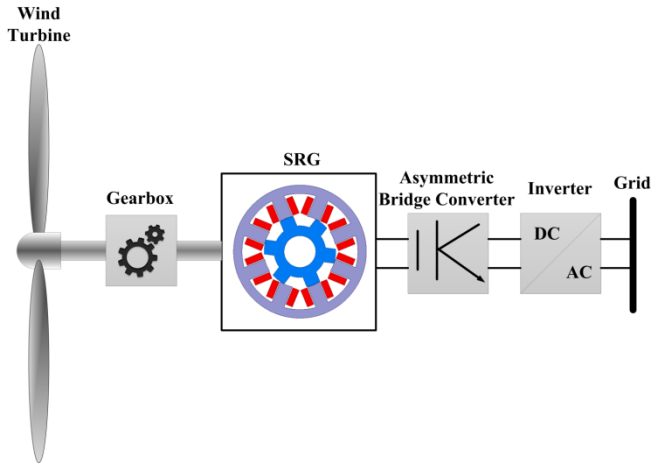

Fig. 5.1. A typical wind power generation system configuration with switched reluctance generator.

Moreover, the magnetic resolvers are quite easily disturbed by electromagnetic radiation which is abundant in the nacelle of WECS. In addition, the transmission

channel, the power source and the related modulation and measurement circuits of the position signal may also be intervened by the external electromagnetism sources.

Thus the above mentioned factors may eventually result in intermittent or permanent faults in the software or hardware of the rotor position sensing systems. The false signals from the faulty rotor position sensor may affect the normal function of the feedback loop and the control system of the WECS. The incipient sensor fault could influence the power generation capacity of the WECS, while more serious sensor faults may lead to catastrophic failures of the WECS.

5.3. MAGNETIZATION CHARACTERISTICS ACQUISITION VIA FEM

Magnetization characteristics, which demonstrate the relationship among flux linkage, phase current and rotor position, is the foundation for rotor position estimation. 2D finite element model of a 7.5kw 8/6 poles four-phase SRG is developed using ANSYS MAXWELL to obtain the magnetization characteristics.

The fully unaligned position is defined as 0°, while the fully aligned position is 30°. The distributions of the flux line at the fully unaligned and aligned positions are shown in Fig. 5.2. Fig. 5.3 displays the magnetic curve clusters of phase A with the rotor position interval of 1.2°. As can be seen in Fig. 3, the flux linkage rises monotonically with the increase of phase current at each position. When the phase current reaches to certain extent, the variation tendency of the flux linkage is becoming unapparent owning to the flux saturation. At each fixed phase current, the flux linkage increases while the rotor position rotates from the fully

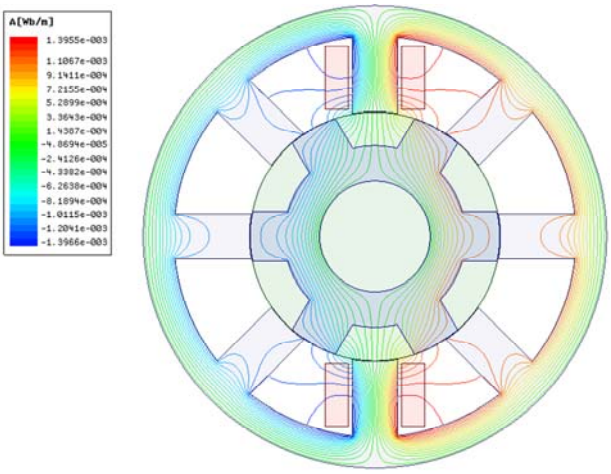

(a)

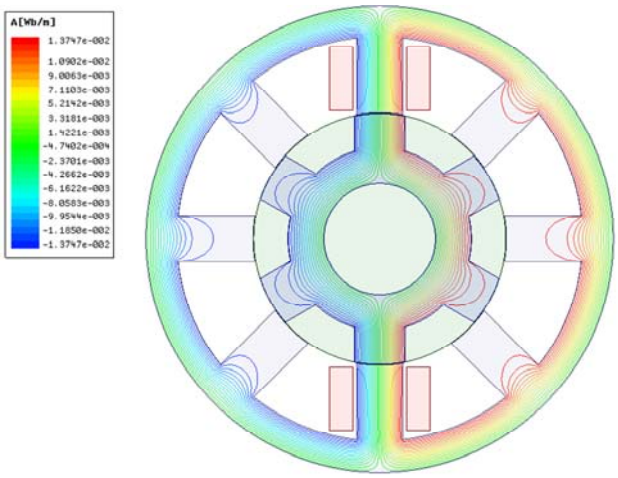

(b)

Fig. 5.2. Flux line distribution at different positions, (a) fully unaligned position, (b) fully aligned position.

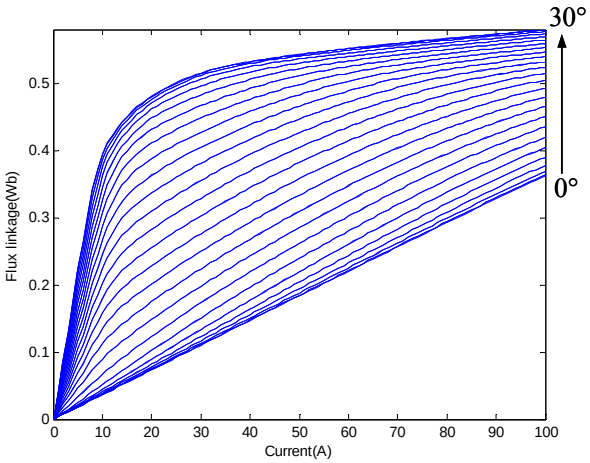

Fig. 5.3. The magnetic curve clusters of the studied SRG.

unaligned position (0°) to aligned position (30°). Near the fully aligned position, the relationship between flux linkage and phase current is nonlinear, on the other hand, there is a nearly linear relationship between flux linkage and phase current near the fully unaligned position.

5.4. ROTOR POSITION ESTIMATION OF SRG BASED ON ELM

5.4.1. EXTREME LEARNING MACHINE

Single hidden layer feedforward neural networks (SLFNs) which have universal approximation ability are widely used in state estimation of electrical machines. Traditional parameter optimization of the SLFNs is based on iterative methods. Gradient descend methods, such as the most commonly used BP algorithm, are used to guide the learning process of parameters tuning iteratively with the training data. These methods are usually time-consuming and hard to get the global optimal solutions. ELM is a recently developed novel learning algorithm for training the SLFNs [29-31]. The name 'ELM' also refers to the SLFNs trained by this algorithm. Thus in the following parts of this chapter, ELM may be either of the two meanings. The only preset parameter of ELM is the number of hidden layer neurons. It is no need to tune the weights and threshold parameters in the learning process of ELM algorithm, the unique optimal parameters can be obtained analytically via simple matrix computations. Thus it offers significant superiorities in term of fast training speed, easy to implement, good generalization ability as well as minimal human involvement.

ELM has been used in power system applications to solve the prediction and state evaluation problems [32-33]. The key principle of ELM for rotor position estimation of SRG is given as follows.

Suppose $\{\boldsymbol{x}_i, \boldsymbol{y}_i\}_{i=1}^{N}$ is n sample dataset of a nonlinear system, where $\boldsymbol{x}_i \in \boldsymbol{R}^n$ with $\boldsymbol{x}_i = [x_{i1}, x_{i2}, \dots, x_{in}]^T$, $\boldsymbol{y}_i \in \boldsymbol{R}^m$ **with** $\boldsymbol{y}_i = [y_{i1}, y_{i2}, \dots, y_{im}]^T$, n, m is the dimension of $\boldsymbol{x}_i$, $\boldsymbol{y}_i$, respectively. The goal is to approximate a model in the form of,

$$f(\boldsymbol{x}_j) = \sum_{i=1}^{K} \boldsymbol{\beta}_i \, g(\boldsymbol{\omega}_i \cdot \boldsymbol{x}_j + b_i), \qquad j = 1, \dots, N \tag{5.1}$$

where $\boldsymbol{\omega}_i = [\omega_{i1}, \omega_{i2} \dots, \omega_{in}]^T$ is the weight vector connecting the i th hidden neuron and the input neurons, $\boldsymbol{\beta}_i = [\beta_{i1}, \beta_{i2} \dots, \beta_{in}]^T$ is the weight vector connecting the ith hidden neuron and the output neurons, b_i is the threshold of the ith hidden neuron, $g(x)$ is the activation function, K is the number of hidden neurons of ELM.

The ELM can approximate these N samples with zero error means that $\sum_{j=1}^{K} \| f(\boldsymbol{x}_j) - \boldsymbol{y}_j \| = 0$,

$$\sum_{i=1}^{K} \boldsymbol{\beta}_i \, g(\boldsymbol{\omega}_i \cdot \boldsymbol{x}_j + b_i) = \boldsymbol{y}_j, \qquad j = 1, \dots, N \tag{5.2}$$

The above equations can be rewritten in a compact form,

$$\boldsymbol{G\beta} = \boldsymbol{Y} \tag{5.3}$$

where

$$\boldsymbol{G} = \begin{bmatrix} g(\boldsymbol{\omega}_1 \cdot \boldsymbol{x}_1 + b_1) & \cdots & g(\boldsymbol{\omega}_K \cdot \boldsymbol{x}_1 + b_K) \\ \vdots & \ddots & \vdots \\ g(\boldsymbol{\omega}_1 \cdot \boldsymbol{x}_N + b_1) & \cdots & g(\boldsymbol{\omega}_K \cdot \boldsymbol{x}_N + b_K) \end{bmatrix}_{N \times K}$$

$$\boldsymbol{\beta} = [\boldsymbol{\beta}_1 \quad \cdots \quad \boldsymbol{\beta}_K]^{\boldsymbol{T}}$$

$$\boldsymbol{Y} = [\boldsymbol{y}_1 \quad \cdots \quad \boldsymbol{y}_K]^{\boldsymbol{T}}$$

here $\boldsymbol{G}$ is the hidden-layer output matrix of the SLFN, while $\boldsymbol{\beta}$ is the output weight matrix, $\boldsymbol{Y}$ is the target matrix.

The smallest norm least squares solution of the above regression system is

$$\widehat{\boldsymbol{\beta}} = \boldsymbol{G}^{\dagger}\boldsymbol{Y} \tag{5.4}$$

where $\boldsymbol{G}^{\dagger}$ is the Moore-Penrose generalized inverse of matrix $\boldsymbol{G}$. The $\boldsymbol{G}^{\dagger}$ can be obtained via Singular Value Decomposition (SVD).

Thus the estimated output of the regression system $f(\boldsymbol{x}_j)$ can be expressed as,

$$\boldsymbol{F} = \boldsymbol{G}\widehat{\boldsymbol{\beta}} = \boldsymbol{G}\boldsymbol{G}^{\dagger}\boldsymbol{Y} \tag{5.5}$$

The Mean Square Error (MSE) of the regression system is,

$$\|\boldsymbol{e}\|^2 = \frac{1}{N}\|\boldsymbol{F} - \boldsymbol{Y}\|^2 = \frac{1}{N}\left\|\boldsymbol{G}\boldsymbol{G}^{\dagger}\boldsymbol{Y} - \boldsymbol{Y}\right\|^2 \tag{5.6}$$

5.4.2. ROTOR POSITION ESTIMATION OF SRG

The voltages and currents of the four phase windings will be delivered to a flux linkage calculator to calculate the flux linkage of each phase. If the leakage inductance between the phases is neglected, the flux linkage of the phase *k* can be calculated by,

$$\psi_k(t) = \int_0^t (u_k - R_k i_k)dt + \psi_k(0), k = 1,2,\ldots,4 \tag{5.7}$$

where u_k , R_k , i_k are the phase voltage, phase resistance and phase current respectively. Then the current and flux linkage will be input to the corresponding

ELM position estimator. There are four ELM estimators, each of which works in its own best estimation region. This will be introduced in detail in the next section.

Offline training and online estimation strategy, which may improve the efficiency of the ELM, is used in this study. After the training process, all the weights and biases parameters of the ELM rotor position estimator are determined. These parameters are configured into the online ELMs for real time rotor position estimation.

5.5. POSITION SENSOR FAULT DIAGNOSIS AND RESULTS ANALYSIS

5.5.1. SIMULATION

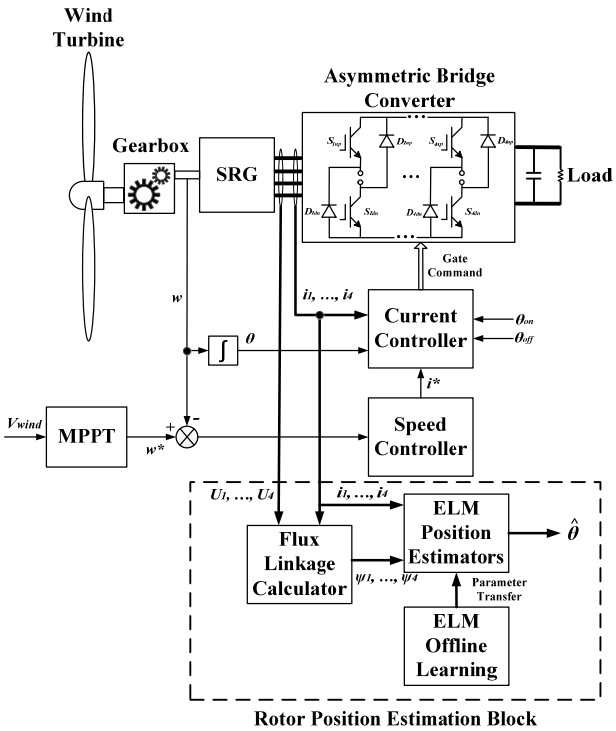

Fig. 5.4. Configuration of the SRG system and the rotor position estimation module.

The configuration of the studied 7.5kw 8/6 poles four-phase SRG system is demonstrated in Fig. 5.4. The current chopping control strategy is deployed in the simulation for the current control, the hysteresis band width is ±3A. The DC exciting voltage is 120V. Due to the generating mode of SRM, the turn-on and turn-

off angles are set to be 30° and 60°. The nominal rotor speed is 1000 rpm while the nominal wind speed is 12m/s. The simulation is implemented in Matlab/Simulink® environment. Each phase is working on the current chopping mode with the reference current 62.5A and the hysteresis band width ±3A. Adjacent phases have a phase shift of 15°.The optimal rotor speed of the SRG is determined by referring to the wind speed to extract the maximum power from the wind [34], which is shown in Fig. 5.5.

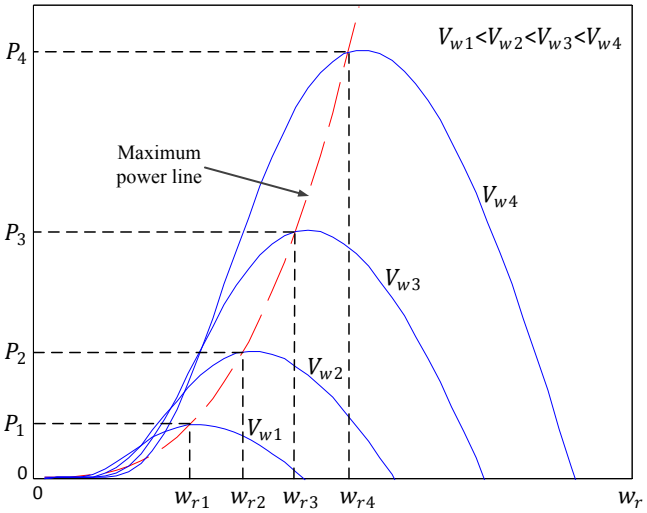

Fig. 5.5. Maximum power point tracking.

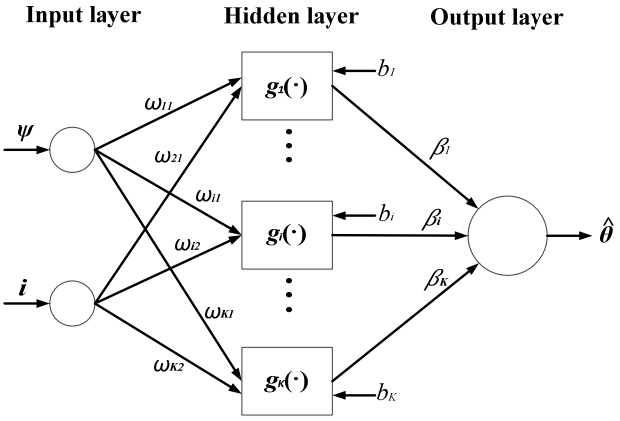

Fig. 5.6. Structure of the ELM position estimator.

1299 samples are collected from the flux linkage-current-angle relationship. The input weights $\boldsymbol{\omega}_i$ and bias $\boldsymbol{b}_i$ are generated randomly, the output weights $\boldsymbol{\beta}_i$ are analytically calculated using the extremely fast ELM. The structure of the ELM position estimator is illustrated in Fig. 5.6. There are two neurons in the input layer, one neuron in the output layer. Sigmoid activation function is used in this study. The number of neurons in the hidden layer is 500. It takes only 0.8292s to learn the 1299 samples, which is almost impossible for other iterative algorithms given the same hardware conditions. The ELM estimator only has the angle estimation range of 30° which is restricted to the magnetic characteristics. Thus, when the current and flux linkage of certain phase are nonzero, they could be used for the ELM to estimate a 30° range of the rotor angle.

Three types of sensor faults are simulated in this study to verify the effectiveness of the proposed diagnosis method. The faults include bias fault, drifting fault and intermittent fault. The bias fault is simulated by adding a constant shift to the output of the position sensor. A monotone increase is superimposed to the sensing signal to simulate the drifting fault. For the intermittent fault, a narrow bandwidth long flat-top pulse is imposed on the sensor's output.

5.5.2. RESULT ANALYSIS

The estimation results of the four separate ELMs when the wind speed is 12 m/s and the generator speed is 1000 rpm are show in Fig. 5.7. Theoretically, only two phases with 30° phase shift (such as phase C and A) is enough to estimate the whole 60° angle cycle. However, as can be seen in Fig. 5.8, the estimation results are undesirable, which is due to the nonlinear magnetization characteristics of the SRG. As shown in Fig. 5.3, the magnetic curves near the aligned, unaligned as well as low current regions are crowed together or even intersecting, which may reduce the accuracy of even advanced estimation algorithms. For the intersection points in the magnetic curves, it is impossible to estimate the rotor position precisely only using flux linkage-current-angle relationship because of the non-unique mapping. In fact, there is a distinguished region among the aligned, unaligned and the certain current and flux linkage range for rotor position estimation, which results in the relatively accurate estimation range of about 20° shown in Fig. 5.7. Therefore, 15° sensitive region of each ELM is selected to contribute the whole 60° range angle estimation. To be specific, ELM1 is responsible for estimation of 41° - 55°, ELM2 takes charge of angle span of 56° - 10°, ELM3 is used to evaluate the position between 11° - 25°, ELM4 is in charge of 26° - 40°. The improved results are demonstrated in Fig. 5.8. The estimated rotor angle is very close to the real rotor position as shown in Fig. 5.8.

The detailed estimation results under various operating conditions are presented in the following section.

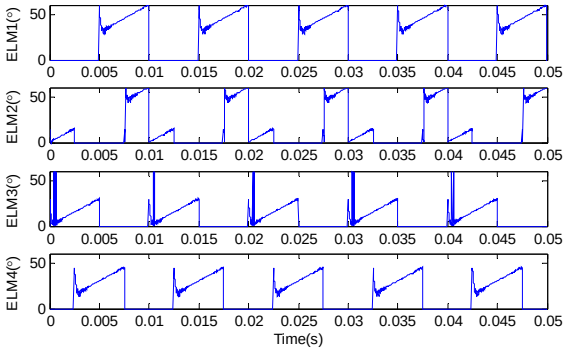

Fig. 5.7. Outputs of ELM estimators.

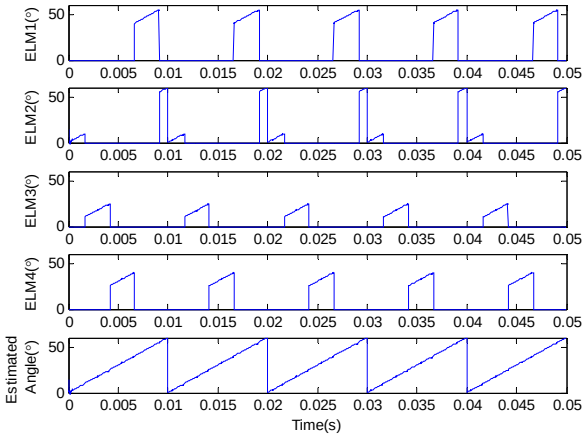

Fig. 5.8. Outputs of the improved assembled ELM estimators and estimated rotor angle.

The assembled ELM estimation results under different operating conditions are shown in Fig. 5.9, Fig. 5.10 and Fig. 5.11, respectively.

Table 5.1. The ELM estimation error at different operating conditions

	Operating Condition (wind speed, m/s)		
	8 (667rpm)	12 (1000rpm)	6-12 (500-1000rpm)
MAE (°)	0.7273	0.5748	2.3633
RMSE (°)	0.1949	0.1617	0.2870

In the case of 12 m/s wind speed, the generator speed is 1000 rpm. As shown in Fig. 5.8(b), the Maximum Absolute Error (MAE) of ELM estimation is 0.5748°, the Root Mean Squared Error (RMSE) is 0.1617°. The MAE and RMSE are both higher with 8 m/s wind speed. As the wind speed increases linearly from 6 to 12 m/s, the generator speed increases from 500 to 1000 rpm, the estimation error is bigger in the low speed stage. The MAE and RMSE results are presented in Tab. 5.1. Although the MAE in the 500 to 1000 rpm acceleration operating condition is relatively larger, the RMSEs are very low (no greater than 0.3°) in all the three operation conditions which indicate the overall estimation performance of the proposed method is good.

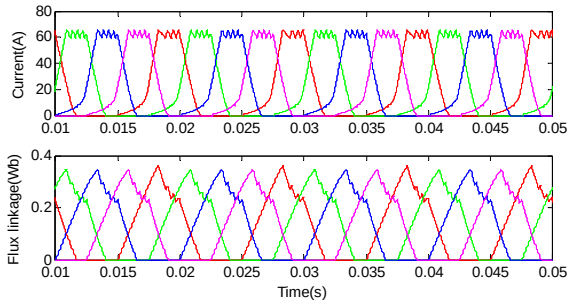

(a)

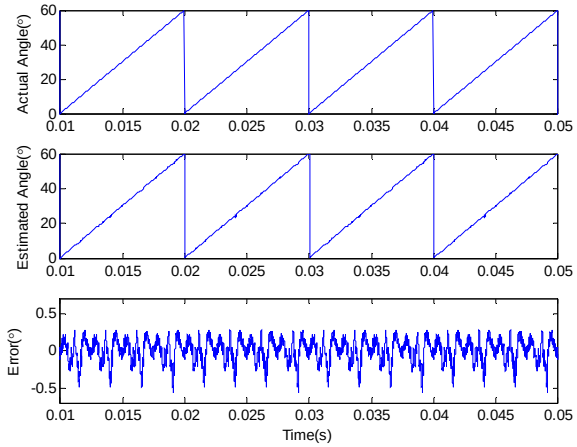

(b)

Fig. 5.9. Assembled ELM estimation result when wind speed is 12m/s ($w_r = 1000$) rpm, (a) current and flux linkage waveforms, (b) estimation result.

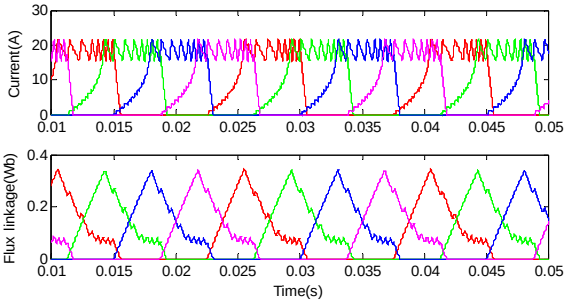

(a)

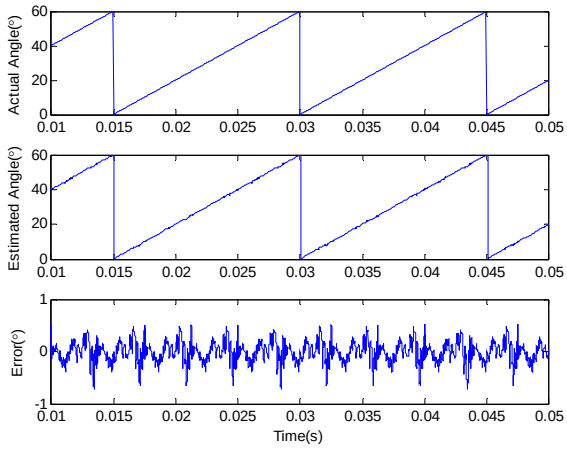

(b)

Fig. 5.10. Assembled ELM estimation result when wind speed is 8m/s ($w_r = 667$) rpm, (a) current and flux linkage waveforms, (b) estimation result.

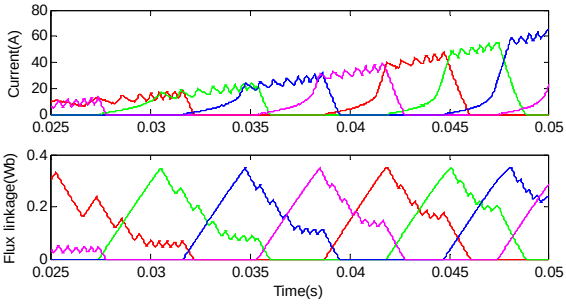

(a)

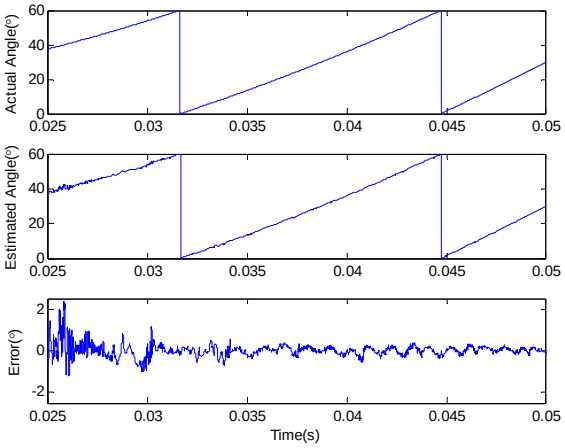

(b)

Fig. 5.11. Assembled ELM estimation result when wind speed from 6 m/s to 12 m/s, w_r from 500 to 1000 rpm, (a) current and flux linkage waveforms, (b) estimation result.

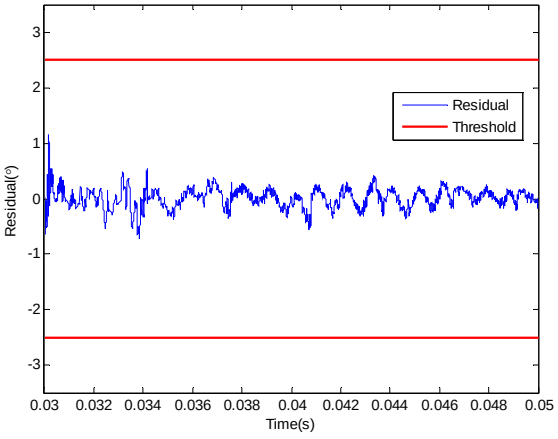

Fig. 5.12. Residual under normal sensor condition when wind speed from 6 m/s to 12 m/s.

It is noted that the MAEs in the cases of 8 m/s wind speed and 12 m/s wind speed conditions always appear when the corresponding current and flux linkage are in the transitional area between the distinguished and crowed regions of the magnetization characteristic curve, which may affect the performance of the ELM estimators. However, 0.7273° and 0.5748° of MAE are satisfying for position estimation. For the wind speed increasing from 6 to 12 m/s operating condition, the MAE is

2.3633°, the relative large errors are all appear before 700 rpm (0.035s).

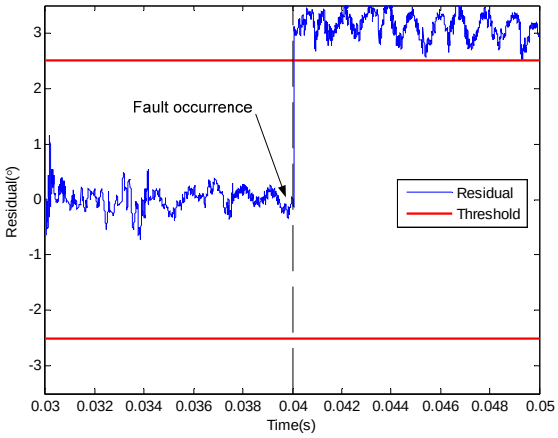

Fig. 5.13. Residual under sensor bias fault condition when wind speed from 6 m/s to 12 m/s.

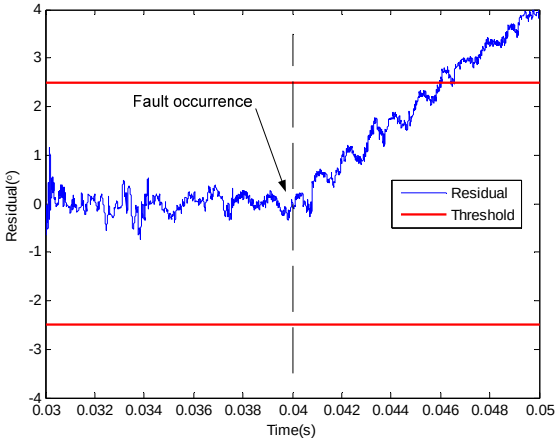

Fig. 5.14. Residual under sensor drifting fault condition when wind speed from 6 m/s to 12 m/s.

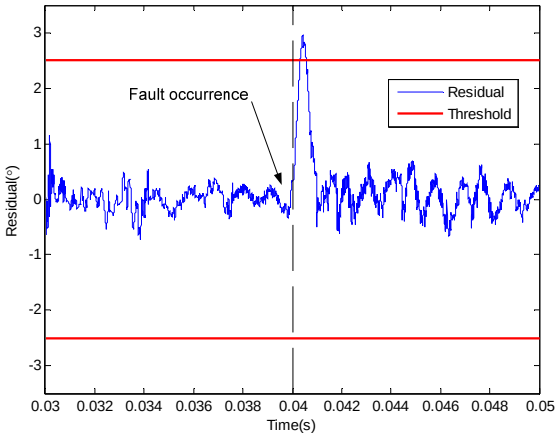

Fig. 5.15. Residual under sensor intermittent fault condition when wind speed from 6 m/s to 12 m/s.

The corresponding current and flux linkage in this case are in the crowed region of the magnetization characteristic curve which is inevitable in this operation condition.

The residual generated under normal sensor condition when wind speed varies from 6 m/s to 12 m/s is shown in Fig. 5.12. The residual generated under the bias fault, drifting fault and intermittent are demonstrated in Fig. 5.13, 5.14, and 5.15, respectively. Since the MAE is 2.3633° in this variable speed operating condition which is shown in Table 5.1, the threshold to determine the normal/abnormal status of the sensor is set to be ±2.5°. As can be seen in Fig. 5.12, the residual from 0.03s to 0.05s when the sensor is healthy and the wind speed is variable has little variations which are all within the threshold range.

As shown in Fig. 5.13, the bias fault occurs at 0.04s until 0.05s, the generated residual has a rapid rise and exceeds the set upper threshold of 2.5° quickly just after the occurrence of this sensor fault. It is observed that the average residual fluctuation also has a slight increase compared with the normal case.

Fig. 5.14 presents the residual curve under sensor drifting fault condition when wind speed from 6 m/s to 12 m/s. The residual in the drifting fault occasion keeps gentle increase between 0.03s and 0.05s. The fault residual reaches and passes the upper threshold at about 0.046s. The fault alarm can be triggered at around 0.047s dependent on the setting.

As is described in Fig. 5.15, a peak pulse of the residual is produced between 0.04s and 0.041s in the intermittent sensor fault circumstance when wind speed from 6 m/s to 12 m/s. It is noted that the average residual fluctuation also has an increase compared with the normal case.

To summarize, when the rotor position sensor has a fault, the output of the sensor can't represents the real rotor position while the proposed assembled ELM estimator can still estimate the rotor position in a high accuracy, which generates residuals. Once the residual exceeds the set threshold, the fault alarm can be triggered which indicates the fault is detected. By analyzing the generated residuals, different kinds of rotor position fault are identified. According to the simulation and results analysis, the common faults such as bias fault, drifting fault and intermittent fault have been detected and diagnosed accurately by using the proposed position sensor fault diagnostic scheme.

5.6. SUMMARY

This chapter presents a novel rotor position sensor fault diagnostic scheme for SRG based on assembled ELM. Simulation results show that the learning speed of ELM is extremely fast, the rotor position estimation accuracy is also very high with the best RMSE of 0.1617°. The sensor faults including bias fault, drifting fault and intermittent fault have been detected and diagnosed accurately by using the proposed position sensor fault diagnostic approach. The rotor position estimation method as well as sensor fault diagnostic scheme proposed in this chapter are of great significance for cost reduction, reliability improvement and predictive maintenance of SRG. It has vast potentials in the application of virtual sensor, position sensor redundancy, sensor-less control and sensor fault tolerant control of SRG.

BIBLIOGRAPHY

[1] D. A. Torrey, "Variable-reluctance generators in wind-energy systems," in *Proc. IEEE PESC'93*, 1993, pp. 561–567.

[2] R. Cardenas, W. F. Ray, and G. M. Asher, "Switched reluctance generators for wind energy applications," in *Proc. IEEE PESC'95*, 1995, pp. 559–564.

[3] K. Park and Z. Chen, "Self-tuning fuzzy logic control of a switched reluctance generator for wind energy applications," in *Proc. IEEE 3rd Int. Symp. Power Electron. Distrib. Gener. Syst.*, 2012, pp. 357–363.

[4] R. Cardenas, R. Pena, M. Perez, J. Clare, G. Asher, and P. Wheeler, "Control of a switched reluctance generator for variable-speed wind energy applications," *IEEE Trans. Energy Convers.*, vol. 20, no. 4, pp. 781–791, Dec. 2005.

[5] E. Echenique, J. Dixon, R. Cardenas, and R. Pena, "Sensorless control for a switched reluctance wind generator, based on current slopes and neural networks," *IEEE Trans. Ind. Electron*., vol. 56, no. 3, pp. 817–825, Mar. 2009.

[6] S. Mendez, A. Martinez, W. Millan, C. E. Montano, and F. Perez-Cebolla, "Design, Characterization, and Validation of a 1-kW AC Self-Excited Switched Reluctance Generator," *IEEE Trans. Ind. Electron*., vol. 61, no. 2, pp. 846–855, Feb. 2014.

[7] D. A. Torrey, "Switched reluctance generators and their control," *IEEE Trans. Ind. Electron*., vol. 49, no. 1, pp. 3–14, Feb. 2002.

[8] H. Chen and S. Lu, "Fault diagnosis digital method for power transistors in power converters of switched reluctance motors," *IEEE Trans. Ind. Electron.*, vol. 60, no. 2, pp. 749–763, 2013.

[9] S. Gopalakrishnan, A. M. Omekanda, and B. Lequesne, "Classification and Remediation of Electrical Faults in the Switched Reluctance Drive", *IEEE Trans. Ind. Appl.*, vol. 42, no. 2, 2006, pp.479–486.

[10] B. Schinnerl and D. Gerling, "Analysis of winding failure of switched reluctance motors," in *Proc. IEEE IEMDC'09*, 2009, pp. 738–743.

[11] J. F. Marques, J. O. Estima, N. S. Gameiro, and A. J. M. Cardoso, "A New Diagnostic Technique for Real-Time Diagnosis of Power Converter Faults in Switched Reluctance Motor Drives," *IEEE Trans. Ind. Appl.*, vol. 50, no. 3, pp. 1854–1860, May./Jun. 2014.

[12] H. Torkaman and E. Afjei, "Comprehensive detection of eccentricity fault in switched reluctance machines using high frequency pulse injection," *IEEE Trans. Power Electron.*, vol. 28, pp.1382 -1390, 2013.

[13] J. Cai, Z. Q. Deng, and R. G. Hu, "Position Signal Faults Diagnosis and Control for Switched Reluctance Motor," *IEEE Trans. Magn*., Early Access Article, 2014.

[14] G. Scelba, G. De Donato, F. Bonaccorso, G. Scarcella, F. Giulii Capponi, "Fault Tolerant Rotor Position and Velocity Estimation Using Binary Hall-Effect Sensors for Low Cost Vector Control Drives," *IEEE Trans. Ind. Appl.*, Early Access Article, 2014.

[15] M. Ehsani and B. Fahimi, "Elimination of position sensors in switched reluctance motor drives: State of the art and future trends," *IEEE Trans. Ind. Eletron.*, vol. 49, no. 1, pp.40–47, Feb. 2002.

[16] I. H. Al-Bahadly, "Examination of a sensorless rotor position measurement method for switched reluctance drive", *IEEE Trans. Ind. Eletron.*, vol. 55, no. 1, pp. 288–295, 2008.

[17] L. Xu and C. Wang, "Accurate rotor position detection and sensorless control of SRM for super-high speed operation," *IEEE Trans. Power Electron.*, vol. 17, no. 5, pp. 757–763, 2002.

[18] J. P. Lyons, S. R. MaHMinn, and M. A. Preston, "Flux-current methods for SRM rotor position estimation," in *Proc. Conf. Rec. IEEE-IAS Annu. Meeting*, 1991, pp. 482–487.

[19] A. D. Cheok and N. Ertugrul, "High robustness and reliability of fuzzy logic based position estimation for sensorless switched reluctance motor drives," *IEEE Trans. Power Electron.*, vol. 15, no. 2, pp.319–334, 2000.

[20] A. D. Cheok and Z. F. Wang, "Fuzzy logic rotor position estimation based switched reluctance motor DSP drive with accuracy enhancement," *IEEE Trans. Power Electron.*, vol. 20, no. 4, pp. 908–921, 2005.

[21] N. Ertugrul and A. D. Cheok, "Indirect angle estimation in switched reluctance motor drive using fuzzy logic based motor model," *IEEE Trans. Power Electron.*, vol. 15, no. 6, pp. 1029–1044, 2000.

[22] A. D. Cheok and N. Ertugrul, "Use of fuzzy logic for modeling, estimation, and prediction in switched reluctance motor drives," *IEEE Trans. Ind. Electron.*, vol. 46, no. 6, pp. 1207–1224, 2000.

[23] A. D. Cheok and N. Ertugrul, "High robustness of an SR motor angle estimation algorithm using fuzzy predictive filters and heuristic knowledge-based rules," *IEEE Trans. Ind. Electron.*, vol. 46, no. 5, pp. 904–916, 2000.

[24] E. Mese and D. A. Torrey, "An approach for sensorless position estimation for switched reluctance motors using artificial neural networks," *IEEE Trans. Power Electron.*, vol. 17, no. 1, pp. 66–75, 2002.

[25] L. Henriques , L. Rolim , W. Suemitsu , J. Dente and P. Branco, "Development and experimental tests of a simple neuro-fuzzy learning sensorless approach for switched reluctance motors, " *IEEE Trans. Power Electron.*, vol. 26, no. 11, pp. 3330–3344, 2011.

[26] S. Paramasivam, S. Vijayan, M. Vasudevan, R. Arumugam, and R. Krishnan, "Real-time verification of AI based rotor position estimation techniques for a 6/4 pole switched reluctance motor drive," *IEEE Trans. Magn.*, vol. 43, no. 7, pp. 3209–3221, 2007.

[27] C. A. Hudson, N. S. Lobo, and R. Krishnan, "Sensorless control of single switch-based switched reluctance motor drive using neural network," *IEEE Trans. Ind. Electron.*, vol. 55, no. 1, pp. 321–329, 2008.

[28] R. Isermann, "Model-based fault-detection and diagnosis–Status and applications," *Annu. Rev. Control*, vol. 29, no. 1, pp.71–85, 2005.

[29] G. B. Huang, Q. Y. Zhu, and C. K. SiewK, "Extreme learning machine: Theory and applications," *Neurocomputing*, vol. 70, nos. 1–3, pp. 489–501, Dec. 2006.

[30] N. Y. Liang, G. B. Huang, P. Saratchandran, and N. Sundararajan, "A fast and accurate online sequential learning algorithm for feedforward networks," *IEEE Trans. Neural Netw.*, vol. 17, no. 6, pp. 1411–1423, Nov. 2006.

[31] G. B. Huang, H. M. Zhou, X. J. Ding, and R. Zhang, "Extreme learning machine for regression and multiclass classification," *IEEE Trans. Syst.*, *Man*, *Cybern.*, *B*, *Cybern.*, vol. 42, no. 2, pp. 513–529, Apr. 2012.

[32] C. Wan, Z. Xu; P. Pinson, Z. Y. Dong, and K. Wong, "Probabilistic Forecasting of Wind Power Generation Using Extreme Learning Machine", *IEEE Trans. Power Syst*., pp. 1033–1044, vol. 29, no. 3, May 2014.

[33] A. H. Nizar, Z. Y. Dong, and Y. Wang, "Power utility nontechnical loss analysis with extreme learning machine method," *IEEE Trans. Power Syst*., vol. 23, no. 3, pp. 946–955, Aug. 2008.

[34] F. Deng and Z. Chen, "Power Control of Permanent Magnet Generator Based Variable Speed Wind Turbines," in *Proc. ICEMS'09*, 2009, pp. 1–6.

CHAPTER 6. CONCLUSIONS AND FUTURE WORKS

6.1. CONCLUSIONS

The objective of this project has been to enhance the RAP of SRG based WTs by applying advanced HMFD technologies. This dissertation has investigated the health monitoring and fault diagnostics of WTs with focuses on gearboxes and generators.

Since metal debris in lubricating oil contains abundant information regarding the ageing and wear/damage of WT gearboxes. The health condition of the lubricated WT gearboxes can be indicated by the concentration and size of the metal abrasive particles, which may provide very early warnings of faults/failures and benefit the condition based maintenance. A new inductive sensor which uses saddle-coil probe to generate a uniform magnetic field for performance improvement on the metal particle detection is proposed. The detailed geometry and the performance analysis are presented by using finite element analysis. The results demonstrate that the proposed saddle-coil inductive sensor possesses good identification ability of recognizing the ferromagnetic and non-ferromagnetic oil debris particles whose diameters are as small as 100 μm.

FD of WT gearboxes is highly desired by the wind farm operators to benefit the predictive maintenance and to reduce the cost of wind power. A new method for detection of early degradation in WT gearboxes is presented. Tri-axis vibration signals, which are used as the medium for the fault detection, are collected from an experimental gearbox test bench with incipient gear tooth wear fault. Twenty four statistical features in time domain are extracted from the vibration signals in each sampled instance. The intrinsic low dimensional manifold embedded in the twenty four dimensional fault characteristic space is learned by using the *t*-Distributed Stochastic Neighbor Embedding (*t*SNE) which is an advanced nonlinear dimensionality reduction algorithm. The incipient gear tooth fault has been successfully detected under different operation conditions only via a simple K Nearest Neighbor (KNN) classifier using the reduced features in the manifold.

Stator winding is one of the most vulnerable parts in Switched Reluctance Machine (SRM), especially under thermal stresses during frequently changing operation circumstances and susceptible heat dissipation conditions. Thus real-time online thermal monitoring of the stator winding is of great significance to the system protection and lifetime extension of SRM. A sensor-less approach for online thermal monitoring of stator winding of SRM is proposed, only voltage and current measurements which already exist in the control system are needed to estimate the

temperature of stator winding, only reference stator resistance R_0 is needed, neither other machine parameters nor thermal impedance parameters are required in the scheme. Simulation results under various operating conditions confirm the proposed sensor-less online thermal monitoring approach. It doesn't need parameters of the machine, it is nondestructive, and can be easily implemented in the machine control and monitoring system only by adding the temperature estimation algorithms in the software. It is cost-effective and has a vast application potential on the online condition monitoring and health management of SRMs.

Fast and accurate fault diagnosis of the position sensor is of great significance to ensure the reliability as well as sensor fault tolerant operation of the Switched Reluctance Wind Generator. A novel rotor position sensor fault diagnostic scheme has been proposed for SRG based on assembled ELM. Simulation results show that the learning speed of ELM is extremely fast, the rotor position estimation accuracy is also very high with the best RMSE of 0.1617°. The sensor faults including bias fault, drifting fault and intermittent fault have been detected and diagnosed accurately by using the proposed position sensor fault diagnostic approach. The proposed rotor position estimation method as well as sensor fault diagnostic scheme are of great significance for cost reduction, reliability improvement and predictive maintenance of SRG. It has vast potentials in the application of virtual sensor, position sensor redundancy, sensor-less control and sensor fault tolerant control of SRG.

As concluded above, this PhD dissertation has addressed some of the major issues regarding health monitoring and fault diagnostics of wind turbines. Issues with oil debris sensor improvement, incipient fault detection of WT gearboxes, online sensor-less thermal monitoring of SRM, and position sensor fault diagnosis in SRG have been covered. Simulation and experimental results have showed that these proposed methodologies are able to successfully address these issues.

6.2. FUTURE WORKS

Although many aspects regarding health monitoring and fault diagnostics of wind turbines have been covered by this dissertation, several other issues are interesting for future investigation. Some of the issues that are deemed valuable are listed as follows,

1. This research concentrates on the HMFD of gearbox and generator in WTs, other subsystems or components in WTs, such as blade, tower, main bearing, power converters, have not been included. As a matter of fact, blade and main bearing may also cause long downtime of WTs, power converters has high failure rate. The scope of the HMFD should be extended to blade, tower, main bearing and power converters in the future research.

2. From maintenance point of view, the decision makers of wind farm operators would like to know the remaining service time of the faulty subsystem/component in WT after the detection of the fault, thus failure prognostic technologies including physics of failure based prognosis, data driven prognosis as well as fusion prognosis need to be further investigated for the health management of WTs.

3. About the oil debris sensor improvement for online health monitoring of WT gearboxes, experimental tests need be followed to verify the proposed new saddle-coil probe. Furthermore, the sensitivity of the new oil debris sensor should be evaluated. Moreover, triple-coil structure oil debris sensor with uniformity improvement of magnetic field is also a valuable research topic. In addition, signal processing technologies for the oil debris identification, life time prediction of WT gearboxes based on oil debris information in the lubricating oil could also be investigated.

4. For the incipient fault detection of WT gearboxes, detection of gear wear fault is the focus in this project, the proposed approach could also be extended to detection of bearing and shaft faults. In addition, FD of WT gearbox based on data fusion of multiple sensors including vibration sensor, thermal sensor and oil debris sensor is also worthy of study in the future.

5. Experimental verification of the proposed sensor-less thermal monitoring of SRM should be conducted. In addition, thermal modeling and temperature rise analysis of SRM could also be studied based on FEA. Sensor-less thermal monitoring may be investigated for the generators in DFIG and PMSG based WTs.

6. Sensor-less control and sensor fault tolerant control of SRG could be the continued research based on the position sensor fault diagnostic approach proposed in this project. Experimental verification of the proposed sensor diagnosis methods should also be followed. Fault modeling and diagnosis of windings in the stator of SRG could be carried out to improve the reliability of SRG based WTs.

ISSN (online): 2246-1248
ISBN (online): 978-87-7112-710-2

AALBORG UNIVERSITY PRESS